

Debris flows on Mars: An experimental analysis

L. Braat
L.Braat@students.uu.nl
Student nr. 3471748

Supervisors:
Dr. M. G. Kleinhans
T. de Haas MSc

Master Thesis Earth Sciences
2nd version
11 June 2014



Universiteit Utrecht

ABSTRACT

Morphological indications for debris flows on Mars were discovered by several authors since the discovery of gullies by Malin and Edgett in 2000. Although most processes related to debris flows are well understood, mechanisms that define dimensions of debris-flow deposits are still uncertain. The aim of this thesis is to find relations between debris-flow morphology and initial and boundary condition (volume, slope, angle, channel dimensions, sediment composition, water content and flow characteristics) by the use of small-scale experiments. These relations will be used to the gain information about Martian conditions. 206 debris-flow experiments were performed to develop a large dataset in which the sensitivity to different initial and boundary conditions was tested. Secondly, 3 alluvial fans were built by multiple debris flows to find more morphologic characteristics (fan slope, fan dimension, sorting patterns and debris-flow dimensions on the fan). Recognizable morphologies similar to the experiments were found on Martian fans strengthening the hypothesis that they were formed by debris flows. From comparison with the data it was found that the studied Martian debris flows contain approximately less than 6wt% clay, 10-30wt% coarse material and more than 27wt% water.

KEYWORDS: DEBRIS FLOW, ALLUVIAL FAN, MARS, EXPERIMENTS, MORPHOLOGY

CONTENTS

Abstract.....	2
List of figures	5
List of tables.....	8
Preface	9
Introduction	10
Thesis outline.....	11
Debris flows	12
Mobilization	12
Motion.....	12
Deposition.....	14
Characteristics	16
Debris-flow fans	16
Why small-scale experiments?	16
Methodology	18
Experimental configuration.....	18
Debris-flow composition.....	19
Terrain parameters	20
Measurement methods	20
Yield stress	21
Permeability	23
Diffusivity	25
Results	27
Single debris-flow experiments	27
General processes - Reference experiments	27
Effect of composition on debris flow morphology	28
Effect of terrain parameters on debris flow morphology	37
Effect on Flow characteristics: velocity and flow depth.....	41
Effect of boundary and initial conditions on debris flow morphology.....	43

Fan experiments	46
Discussion	51
Implications for debris flow risk assessment	51
Comparisson other small scale experiments	51
Comparisson natural debris flows.....	54
Non-dimensional parameters	54
Stopping mechanism.....	58
Scaling parameters	60
Martian debris-flow fans.....	62
Improvements and future research	64
Conclusion.....	66
Acknowledgements.....	66
References.....	67
Appendix.....	71
Appendix I: All experiments.....	71
Appendix II: Fan composition.....	71
Appendix III: Permeameter	71
Appendix IV: Yield strength	71
Appendix V: Non-dimensional numbers.....	71
Appendix VI: Martian lobe dimensions.....	71

LIST OF FIGURES

<i>Figure 1: Gullies with fans on the inside of a crater wall on Mars (-35.121°N, 165.314°E). A) overview of gullies, fans and crater rim, B) zoomed in on fans, C) zoomed in on lobate texture. (HiRISE image: PSP_003162_1445, NASA/JPL/University of Arizona)</i>	10
<i>Figure 2: Gullies with fans on the inside of a crater (-45.109°N, 274.193°E). A) overview of the north side on the crater, B) zoomed in on fans, C) zoomed in on lobate texture. (HiRISE image: PSP_006837_1345_RED, NASA/JPL/University of Arizona)</i>	11
<i>Figure 3: Stress-strain relations for idealized liquid and plastic rheologic bodies (Pierson and Costa, 1987). 13</i>	
<i>Figure 4: Surface velocities experiments USGS debris-flow flume 3.5 s after flow reaches the flume mouth (x=0). A) Surface velocity field in a stationary frame. B) Same velocity field, but in a frame moving at the speed of the flow front. Shaded material in figure A and red arrows in B move less than 4 cm/s. Scale bars relate arrow length to corresponding surface speed. (Johnson et al., 2012)</i>	14
<i>Figure 5: A) debris flow deposit on Spitsbergen (photo by Tjalling de Haas, Maarten Kleinhans and Patrice Carbonneau), B) debris flow levees Sacagawea peak (photo by Travis Corthouts).....</i>	15
<i>Figure 6: Schematic of common processes on debris-flow dominated alluvial fans. Feeder channel (FC), fan apex (A), incised channel (IC), intersection point (IP). (Blair and McPherson, 2009).....</i>	17
<i>Figure 7: Experimental setup, A) overview, B) side view schematization.</i>	18
<i>Figure 8: Photograph of experimental debris-flow deposit. Indicated on the photograph are how and where the measurements were taken from the DEMs. A) Overview, B) cross section.</i>	21
<i>Figure 9: Grain size distribution obtained by sieving. A) Mass percentage plotted against fraction diameter. B) Cumulative sediment percentage as a function of grain size.</i>	22
<i>Figure 10: Yield stress experiment. Clay rich mass visible in the flume under a very high slope (high yield stress). Movie showing the experiment for a mixture without coarse material. (http://youtu.be/bEW1631M674)</i>	23
<i>Figure 11: A) Permeameter. A water reservoir with a constant head. Burettes at the front and on top a system for measuring detailed water heights. B) Sample holder of the permeameter. Sample is covered with a gauze and a small metal raster.</i>	24
<i>Figure 12: Permeability as a function of sample time for reference mixtures.....</i>	24
<i>Figure 13: A) Setup of diffusivity experiment. B) Photograph experiment in progress and movie about diffusivity experiment. (http://youtu.be/9XGQ75FAVYk).</i>	25
<i>Figure 14: Schematization of one-dimensional gravity-driven consolidation of a saturated slurry overlying an impermeable bed. H is the original surface position, z is the elevation positive upwards, u is the change in surface position, P_h is the hydraulic pressure, P^* is the excess pore pressure, P_t is the total fluid pressure, P_{t0} is the initial total fluid pressure at the slurry base, σ_t is the total normal stress and σ_e is the effective normal stress. A) Initial, liquefied state, B) Consolidation state, C) Drained state. (Major, 2000).....</i>	26
<i>Figure 15: Photographs experiment 230 with 4x coarse material. A) coarse snout, B) cross-section coarse levees, C) overview.....</i>	27
<i>Figure 16: Movie of the first reference experiment exp003 (youtu.be/NeYvwnYxyEM).....</i>	28

Figure 17: Top-view photographs of experimental debris-flow deposits for different percentages of coarse material. A) exp030 0%, B) exp225 13.85% reference mixture, C) exp029 23.46%, D) exp227 49.01%...... 29

Figure 18: Different variables as a function of mass percentage coarse material (basalt). a) runout length, b) velocity in the channel, c) snout deposit height, d) maximum and snout deposit width, e) levee length, f) levee height in reference to the inside and outside of the deposit, g) yield strength, h) diffusivity, i) permeability. ..31

Figure 19: Hill shade DEMs of experimental debris-flow deposits for different percentages of clay content. A) exp119 0%, B) exp166 10.80% C) exp165 18.03%, D) exp163 22.30%. 32

Figure 20: DEMs of experimental debris-flow deposits for different percentages of water content. A) exp146 20.00%, B) exp132 23.08% reference mixture, C) exp148 26.47%, D) exp161 31.03%. 33

Figure 21: Different variables as a function of mass percentage clay (kaolinite). a) runout length, b) velocity in the channel, c) snout deposit height, d) maximum and snout deposit width, e) levee length, f) levee height in reference to the inside and outside of the deposit, g) yield strength, h) diffusivity, i) flow depth at the apex, j) permeability, k) porosity..... 34

Figure 22: Hillshades of experimental debris-flow deposits for different amounts. A) exp207 2600g, B) exp211 11050g. 35

Figure 23: Different variables as a function of mass percentage water. a) runout length, b) velocity in the channel, c) snout deposit height, d) maximum and snout deposit width, e) Levee length, f) Levee height in reference to the inside and outside of the deposit..... 36

Figure 24: Different variables as a function of total amount. a) runout length, b) velocity in the channel, c) snout deposit height, d) maximum and snout deposit width, e) Levee length, f) Levee height in reference to the inside and outside of the deposit, g) flow depth at the apex. 37

Figure 25: Different variables as a function of outflow plain slope. a) runout length, b) snout deposit height, c) maximum and snout deposit width, d) Levee length, e) Levee height in reference to the inside and outside of the deposit. 38

Figure 26: Different variables as a function of channel slope. a) runout length, b) velocity in the channel, c) snout deposit height, d) maximum and snout deposit width, e) levee length, f) levee height in reference to the inside and outside of the deposit, g) flow depth at the apex. 39

Figure 27: Different variables as a function of channel width. A) runout length, B) velocity in the channel, C) snout deposit height, D) maximum and snout deposit width, E) levee length, F) levee height in reference to the inside and outside of the deposit. 40

Figure 28: A) Runout length and B) velocity as a function of channel slope. Long channel experiment shown in red. 41

Figure 29: Time lapse, top view photographs..... 41

Figure 30: Simplified flow geometry A) with increasing grain volume and constant bed speed, B) with increasing bed speed for constant sediment mixture (Davies, 1990). 42

Figure 31: Flow depth plotted against velocity for all data sorted by tested variable. Trends lines are plotted for channel slope and amount of material series 42

Figure 32: Snout height plotted against snout width. 44

Figure 33: Velocity as a function of maximum width. 44

Figure 34: Levee height measured on the outside of the deposit as a function of velocity.	44
Figure 35: Levee height measured relative to inside of the deposit as a function of infill area. Infill area is calculated by deposit width times length.	44
Figure 36: levee length of all experiments as a function of outflow length.	45
Figure 37: Photograph fan 1, 22 debris flows with 2x coarse material content (23.47wt%).	47
Figure 38: Different debris flows indicated with a different color on a hill shade map. Every color is the difference between two successive DEMs.	47
Figure 39: Top-view photographs of different steps in the formation of fan 1 after debris flows 2, 9, 16 and 22. Movie showing all top-view photographs (http://youtu.be/-_bWJwCAXD0).	48
Figure 40: Top-view photographs of different steps in the formation of fan 1 after debris flows 2, 3, 4 and 6. Movie showing all top-view photographs (http://youtu.be/C5SjM3InZ0g).	48
Figure 41: Top-view photographs of different steps in the formation of fan 1 after debris flows 2, 5, 12 and 19. Movie showing all top-view photographs (http://youtu.be/B_oqo4FnRHw).	48
Figure 42: Long profile elevation of fans 1, 2 and 3. Red line indicates the bed elevation.	49
Figure 43: Cross-sections of fan 1 at 8, 24 and 44 cm from the apex.	49
Figure 44: Cross sections of fan 3 at 10, 20 and 40 cm from the apex.	49
Figure 45: Cross-sections fan 1. A) Elevation, B) location of cross-sections and long profile.	50
Figure 46: Cross-sections fan 3. A) elevation, B) location of cross-sections and long profile.	50
Figure 47: Small-scale debris-flow experiments by different authors, a+b) Fairfield (2011), c) Bettella et al. (2012).	52
Figure 48: Small-scale debris-flow experiments by different authors, a) Liu (1996), b) van Steijn et al. (1989).	53
Figure 49: Photographs of natural debris flows. A) Downfan view from apex of Dolomite fan, Owens Valley, of paired levees 150–250 cm tall deposited during a 1984 debris-flow event (Blair and McPherson, 2009). B) Overview of 1984 debris-flow deposits (light) on the Dolomite fan consisting of proximal levees (upper arrow) and distal lobes (lower arrow) (Blair et al., 2009). C) Lobe-shaped deposits produced by the 1993 pyroclastic flows of Lascar volcano (Chile), levees enriched in large pumices (flow moving ahead) (Felix and Thomas, 2004). D) Natural levee along debris flow channel a few years after the event, Cresta Reit, Bormio (Sondrio), Italy (Zanuttigh and Lamberti, 2007).	53
Figure 50: Non-dimensional numbers a,b) Bagnold number, c,d) Savage number, e,f) Friction number, g,h) Mass number, i,j) Darcy number, k,l) Reynolds number as a function of a,c,e,g,i,k) coarse material content and b,d,f,h,j,l) clay content.	59
Figure 51: Histogram with width/height ratios of Martian debris flow lobes (dataset Tjalling de Haas).	63
Figure 52: Experimental width/height ratios for a) coarse material content, b) clay content and c) water content.	64

Figure 53: HiRISE (PSP_006837_1345_RED) image with debris-flow fans Mars. A) Overview with frames indicating location of other images. Zoomed in on, B) boulders, C) levees, D) lobes. 65

LIST OF TABLES

Table 1: Tested initial and boundary conditions and their ranges. Number of experiments is indicated for each variable. Left column experiments of this thesis, right column experiments of Lokhorst (2013). 20

Table 2: Results of reference experiments..... 28

Table 3: Ranges and values of different properties. Values are shown for this thesis, the USGS flume and three real debris flows (Oddstad 1982, South Toutle river 1980, Osceola mudflow 5700 B.P.). Additionally typical values are given. (Iverson, 1997)..... 55

Table 4: Dimensionless parameters calculated for USGS flume, three real debris flows (Iverson, 1997) and experiments of this thesis..... 58

Table 5: Values for dimensionless scaling parameters for different debris-flow sizes of similar composition ($\delta=0.01\text{m}$, $\rho_s=2700\text{kg/m}^3$, $\rho_f=1200\text{kg/m}^3$, $\tau_y=100\text{ Pa}$, $\mu=0.1\text{ Pa}\cdot\text{s}$, $D=10^{-5}\text{ m}^2/\text{s}$) (Iverson et al., 2010). Second column range of the parameters for this thesis is included, same composition was not possible. 61

Table 6: Martian lobe dimensions (Tjalling de Haas) and average dimensions reference experiments. 62

PREFACE

After my bachelor in Earth Sciences at Utrecht University I started the master Earth Surface and Water with a specialization in the direction Coastal Dynamics and Fluvial Systems. This thesis is a mandatory part of my educational program and was set up to contribute to the active research of my second supervisor, PhD candidate Tjalling de Haas. This thesis contains a practical research of 30 ECTS.

This subject was provided by my first supervisor Dr. Maarten Kleinhans. The research continues on work done by Ivar Lokhorst for his BSc thesis and KNAW lab assistant Jasper Leuven BSc. They developed the experimental method and started the dataset that was used in this thesis. The data and appendices of this thesis are not included but can be requested by contacting me or Tjalling de Haas.

Lisanne Braat, 11th April 2014, Utrecht

INTRODUCTION

In the search for recent fluvial activity on Mars, debris flows have become an important geomorphologic indicator for liquid water. Indications for debris flows on Mars were discovered with MOC (Mars Orbiter Camera) images on board of the Mars Global Surveyor (MGS) and HiRISE (High Resolution Imaging Science Experiment) on board of the Mars Reconnaissance Orbiter (MRO). For example, debris flows were found on fans in Protonilus Mensae (44°N, 51°E; Levy et al, 2010), on dunes in the Russel crater (54°S, 347°W; Mangold et al., 2003) and in impact unnamed craters at 45.109°S, 274.193°E (Johnsson et al., 2014), 38.390°S, 96.804°E and 35.121°S, 165.314°E (Lanza et al., 2010). On Mars these alluvial fans are mostly found at the lower end of gullies (*Figure 1* and *Figure 2*). Gullies with fans are abundant on Mars and can develop on the inside of crater walls, on dunes and on the sides of mesas.

Most of the gullies and fans are covered with relatively few impact craters and little dust. They are thought to be one of the youngest geological features (Malin and Edgett, 2000; Costard et al., 2002; Reiss et al., 2004; Malin et al., 2006; Schon et al., 2009; Lanza et al., 2010), which is supported by crater dating, cross-cutting relationships and stratigraphic analysis. Even though liquid water can currently not exist at the surface of Mars, because of the low atmospheric pressure and cold temperature, it is unlikely that these morphologies were formed by dry granular flow. Fan morphologies formed by dry granular flows differ significantly from those formed by debris flows.

Some alluvial fans show many morphological features that are characteristic for debris-flow fans and deposits on Earth. Recognizable morphologies include channels, sinuous gullies, levees, boulders in deposits, debris aprons and lobate deposits (Mangold et al., 2003; Lanza et al., 2010; Levy et al., 2010). Since these similar morphologies are found, it is assumed that these morphologies are developed by the same processes as on Earth (Costard et al., 2002; Mangold et al., 2003; Conway et al., 2008; Lanza et al., 2010). Debris flows are therefore often mentioned as a major formative mechanism for alluvial fans on Mars.

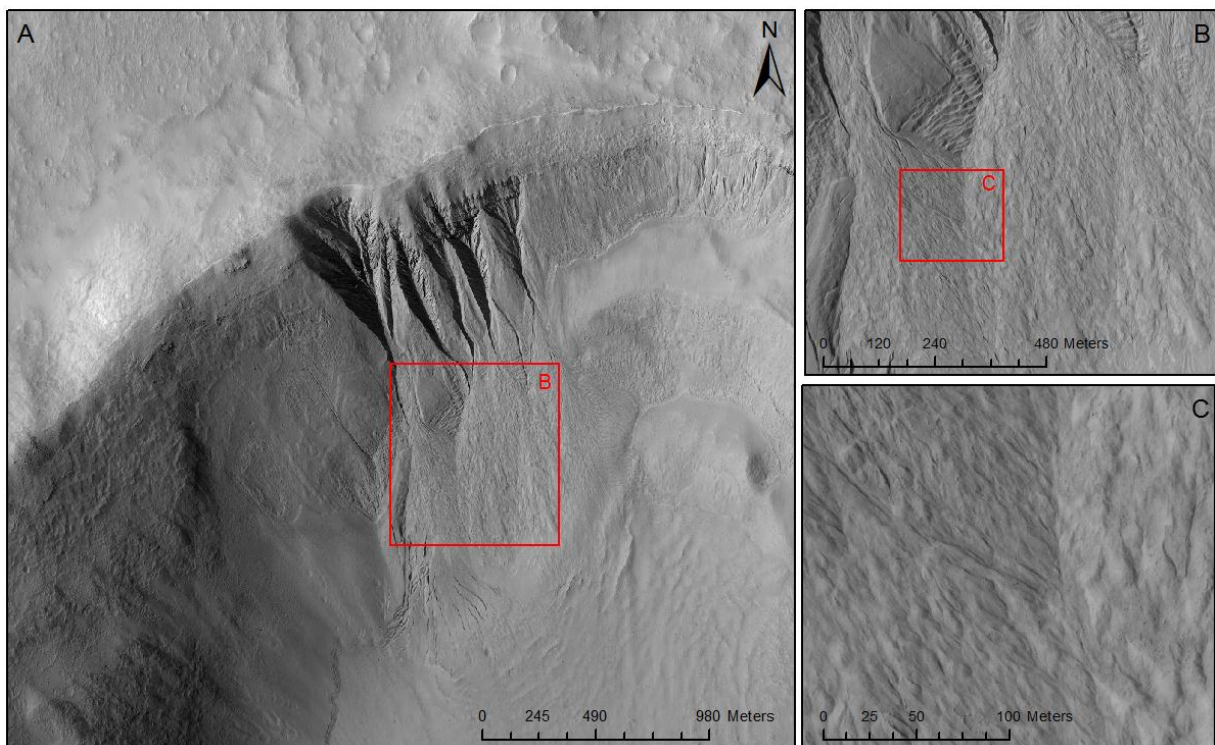


Figure 1: Gullies with fans on the inside of a crater wall on Mars (-35.121°N, 165.314°E). A) overview of gullies, fans and crater rim, B) zoomed in on fans, C) zoomed in on lobate texture. (HiRISE image: PSP_003162_1445, NASA/JPL/University of Arizona)

Although most processes related to debris flows are well understood, mechanisms that define dimensions of the debris flow are still uncertain. Examples of open questions are which mechanism defines the characteristic width of lobate deposits, and how do width and height of levee channeled flows influence runout length (Johnson et al, 2012).

The aim of this thesis is to find relations between debris-flow deposit dimensions and initial and boundary conditions by the use of small-scale experiments. A better understanding about the influence of volume, slope angle, channel dimensions, sediment composition and water content on deposit dimensions is necessary to uncover such relations. These relations can be used to develop better debris-flow prediction and risk assessment methods. However, this thesis aims to use the relations to gain information on Martian conditions from debris-flow morphologies that are visible at the surface. This information is essential in assessing the amount, origin and timing of liquid water in certain areas on Mars.

THESIS OUTLINE

The part of this chapter provides background information about debris flows and debris-flow fans. In chapter 2 the methods of the experimental research are discussed and chapter 3 states the results of the experiments. Chapter 4 discusses the results in relation to previous research of other authors and in relation to Mars. The conclusions are formulated in chapter 5.

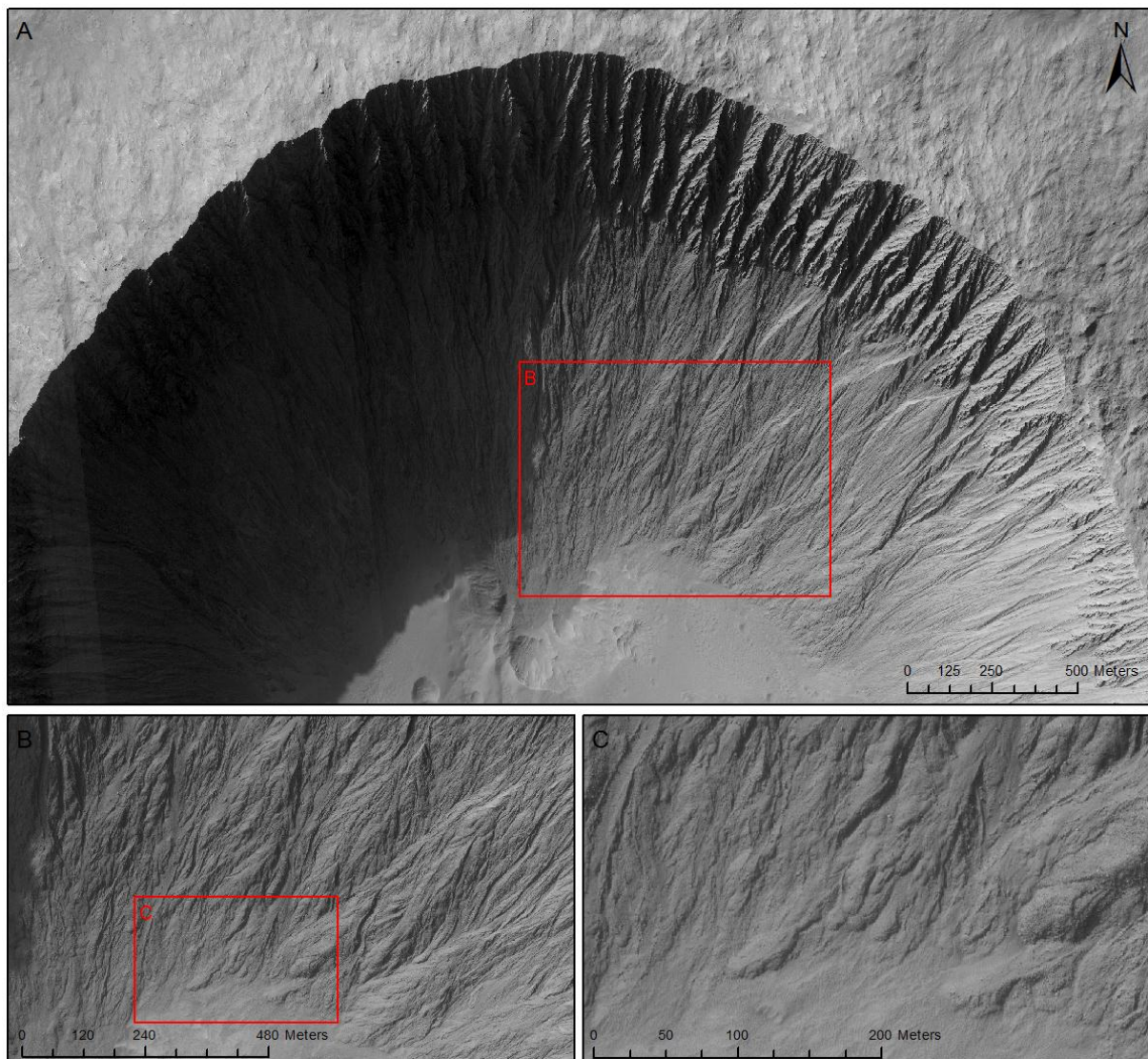


Figure 2: Gullies with fans on the inside of a crater (-45.109°N , 274.193°E). A) overview of the north side on the crater, B) zoomed in on fans, C) zoomed in on lobate texture. (HiRISE image: PSP_006837_1345_RED, NASA/JPL/University of Arizona)

DEBRIS FLOWS

Debris flows are one of the primary processes that develop alluvial fans besides other mechanisms like rock falls, rock slides, rock avalanches, earth flows, colluvial slips, noncohesive sediment-gravity flows (NSGFs), hyperconcentrated streamflow and normal streamflow (Pierson and Costa, 1987; Blair and McPherson, 2009). A debris flow is a sediment-gravity process generated by colluvial slope failure (Blair and McPherson, 2009) or by runoff (Kean et al., 2013). Colluvial slope failure occurs due to the addition of large amounts of water, for example by heavy precipitation or rapid snow and ice melt and sporadically by glacial outburst, dam failure or volcanic crater lake drainage (Costa, 1984). However, it is likely that the sources of water on Mars are different from Earth. Many authors have discussed possible sources of water that could have generated debris flows in the recent past of Mars. These include groundwater (Malin and Edgett, 2000; Gaidos, 2001; Gilmore and Phillips, 2002; Heldmann and Mellon, 2004), melting ground ice (Mellon and Phillips, 2001; Costard et al., 2002; Lanza et al., 2010) and snowmelt (Lee et al., 2001; Christensen, 2003).

Debris flows mobilize from a static, rigid mass of sediment on a slope. When mass movement occurs the sediment-water mixture is liquefied and transported downslope until it transforms back to a rigid deposit (*Figure 5A*) (Iverson, 1997).

Both the moment of generation and the magnitude and force of debris flows are unpredictable. Because of their high density in combination with high velocities they are major natural hazards for people and structures on Earth.

In contrast to rock-gravity and fluid-gravity processes, debris flows consist of a mixture of water and sediment particles with a wide variety in grain sizes that move downslope in a viscous state under the force of gravity (Blair and McPherson, 2009). Solid and fluid forces both play a role in debris-flow physics. Flow properties vary for different water and clay contents, grain size and sorting (Costa, 1984).

MOBILIZATION

Mobilization of debris flows requires (1) mass failure, (2) sufficient water and (3) sufficient energy conversion from gravitational potential energy to kinetic energy (Iverson, 1997). If all three conditions are met, the sliding motion can extend to widespread deformation recognized as flow (Iverson, 1997). Due to visibly abundant weathered material on the surface of Mars, debris flows are limited in frequency and intensity by their water content.

The Mohr-Coulomb criterion describes the state of stress on surfaces where mass failure occurs (*equation 1*). Cohesion, normal stress and internal angle of friction are unlikely to change over time. Changes in resistance are found in the effective stress ($\sigma - p$) by pore pressure change (Iverson, 1997; Lanza, 2010).

$$\tau = (\sigma - p)\mu + c \quad \text{eq. 1}$$

τ = shear strength [N/m^2] or [Pa]

σ = normal stress [Pa]

p = hydraulic pressure [Pa]

μ = internal friction coefficient [-]

c = cohesion [Pa]

MOTION

EXCESS PORE PRESSURE

High pore pressure can overcome shear strength (*equation 1*), leading to downward movement (Blair and McPherson, 2009; Mathewson et al. 1990). Fine sediment like clay fills the pores of the larger grains, preventing water from dissipating. This results in pore pressure excess to the hydrostatic pore pressure, by lowering the hydraulic diffusivity and therefore reducing the

change of basal pore pressure (dp_{bed}/dt) during motion (Iverson et al., 2010). Because of the excess pore pressure buoyancy increases and water carries part of the weight of the solid phase (Pierson and Costa, 1987). The buildup of excess pore pressure causes liquefaction of the sediment water mixture.

A wide diversity of grain sizes is essential to develop excess pore pressure, because small grains fill pores of larger grains preventing water dissipation (Iverson, 1997). Debris flows are more likely when colluvium contains clay which lowers the permeability, increasing pore pressure.

BINGHAM PLASTIC

Debris flows are non-Newtonian fluids, they behave roughly as Bingham plastics. A Bingham plastic behaves as a rigid body under low stresses, but will flow as a viscous fluid when stresses exceed the yield strength (Figure 3; Pierson and Costa, 1987). The plastic flow behavior leads to the formation of distinct morphologic characteristic for debris flows, such as levees, steep lobate fronts and unsorted deposits (Pierson and Costa, 1987).

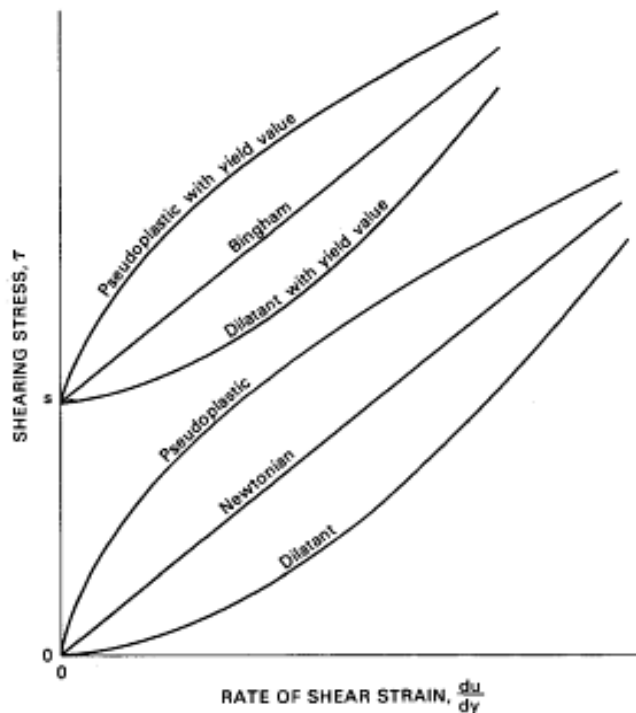


Figure 3: Stress-strain relations for idealized liquid and plastic rheologic bodies (Pierson and Costa, 1987).

GRAIN SEGREGATION

Many authors have discussed the importance of heterogenic debris-flow architecture. It is well known that inversely graded (coarsening upwards) particle size distribution develops during motion (Bagnold, 1954; Gray and Thornton, 2005; Johnson et al., 2012). Different processes are discussed as a cause for this distribution: kinetic sieving and dispersive and buoyancy forces (Sparks, 1976; Iverson and Vallance, 2001; Branney and Kokelaar, 2002). Kinetic sieving causes boulders moving in the debris to concentrate at the top. In the debris, voids open and close during motion. Small grains settle in these voids, which causes vertical sorting resulting in large boulders accumulations at the top of the flow (Gray and Thornton, 2005). Friction at the bottom of the flow causes vertical velocity differences. Therefore, the top of the flow has higher velocities and transports boulder rich material to the front of the flow creating longitudinal sorting. Surface velocities are measured 1.5 times faster than the propagation speed of the flow front (Johnson et al., 2012). A boulder rich, coarse grained, high intergranular friction front develops lacking pore fluid pressure (Iverson, 1997; Hungr et al., 2001). During transport other cobbles, boulders and even trees and cars can be entrained. Because of the lack of pore fluid pressure the debris-flow front tumbles and slides down rather than flows and will eventually stop moving (Iverson, 2003). Fine-grained debris behind the boulder accumulations is still liquefied and pushes the frontal boulders forward and aside (this is called shouldering) creating levees (Figure 4 and Figure 5B) (Sharp & Nobles 1953; Iverson, 1997; Major and Iverson, 1999; Iverson et al., 2010; Johnson et al., 2012). These levees are typically 1 to 2 m wide and 1 to 4 m tall. They are always present in parallel pairs, with approximately 2 to 10 m between the two levees (Blair and McPherson, 2009). The levee length can extend as long as the debris flow and end in a snout, the front of the debris flow. The levees and snout are generally clast-supported while the center of the flow is typically matrix-supported (Blair and McPherson, 2009). Levees

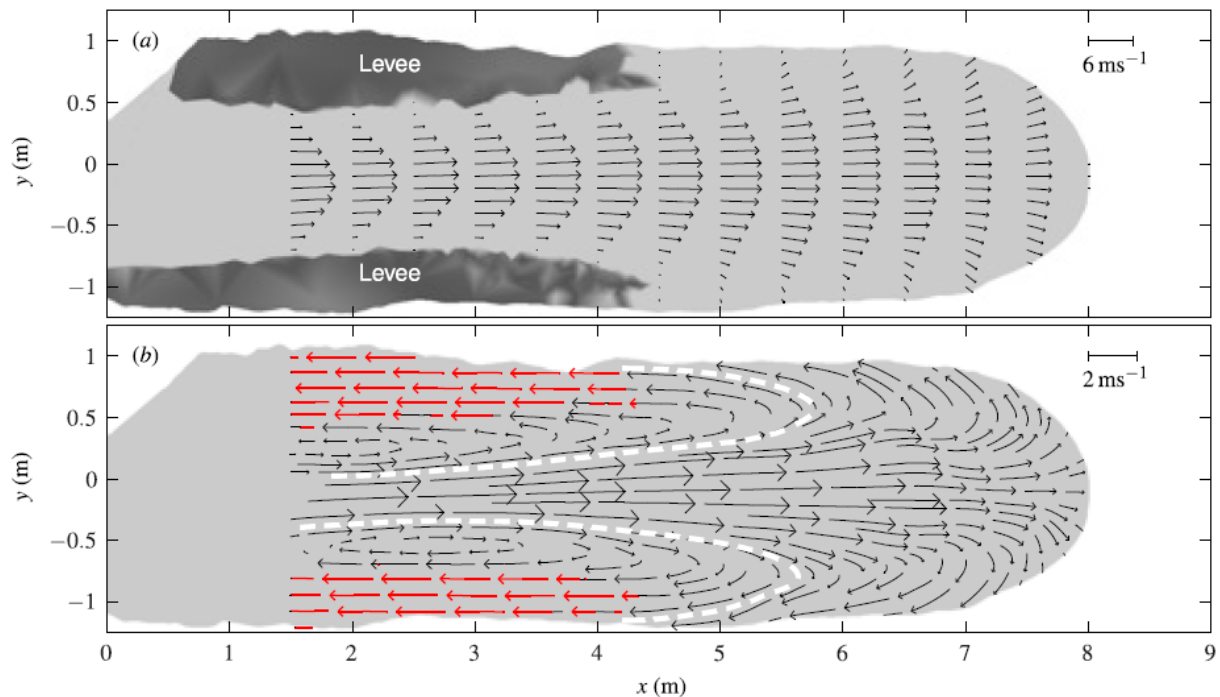


Figure 4: Surface velocities experiments USGS debris-flow flume 3.5 s after flow reaches the flume mouth ($x=0$). A) Surface velocity field in a stationary frame. B) Same velocity field, but in a frame moving at the speed of the flow front. Shaded material in figure A and red arrows in B move less than 4 cm/s. Scale bars relate arrow length to corresponding surface speed. (Johnson et al., 2012)

reduce lateral spreading of the flow resulting in longer run out distances (Iverson, 2003; Zanuttigh and Lamberti, 2007).

Debris flows moving downslope consist of multiple surges or waves (Pierson, 1980; Zanuttigh and Lamberti, 2007). A typical debris-flow surge forms a steep flow front similar to a bore which is followed by a gradual thinning body. The flow front consists (as discussed before) of very coarse material. The main body consists of average-sized material and ends in a watery tail (Davies, 1990). Surges can arise spontaneously without flow perturbation (Iverson, 1997). They appear as low-amplitude surface waves that look similar to roll waves of water on steep slopes (Iverson, 1997).

DEPOSITION

Debris flows come to a halt when gravity cannot overcome shear strength anymore, so the plastic yield strength equals the shear strength (*equation 1*). Lessening of the slope and losing excess pore pressure can contribute to an increase in shear strength, but is not necessary, since shear strength also increases when the flow thins due to lateral expansion.

Which process actually increases the shear stress is under debate. Authors have discussed excess pore pressure, intrinsic viscoplastic yield strength (Iverson, 2003) and grain-collision stresses (Major and Iverson, 1999; Iverson, 2003) to explain debris-flow deposition. Because the snout contains a large amount of boulders and other coarse material the water content is low and the head tends to slow down, causing a lot of friction (Major and Iverson, 1999).

After deposition, consolidation occurs in the form of water escaping from the deposit by evaporation and/or infiltration. Until pore pressure decreases, a slight chance remains that the deposit starts moving again by a second triggering mechanism, e.g. an earthquake. The time it takes for the deposit to consolidate is dependent on the diffusion quotient, the bed and deposition height (*equation 2* and *equation 3*).

$$D = kE/\mu \quad \text{eq. 2}$$

$D = \text{hydraulic diffusivity [m}^2/\text{s]}$
 $k = \text{permeability [m}^2]$
 $E = \text{Young's modulus [Pa]}$
 $\mu = \text{viscosity [Pa} \cdot \text{s]}$

$$t = h^2/bD \quad \text{eq. 3}$$

$t = \text{time for consolidation [s]}$
 $h = \text{deposition height [m]}$
 $b = 1 \text{ for an impermeable bed,}$
 $2 \text{ for a permeable bed}$
 $D = \text{hydraulic diffusivity [m}^2/\text{s]}$

Even though there is grain segregation during the flow, debris flows often result in non-stratified deposits with only locally inversely graded beds. Longer runout distances and long events generally result in more pronounced grain size variations within the deposit (Major, 1997). Inversely graded beds distinguish the deposit from fluid flow deposits which are normally graded. Because the density is large, selective particle settling does not take place in debris flows when velocity decreases (Pierson, 2005). The grains are already packed together and a poorly sorted sediment deposit is formed.

After deposition and consolidation secondary processes will affect the deposit over the course of time (Blair and McPherson, 2009). This has to be taken into account when studying Martian debris flows. Wind erosion is one of the most important reworking processes on Mars. Sand can be blown out or more likely, dust is blown over the deposit. Aeolian ripples and dunes are often observed on top of deposits that are most wind sensitive (Lanza et al., 2010). Some parts of the fans are inactive for long periods of time (Figure 6). These are the areas on the fan that are most affected.

Besides wind erosion, weathering can affect the appearance. On many suspected debris-flow fans, the amount of boulders at the surface is lower than expected. This can be explained by high boulder breakdown rates estimated at 3.5 m/Myr implying boulders are probably removed within 1 Myr (De Haas et al., 2013). This rate was locally estimated on a young (~1.25 Ma) fan in eastern Promethei Terra (35°S, 131°E)



Figure 5: A) debris flow deposit on Spitsbergen (photo by Tjalling de Haas, Maarten Kleinhans and Patrice Carbonneau), B) debris flow levees Sacagawea peak (photo by Travis Corthouts).

CHARACTERISTICS

Slopes that generate debris flows are in the range of 26 to 56 degrees. Higher slopes are too steep for colluvium and lower slopes have lower propensity to fail (Campbell, 1975; Ikeya, 1989; Rickenmann, 2005; Blair and McPherson, 2009). The speed of a debris flow can vary from 1 to 13 m/s (Blair and McPherson). Flows are generally 1 to 10 m thick and decrease in thickness due to lateral expansion on a fan (Blair and McPherson, 2009). Sediment concentrations by weight are between 50 to 90% with usually less than 15% clay and silt (Fairfield, 2011) and clay alone less than 10% (e.g., Major, 1997). Densities range from 1320 to 2600 kg/m³ with most around 2000 kg/m³ (Fairfield, 2011).

When deposited debris flows show elongated deposits ending in a lobe with sizes from 1 to 100 m wide, 0.005 to 2 m thick and hundreds of meters long, their margins are very steep, generally larger than 45 degrees (Blair and McPherson, 2009). This is very similar to dimensions found on Mars. Dimensions of typical debris-flow deposits on Mars are discussed by Levy et al. (2010). The average lobe thickness is estimated at 1.5 m ranging from 0.6 to 2.8 m, the average width is about 11 m ranging from 4 to 50 m and the deposit length is on average 50 m ranging from 10 to 200 m (Levy et al., 2010).

DEBRIS-FLOW FANS

Alluvial fans are conical landforms that develop by deposition of material emerging from a channel flowing out of mountain catchments (Blair and McPherson, 2009). Deposits are generally coarse grained and poorly sorted due to the short transport distance. When alluvial fans become large enough, some parts of the fan become temporarily abandoned and are influenced by secondary processes on the fan.

For optimal alluvial fan development three conditions are necessary: 1) a topographic setting where a catchment drains into a valley, 2) sufficient sediment production and 3) a triggering mechanism for colluvial slope failure, like a high water supply or earthquake (Blair and McPherson, 2009).

Debris-flow fans are classified as CC fans in the classification of Blair and McPherson (2009). Which are fans that develop from cohesive colluviums. CC fans have levees, lobes, rills and gullies as characteristics and secondary processes often result in desert pavement and boulder mantles (Blair and McPherson, 2009).

The average slope of alluvial fans varies from 2 to 35 degrees, but mostly between 2 and 20 degrees (Blair and McPherson, 2009; Ikeya, 1989; Campbell, 1975). More specifically debris-flow levees are often seen on 9-18 degree slopes, clast-rich lobes on slopes of 4-9 degrees and clast poor lobes on 2 - 4 degree slopes (Blair and McPherson, 2009).

The slopes found on Mars by Levy et al. (2010) are within or close to Terrestrial values. Gullies are generally found on slopes of ~27° (24°-32°) and fans initiate on slopes of ~21° (14°-24°). The lobate flows are present on slopes of ~18° (8°-25°) and their snouts on slopes of ~14° (6°-20°). Parsons et al. (2008) have slightly different results, the highest slopes found near the alcove are ~30°, ~23° slopes are found for gullies and deposition starts at 17°. This is all in agreement with the ranges on Earth.

WHY SMALL-SCALE EXPERIMENTS?

For this thesis small-scale debris-flow experiments were performed in the physical geography laboratory at Utrecht University. Laboratory experiments have many advantages over field observations. Field data are generally limited to the measurements of the situation after the event, while the initial and original boundary conditions such as water content and initial slope are unknown or irreproducible. Field observations related to origination, transportation and

deposition processes are rare because of the long recurrence interval and low predictability of debris flows. Additionally, this type of field monitoring is expensive and time consuming.

In small-scale laboratory experiments all initial and boundary conditions can be controlled. Processes involved in the formation of debris-flow deposits can be studied in detail because many quantities such as velocity and flow depth can be measured. The morphology can also be studied in detail, because weathering and secondary processes are not an issue, which is important for the comparison with Martian fans. Furthermore, the influence of individual initial and boundary conditions can be tested. Because the experiments are quick (1½ hour) and relatively easy, many experiments can be performed which increases the reliability of the measurements and results.

Small-scale debris-flow experiments are often discussed to have major scaling problems. The influence of fluid pressure and friction is said to become relatively small in relation to the influence of yield strength and viscosity (Iverson et al., 2010; Johnson et al., 2012). This problem with small-scale experiments is considered in the discussion.

An exception to scaling problems are the large-scale experiments in the large scale flume of the USGS (e.g. Major, 1997; Major and Iverson, 1999; Iverson et al., 2010; Johnson et al., 2012). Although these experiments are probably more realistic if compared to natural debris flows, only a limited amount of boundary conditions can be varied because of the size of the setup. Furthermore, less experiments can be performed in the same amount of time because they are less easy and more expensive.

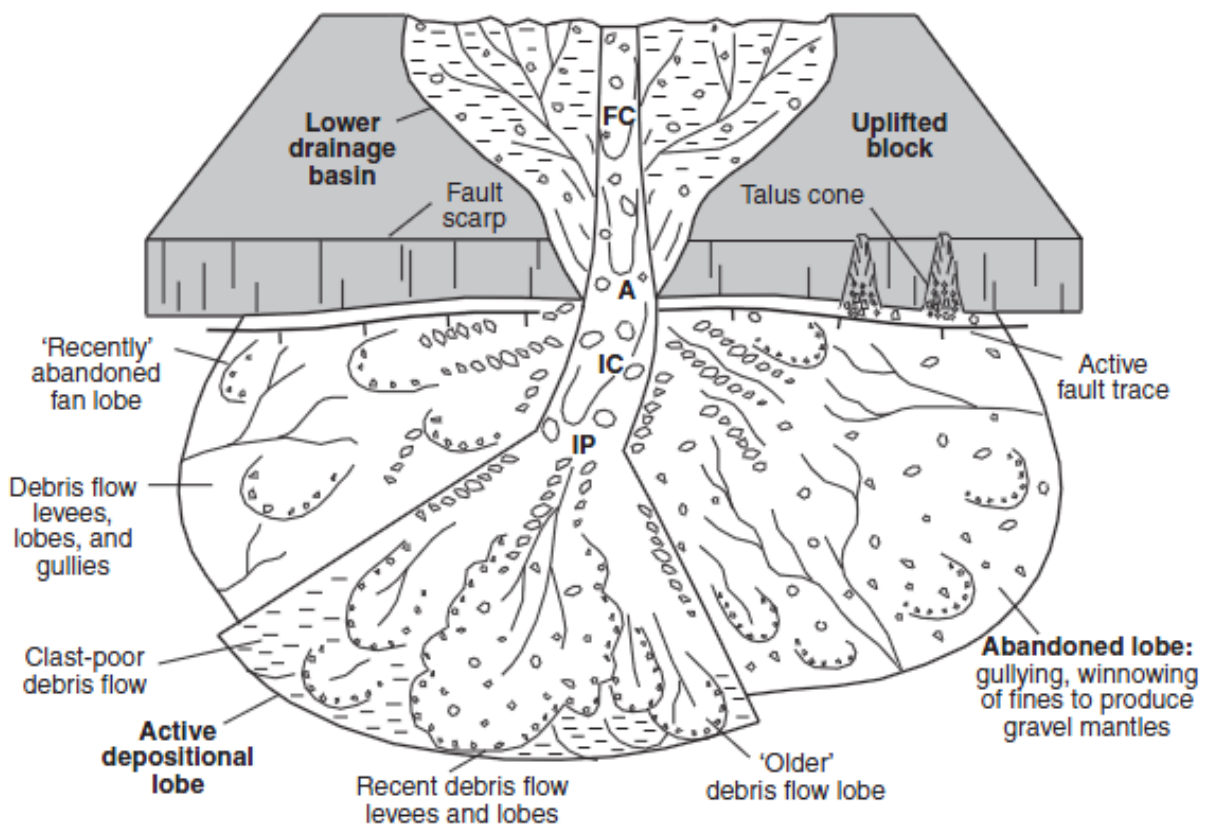


Figure 6: Schematic of common processes on debris-flow dominated alluvial fans. Feeder channel (FC), fan apex (A), incised channel (IC), intersection point (IP). (Blair and McPherson, 2009)

METHODOLOGY

To compare debris-flow fans to suggested debris-flow fans on Mars, small-scale experiments were performed in the physical geography laboratory at Utrecht University. As discussed in the introduction, small-scale laboratory experiments have many advantages over field data. The most important advantage is that they offer the opportunity to produce data in a controlled environment.

Experiments were performed in two steps. In the first step multiple debris-flow experiments were performed to develop a large dataset in which the sensitivity to different initial and boundary conditions (e.g. slopes, sediment concentration, water content and channel dimensions) was tested. Additionally, this sensitivity analysis was used to find optimum sediment mixtures, water concentrations and terrain parameters for the creation of realistic debris flows in the laboratory.

In the second step alluvial fans were built with multiple debris flows on top of each other to discover morphologic characteristics. In total 206 single debris-flow experiments and 3 alluvial fan experiments were performed.

EXPERIMENTAL CONFIGURATION

The experiments are conducted in a 2 m long and 11.9 cm wide outflow channel (*Figure 7*). The channel is covered with sandpaper to simulate the roughness of a natural channel. Lines are drawn on the channel 10 cm apart to help the velocity measurements and a tape-measure is glued vertically in the channel at the apex to measure flow depth.

A barrel with an impeller inside is connected at the top of the channel. The impeller is connected to a handle with which sediment and water can be mixed. After mixing the hatch in the barrel is opened electronically by pushing a button. Attached to the hatch is a sponge, to prevent water flowing out of the barrel during mixing. 1.5 seconds after the hatch is opened a second hatch opens automatically in the channel to remove the watery tail of the flow. This is necessary due to scaling issues. In scale experiments the influence of viscosity and yield stress is relatively large, and due to this the flow stops sooner than in nature (Johnson et al., 2012). If the tail of the flow is not removed, space between the levees would be filled and the material floods the debris flow occasionally. By diverting the flow after 1.5 seconds the morphology of the debris flow stays intact.

The part of the mixture that passes the second hatch flows further through the outflow channel into a larger flume. The bottom of the flume is covered with two rasters of 1.15 by 1.50 m with a cloth in between. The top raster is covered with sediment so water can drain easily. For every experiment a thin bed of loose sediment of about 1 cm high is placed under the outflow channel

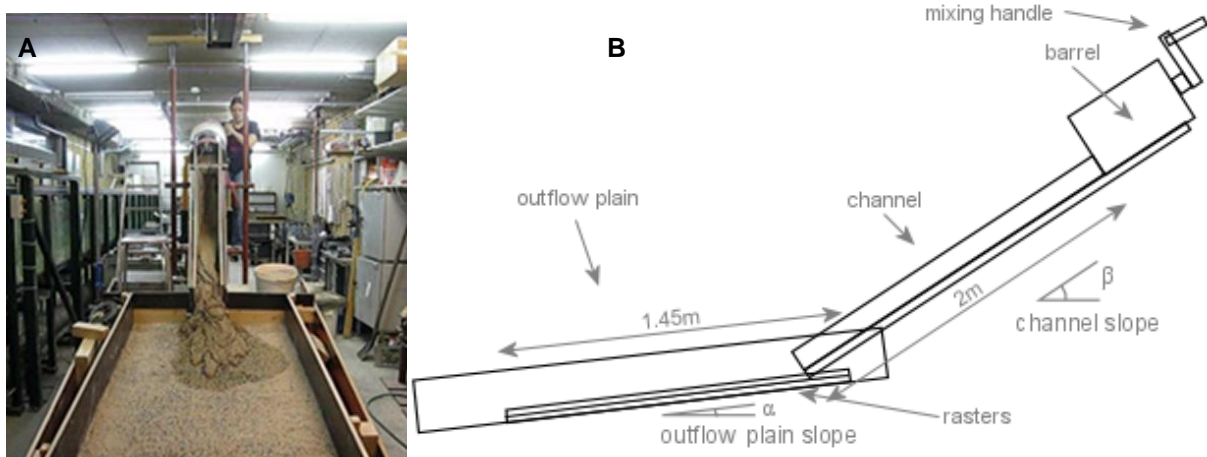


Figure 7: Experimental setup, A) overview, B) side view schematization.

to enhance drainage even more. This bed is replaced after each experiment. The same set up is also used to develop debris-flow fans in the second step. The fan is dried after each debris flow with a small heater and ventilator for better preservation of the morphology of the debris flows on the fan.

The set up simulates a feeder channel flowing onto an outflow plain on which fans can develop (*Figure 6*). The outflow channel represents the feeder channel, normally fed by many tributaries, but now by the barrel. The bottom of the outflow channel is the fan apex and the rasters in the flume represents the outflow plain.

A similar (but non automatic) setup was already successfully used by KNAW lab-assistant Jasper Leuven and BSc student Ivar Lokhorst at Utrecht University. This setup was slightly improved to decrease the human error by opening the hatches. Experiments 1 to 88 from the dataset were provided by their work of which 3 to 64 were single debris-flow experiments and 65 to 88 were fan experiments. After experiment 218 the setup was moved to a new location, which was an opportunity to further improve the set up. In this new location the channel walls were heightened to make it more suited for fan experiments and the whole setup was lowered to the ground to capture more data with the electronic equipment on the ceiling.

DEBRIS-FLOW COMPOSITION

A reference sediment mixture of 5 kg was used for the single debris-flow experiments which consist of 100 g (1.5 wt%) kaolinite clay, 1050g (16.1 wt%) fine sand, 2950g (45.4 wt%) river sand and 900g (13.9 wt%) 2 to 5 mm basalt which will be described as the coarse material content in the rest of this thesis. A wide variety of grain sizes is essential for typical debris-flow behavior, because this creates lower diffusivity generating excess pore fluid pressure. The different sediments were mixed by hand before they were put into the barrel to be mixed with water. For each reference experiment 1500g (23.1 wt%) water was used which makes a total mixture of 6.5kg mixed in the barrel for each debris flow.

For the sensitivity analysis variations in debris flow composition were tested. The goal was to test each variation on the reference three times to indicate repeatability. The amount of water was varied by simply adding different amounts of water to the sediment mixture. Testing the water concentration had therefore no influence on the amount of sediment used, but did have an effect on the total amount of the mixture. Water content was varied between 19.35 to 33.33 wt%.

Variations in the sediment mixture were tested by varying the amounts of kaolinite clay and 2-5 mm basalt representing coarse material. Clay and coarse material were expected to be important for flow parameters, levee and snout formation. The effects of clay and coarse material were studied separately. The amounts of clay and coarse material were varied by multiplying the reference mass by a scalar (*Table 1*). These resulting percentages were used to calculate the amount of sediment necessary for 5 kg. The amounts of the three other sediments types remain in this way proportional to each other. The range over which coarse material content was tested was from 0 up to 55.76 wt% (0 – 3624 g or 0 – 12 x). The range over which the clay content was tested was from 0 up to 29.21 wt% (0 – 1899g or 0 – 30 x).

For most of the sediment mixtures sieve curves were made to study the grain size distribution (*Figure 9*). Some problems occurred by sieving clay because of its cohesion, therefore these curves were not added to the figures.

The total amount of water and sediment combined was also varied for the sensitivity analysis in a way that the mass percentages of the different constituents would stay the same. It was varied from a total weight of 1950 to 11050 g.

TERRAIN PARAMETERS

The sensitivity of the morphology to different terrain parameters was also tested (*Table 1*). Experiments were performed with different outflow plain slopes, channel slopes, channel widths and channel lengths. The reference outflow plain slope was set to 10°. The outflow plain slope was varied between 0° to 15°. The reference outflow channel slope was set to 30°. The slope of the outflow channel was varied between 22° and 34°. Below 22° the reference mixture did not come out of the channel and the maximum slope was limited by the ceiling of the laboratory.

The channel width was varied by placing wooden boards on the side of the channel to make it smaller. The width could therefore not be increased in the sensitivity analysis, only decreased. Widths of 4.5, 7, and 9.5 cm were tested and the reference was 11.9 cm.

The effect of channel length was also tested. A longer outflow channel of 3 m was made for this experiment. A maximum slope of 28° was used for experiments with this channel.

Table 1: Tested initial and boundary conditions and their ranges. Number of experiments is indicated for each variable. Left column experiments of this thesis, right column experiments of Lokhorst (2013).

	Variable	Reference	Range	Number of experiments	
Composition	Coarse material fraction	13.85 wt% 900 g 1 x	0 - 55.76 wt% 0 - 3624 g 0 - 12 x	34	9
	Clay content	1.54 wt% 100 g 1 x	0 - 29.21 wt% 0 - 1899 g 0 - 30 x	35	6
	Water content	23.08 wt% 1500 g	19.35 - 33.33 wt% 1200 - 2500 g	16	6
	Total amount	6.5 kg	1.95 - 11.05 kg	11	6
Terrain	Channel slope	30°	22 - 34°	20	6
	Outflow plain slope	10°	0 - 15°	13	6
	Channel width	11.9 cm	4.5, 7, 9.5, 11.9 cm	4	3
	Channel length	2 m	2, 3 m	5	
				5	6 (reference experiments)
				143 + 48 = 191	

MEASUREMENT METHODS

Data of the experiments was obtained by 3 Canon Powershot photo cameras and a ViALUX zSnapper (3D scanner). Two to four point cloud scans were made by the scanner of the resulting morphology of each experiment. These scans were analyzed in Matlab by a code provided by Wouter Marra. With this script, the scans were merged together to form one large grid with z coordinates. From this data digital elevation maps (DEMs), 3D images and cross-profiles were made. From the DEMs and profiles parameters such as length, levee length, maximum width, snout width, levee height and snout height were obtained (*Figure 8*).

One camera was set to make top view photographs on which the whole debris flow was visible. Another camera was used to make a close up movie of the flow at the end of the outflow channel to determine the flow depth. A third camera was used to make an overview movie of the experiment from which flow velocity was determined. Velocity was determined by analyzing at the movie frame by frame obtaining time and travel distance. The third camera was also used to make close-up photographs by hand after the experiment. All this data is analyzed in Matlab together with permeability, yield stress and diffusivity to find relations and to calculate more parameters.

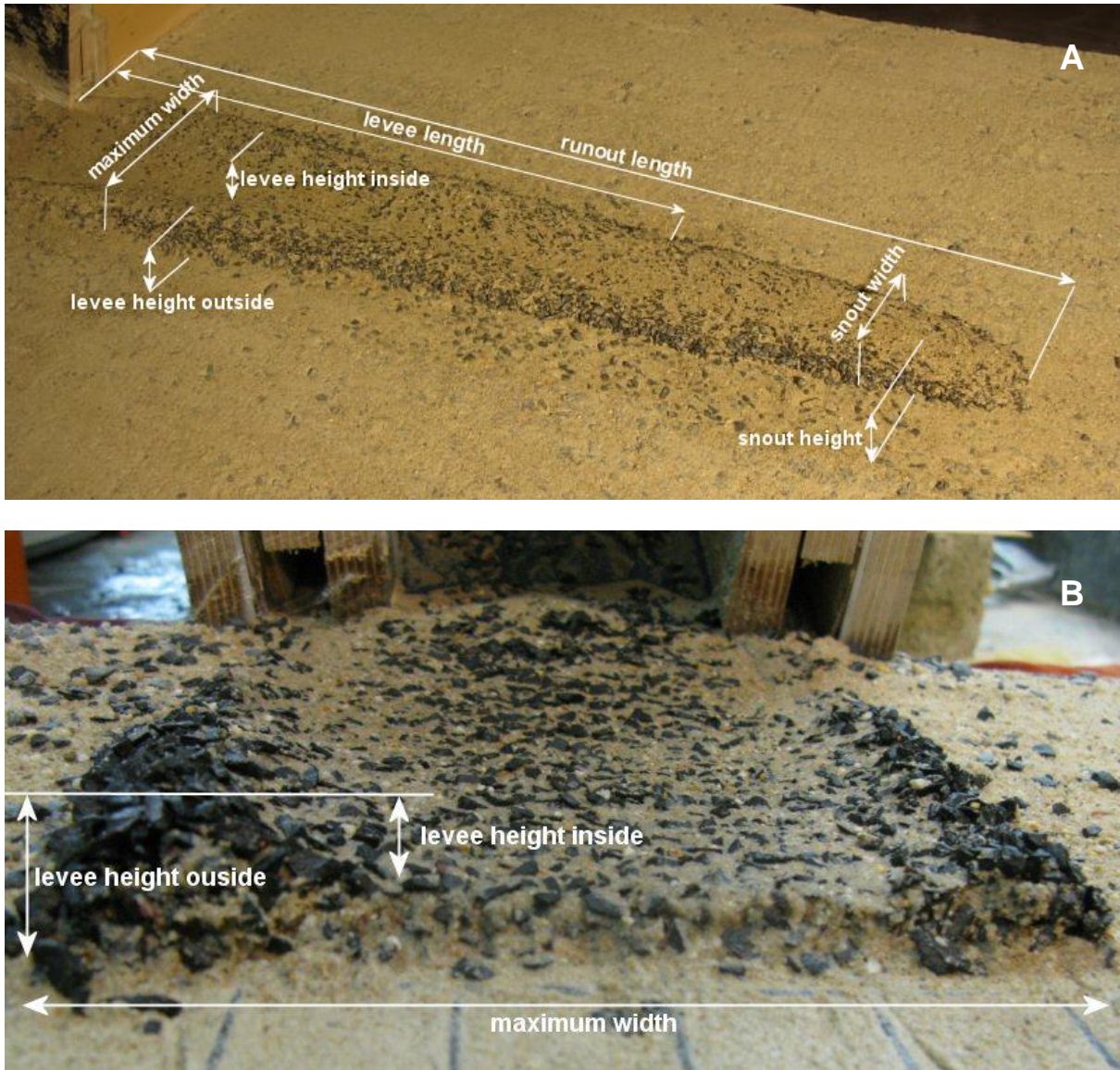


Figure 8: Photograph of experimental debris-flow deposit. Indicated on the photograph are how and where the measurements were taken from the DEMs. A) Overview, B) cross section.

Yield stress

Another variable that was measured outside of the experiments is the yield stress. A method similar to the method used by Yu et al. (2013) was used. Yield stress was measured using 750 g water and 2.5 kg sediment mixtures with varying compositions similar to the debris-flow experiments. The sediment and water was mixed with an impeller on a drill and was then poured in a 2 m long flume with an initial small slope gradient of a few (5 to 6) degrees (Figure 10). When the flow stopped a mass remained on the place where the mixture was poured in the channel. Then the gradient of the channel was increased until the mass started to move again. The mass would then spread out and obtain an almost uniform thickness (Figure 10). This is the maximum accumulation thickness. This thickness and the slope were measured to calculate the yield stress (equation 6). The maximum accumulation was measured with a ruler on 5 different places and then averaged. The precision of these measurements is about 1 mm. In some cases the whole mass did not start moving again, probably because most of the water was already drained. In these cases only the thickness of the parts that moved were measured.

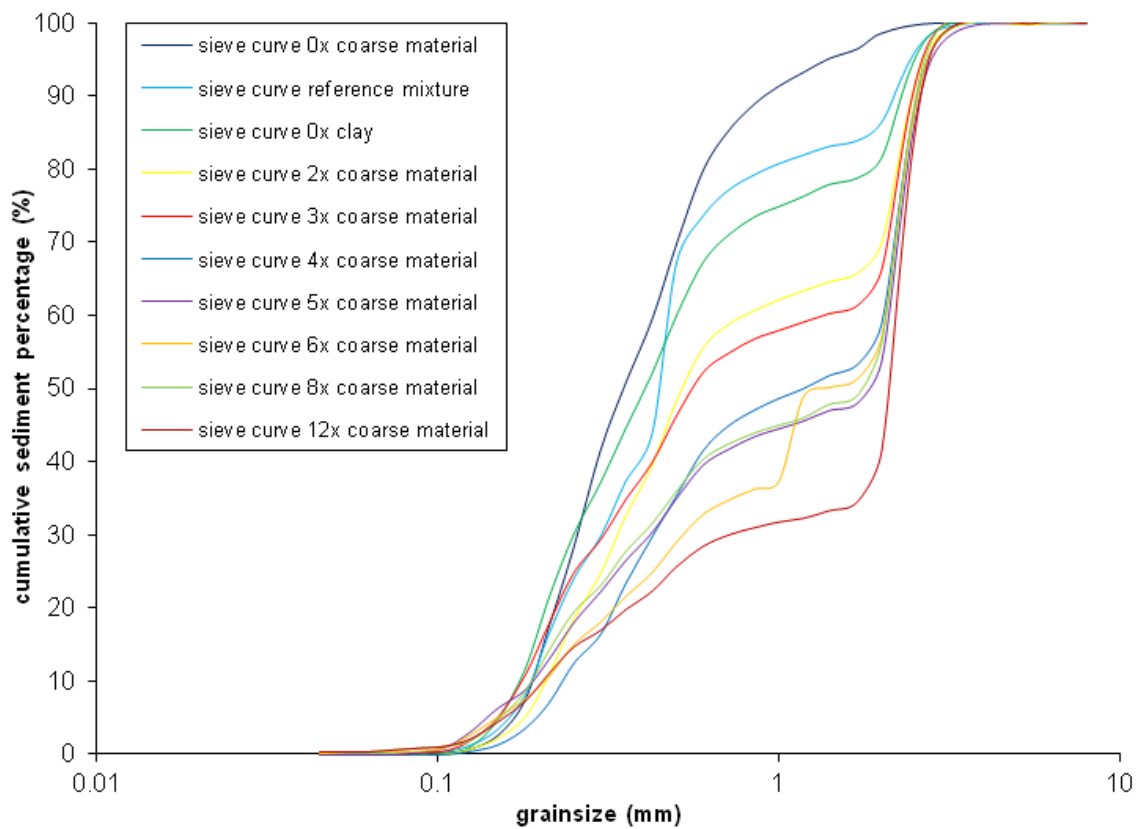
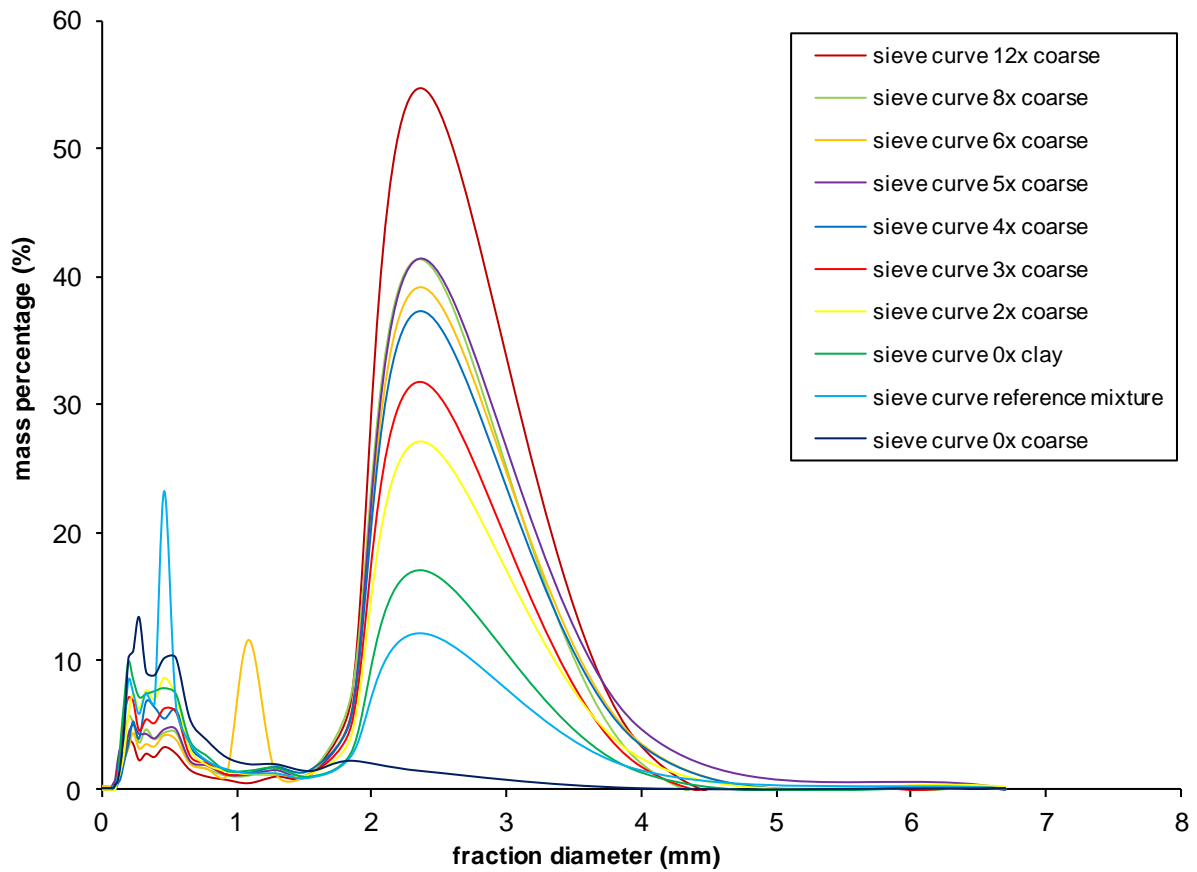


Figure 9: Grain size distribution obtained by sieving. A) Mass percentage plotted against fraction diameter. B) Cumulative sediment percentage as a function of grain size.

$$\tau_y = \rho g h \sin(S) \quad \text{eq. 6}$$

τ_y = yield stress [Pa]

ρ = density [kg/m³]

g = gravitational acceleration [m/s²]

h = maximum accumulation thickness [m]

S = flume slope [°]

Permeability

To obtain the permeability of the different mixtures a constant head permeameter was used (Figure 11a). A similar amount of water and sediment as for the experiments was mixed and poured in a crate with a cloth and raster to stimulate drainage similar to the debris-flow experiments. 20 minutes after the mixture was poured in the crate, 5 samples were taken with sample rings.

After the samples were taken, they were further prepared for the permeameter. Samples were on one side covered with a gauze which was held in place with a plastic, yellow ring and covered with a small metal grate. The whole package was then put into a holder of the permeameter (Figure 11). This holder was placed in the permeameter, which allowed many samples to be tested simultaneously.

The permeameter contained a large amount of water with a constant head. Water from the permeameter flowed through the samples from the bottom to the top. A plastic siphon tapped the water from the top of the samples to burettes in which the amount of water that flowed through the sample could be measured. Additionally, the water level in and outside of the sample was measured.

This was done for a wide range of different mixtures that were used for the experiments. From the results from the permeameter (volume water flowing through the sample in a certain amount of time and water level difference in and outside of the sample) hydraulic conductivity was calculated using equation 4. From the hydraulic conductivity the permeability was calculated using equation 5.

$$K = \frac{VL}{A th} \quad \text{eq. 4}$$

K = hydraulic conductivity [m/s]

V = volume water flown through the sample in a certain time [m³]

L = length sample [m]

A = surface area sample [m²]

t = time [s]

h = difference water level in and outside the samples [m]

$$k = K \frac{\mu}{\rho g} \quad \text{eq. 5}$$

k = permeability [m²]

K = hydraulic conductivity [m/s]

μ = dynamic viscosity [Pa · s] depending on temperature

ρ = density [kg/m³]

g = gravitational acceleration [m/s²]



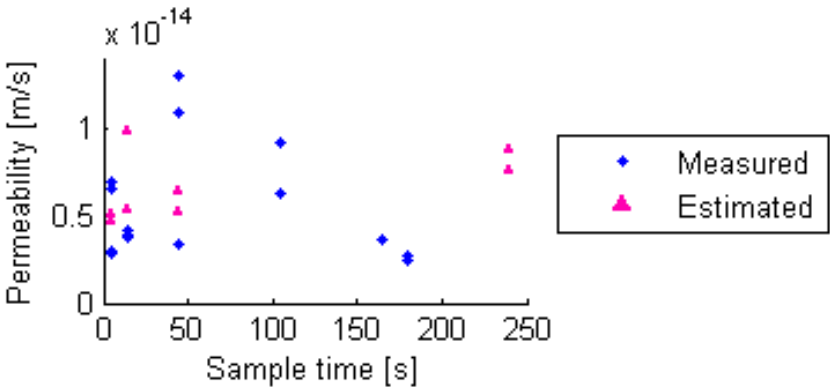
Figure 10: Yield stress experiment. Clay rich mass visible in the flume under a very high slope (high yield stress). Movie showing the experiment for a mixture without coarse material. (<http://youtu.be/bEW1631M674>)

The permeability was measured for 66 samples (*Appendix III*). This includes some tests with reference mixtures. The sensitivity of the reference mixtures to sample time was tested. Sample time is defined as the time between pouring the mixture in the crate and taking the sample from the crate. During this time the water can drain and the mixture can consolidate. *Figure 12* shows that the permeability results for the reference mixtures are randomly distributed for sample time. This indicates that the sample time has no clear effect on the permeability (*Figure 12*). It is assumed from these results that the effect of water content is negligible. Therefore, further study on permeability only has to be done with varying sediment composition.

For some of the samples not all variables were measured. Most of these variables could be estimated based on measurements of samples from the same mixture. The estimated variables are indicated in red and calculated values that use estimated variables in orange in *Appendix III*. These results are indicated in a different color in the graphs (e.g. *Figure 12*). They do not deviate from the results that are based on measurements and can be used for analysis.



Figure 11: A) Permeameter. A water reservoir with a constant head. Burettes at the front and on top a system for measuring detailed water heights. B) Sample holder of the permeameter. Sample is covered with a gauze and a small metal raster.



Diffusivity

The experiments to measure diffusivity are based on the method used by Major (2000). The diffusivity of the mixtures is measured with pressure sensors. Pressure sensors are connected to a transparent tube on different heights (*Figure 13*). The mixture is not poured directly in the tube, but mixed in another tube with impellers on a drill inside the transparent tube. This is done to protect the pressure sensors from damage. As soon as the mixture is well mixed the mixing tube and drill are pulled up with a rope over a pulley connected to the ceiling. The mixture can in this way flow through the bottom of the mixing tube into the transparent tube with the pressure sensors. The pressure sensors measure the total water pressure on the different heights. This total pressure consists of the hydrostatic pressure plus the excess pore pressure. Over time consolidation generates excess pore-fluid pressure dissipation by seepage (*Figure 13* and *Figure 14*). Eventually the total water pressure will approach the hydrostatic pressure. From the excess pore pressure dissipation over time and elevation the diffusivity coefficient can be determined (*equation 7*).

$$\frac{\partial P_*}{\partial t} - D \frac{\partial^2 P_*}{\partial z^2} = 0 \quad \text{eq. 7}$$

D = hydraulic diffusivity [m^2/s]

P_* = pore fluid pressure [Pa]

t = time [s]

z = elevation [m]



Figure 13: A) Setup of diffusivity experiment. B) Photograph experiment in progress and movie about diffusivity experiment. (<http://youtu.be/9XGQ75FAVYk>).

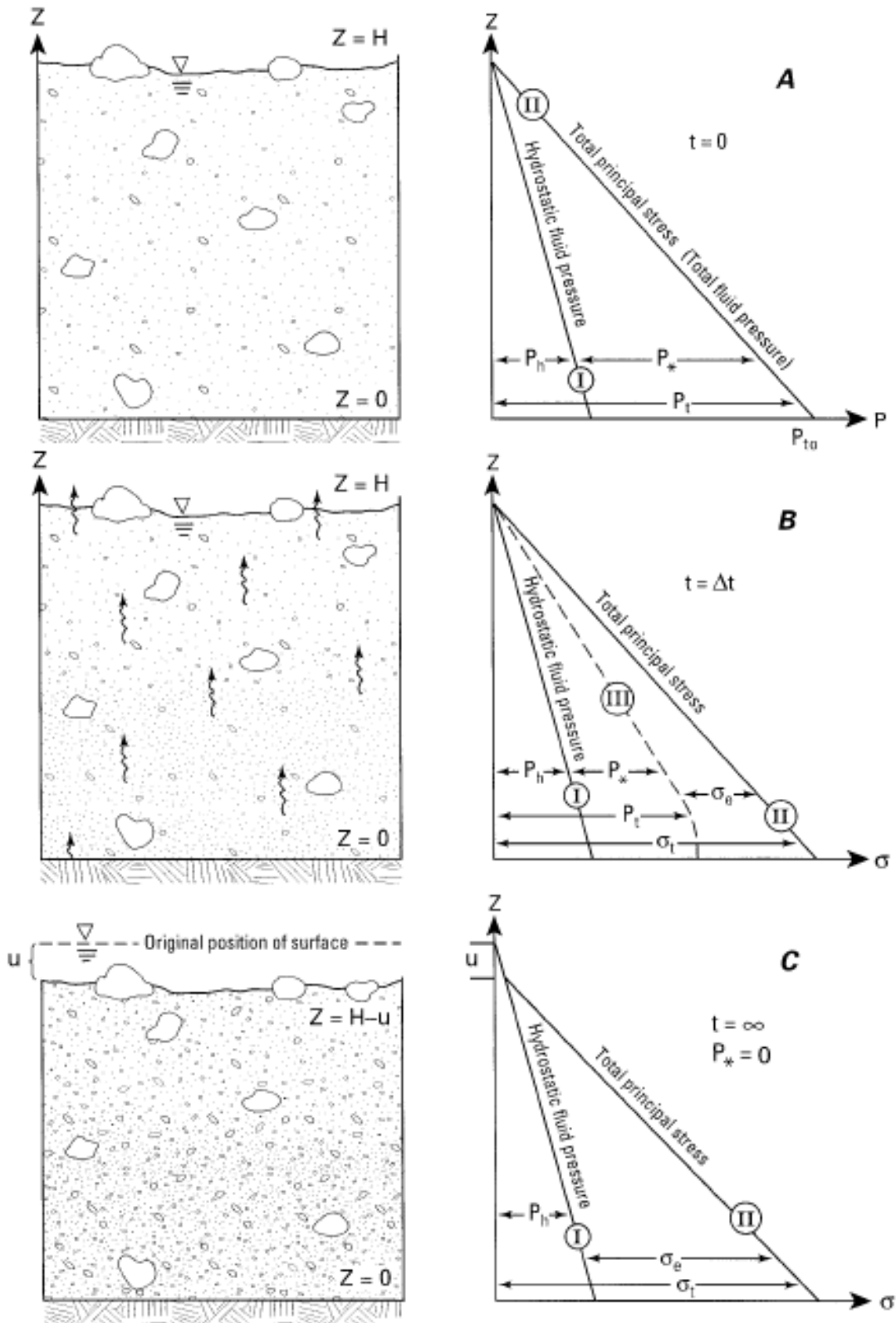


Figure 14: Schematization of one-dimensional gravity-driven consolidation of a saturated slurry overlying an impermeable bed. H is the original surface position, z is the elevation positive upwards, u is the change in surface position, P_h is the hydraulic pressure, P^* is the excess pore pressure, P_t is the total fluid pressure, P_{t0} is the initial total fluid pressure at the slurry base, σ_t is the total normal stress and σ_e is the effective normal stress. A) Initial, liquefied state, B) Consolidation state, C) Drained state. (Major, 2000)

RESULTS

In this chapter the results from the experiments are presented. In the first section the data from the single debris-flow experiments are shown and in the second section the results from the debris-flow fan experiments. Some interpretations are made about the plotted results, but these are more thoroughly analyzed in the discussion.

SINGLE DEBRIS-FLOW EXPERIMENTS

First, the results of the single debris flows are presented, sorted by tested variable: coarse material content, clay content, water content, amount of material, outflow plain slope, channel slope and channel width. Secondly, the results are discussed by measured parameter: velocity, flow depth, snout height, deposit width, levee height, levee length and runout length. But first the general processes are discussed using the reference experiments.

GENERAL PROCESSES - REFERENCE EXPERIMENTS

The single debris-flow experiments exhibited morphologies and transport processes that are also observed in natural debris flows. After the first hatch was opened, a debris flow moved down the slope very rapidly. During the transportation down the channel a coarse flow front and a watery tail developed. This indicates that grain segregation took place in the vertical and longitudinal direction. When the coarse snout entered the outflow plain, levee formation started immediately by shouldering of the coarse snout by the finer material in the middle. Velocities in the middle of the flow were observably larger than at the sides when entering the plain (*Table 2*). The levees confined the flow creating an elongated deposit. Levees were still visible after deposition and consist of coarser material (*Figure 15*). The edges of the deposit were very steep which is typical for debris flows.

From testing the reference experiment multiple times it was discovered that the repeatability is large (*Table 2*), although there is some small variation that might be internal variation or might depend on small factors like cleanness of the channel, dryness of the sub bed, different flume setups and the person that performed the experiment. It was therefore necessary to repeat all experiments at least once. If after two times the variation was large, the experiments were repeated multiple times.

Some experiments with extreme compositions that were tested can probably not be qualified as debris flows. Extreme water, clay or coarse material contents are not likely to occur in natural debris flows. The lower threshold of debris flows is the transition from hyperconcentrated flow to debris flow. This threshold can be defined by a sudden increase in the rate of yield strength increase with sediment concentration (Pierson and Costa 1987; Pierson, 2005). From this point onwards yield strength and buoyancy are sufficient to suspend gravel sized particles of 4 mm (Pierson, 2005). This onset is determined by the increase in internal friction (Rodine, 1974; Pierson and Costa, 1987) and is therefore more pronounced in coarse grained mixtures. (Pierson



Figure 15: Photographs experiment 230 with 4x coarse material. A) coarse snout, B) cross-section coarse levees, C) overview.

and Costa, 1987).

The upper boundary is the transition between debris flow and granular flow. This transition occurs when the flow is no longer liquefied (Pierson and Costa, 1987). This takes place when excess pore fluid pressure has disappeared and collisions and grain-to-grain contact become important (Pierson and Costa, 1987).

Not all experiments that were done are included in the plots. Some of the experiments had technical problems, like one of the hatches did not open or did not open in time. Secondly, data was sometimes missing because one of the cameras was out of memory (or making scans/movies was simply forgotten). Additionally, problems occurred with water content within the setup. For example the wetness of the bed, channel or barrel was sometimes significantly different. Especially the first experiment of the day or after the weekend often looked different than expected, probably because of this. Because this is only a hypothesis and not a technical problem, these experiments were included in the plots, but indicated in orange with yellow marking in the table including all experiments (*Appendix I*).



Figure 16: Movie of the first reference experiment *exp003* (youtu.be/NeYvwnYxyEM)

Table 2: Results of reference experiments.

Exp nr.	Length <i>L</i> [m]	Levee length <i>Ll</i> [m]	Max width <i>Wmax</i> [m]	Snout width <i>Ws</i> [m]	Snout thickness <i>Hs</i> [m]	Levee thickness <i>Hlo</i> [m] <i>Hli</i> [m]		Velocity <i>v</i> [m/s]	Flow depth <i>h</i> [m]
003	0.820	0.250	0.142	0.095	0.014	0.012	0.008	-	-
004	0.910	0.500	0.133	0.109	0.016	0.012	0.004	2.00	-
005	0.800	0.250	0.163	0.086	0.012	0.016	0.006	1.96	-
006	0.780	0.450	0.151	0.067	0.013	0.015	0.004	-	-
007	0.770	0.400	0.168	0.113	0.018	0.016	0.009	-	-
008	0.780	0.300	0.174	0.088	0.018	0.019	0.007	2.04	-
132	0.876	0.583	0.207	0.087	0.028	0.021	0.012	2.32	-
223	0.501	0.251	0.152	0.078	0.020	0.016	0.004	2.22	0.007
224	0.771	0.638	0.120	0.089	0.014	0.008	0.004	2.08	0.008
225	0.770	0.467	0.176	0.102	0.019	0.018	0.008	2.17	-
226	0.726	0.438	0.182	0.088	0.023	0.023	0.009	1.94	-
Min	0.501	0.250	0.120	0.067	0.012	0.008	0.004	1.944	0.007
Avg	0.773	0.412	0.161	0.091	0.018	0.016	0.007	2.093	0.008
Max	0.910	0.638	0.207	0.113	0.028	0.023	0.012	2.317	0.008

EFFECT OF COMPOSITION ON DEBRIS FLOW MORPHOLGY

EFFECT OF COARSE MATERIAL

Coarse material was varied with respect to the reference mixture. For high percentages of coarse material the deposits almost looked like dry rock fall deposits (*Figure 17D*). For low percentages there was no levee formation resulting in a more circular deposit instead of an elongated deposit (*Figure 17A*).

Experimental debris-flow lengths varied from ~0.2 up to ~1.2 m. Deposits were longest with mass percentages between 20 and 30 percent coarse material (2-5 mm basalt) (*Figure 18a*). Increasing or decreasing the mass percentage led to shorter debris-flow morphologies. Channel velocity showed a similar trend as runout length (*Figure 18b*). The optimum in the velocity was similar to the optimum in runout length. Therefore, velocity was determined to be a

very important factor regulating the length of the final morphology. Higher velocities produce longer debris-flow deposits. Velocities varied between 1.4 and 2.8 m/s.

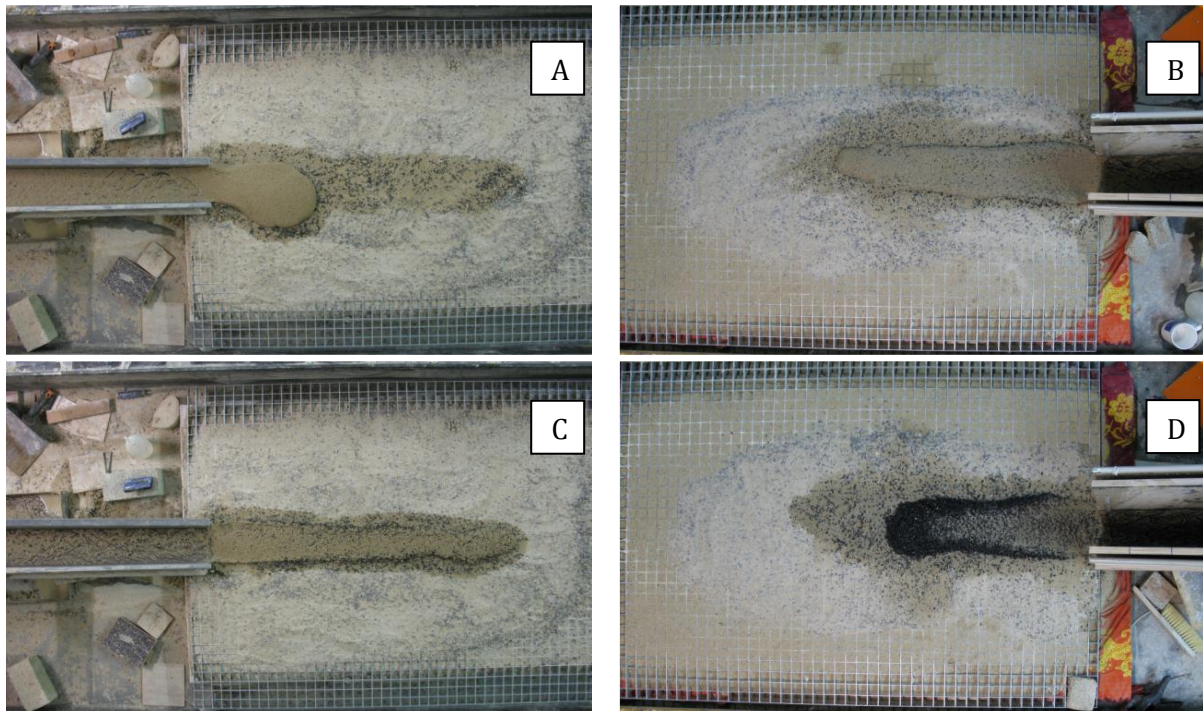


Figure 17: Top-view photographs of experimental debris-flow deposits for different percentages of coarse material. A) exp030 0%, B) exp225 13.85% reference mixture, C) exp029 23.46%, D) exp227 49.01%.

Snout height varies from 1 to 7 cm for the range of coarse material that was tested (Figure 18c). The snout height of the deposit as a function of coarse material shows thicker snouts for large coarse material contents. This is in agreement with the process of particle sorting in debris-flow fronts. Snouts consist generally of coarse material that is sorted to the front of the flow during transport down the channel slope. If there is more coarse material in the mixture more coarse material will collect at the debris-flow front. Large coarse snouts cause a lot of friction between grains and the bed and might be a possible reason why debris flows with a lot of coarse material do not result in a very long runout length. A low snout height occurs for an optimum in velocity and runout length. It is possible that higher velocities cause more downward transport, increasing the length and decreasing the height. The height compromises therefore for longer lengths, leading to an inverse relation.

A same relation as for snout height is visible for snout width (Figure 18d). The same explanations can be given for this relation. For the maximum width on the other hand, no clear trend is observed. Maximum width seems constant for different coarse material contents, although there is a large amount of scatter increasing uncertainty. The maximum width varies around 0.2 m.

Levee length also shows a trend with an optimum similar to runout length and velocity (Figure 18e). The optimum is a little bit closer to 30 than to 20 wt% coarse material compared to the other optima, but that might be due to the scatter. Longer debris flows have longer levees. This confirms that levee formation is an important process in increasing debris-flow length. Until the optimum in debris-flow length is reached the increase in coarse material content supplies the coarse snout with material to build the levees. After the optimum other processes take over which prevent further increase in outflow length.

Levee height was measured in reference to the outside of the deposits, so in reference to the outflow plain level, and in reference to the height of the debris flow in the middle (Figure 8).

When the two levee heights are subtracted from each other the deposition height at the beginning of the flow is obtained. This height is partly determined by the amount of material passing the second hatch, that is mostly determined by velocity. Therefore this height is not a reliable result unless you take the effect of velocity into account. Measurements of levee height relative to the outflow plain show an inverse relation similar to snout height with an optimum for the same mass percentage (*Figure 18f*). This means that low snout height is related to low levees. For a large coarse material content a lot of material is available to build large levees (*Figure 17D*). Surprisingly, the levee height is very high for low coarse material contents. In these cases the height relative to the inside is so small that it is debatable if there is levee formation at all (*Figure 17A*).

In *Figure 18g* and *Figure 18h* yield strength and diffusivity are plotted as a function of coarse material. Yield strength shows a linear decrease from ~44 to 8 for increasing coarse material content. This linear relation shows the transition from a Bingham plastic liquid (with yield strength) to a granular flow roughly resembling a Newtonian liquid (without yield strength). Diffusivity does not show a linear relation but an exponential increase. When the mixture contains more coarse material, water can escape the mixture more rapidly and pore fluid pressure decreases. This decreases debris-flow motion, for which excess pore pressure is essential (*equation 1*).

Figure 18i shows that permeability depends on the debris-flow composition. Larger coarse material contents clearly increase the permeability of the debris-flow mixture. More coarse material creates larger pores through which water can flow more easily.

EFFECT OF CLAY

Secondly, clay content was varied. For the highest percentage tested the debris flow had such observably high viscosity and yield strength that it did not exit the feeder channel. Generally high percentages of clay resulted in thick, viscous, sticky deposits which retained water for long periods of time (*Figure 19C* and *Figure 19D*). Mixtures with low percentages of clay were less viscous and showed unstable and irregular debris-flow snouts (*Figure 19A*).

Varying the clay percentage showed a clear trend for runout length with an optimum for mass percentages between 5 and 15 percent clay (kaolinite) resulting in the longest debris flows up to 1.45 m (*Figure 21a*). Experiments with a very high clay content resulted in the shortest runout lengths down to zero because the mixture could not get out of the channel.

Velocity showed the same trend as runout length (*Figure 21b*). The optimum of ~2.9 m/s is located at the same clay percentage (5-15 wt%) and the velocity also falls to zero for high clay contents. Hence, velocity is directly related to the runout length.

Snout height shows an inverse trend compared to velocity and runout length (*Figure 21c*). Short debris flows are related to thick snouts. The scatter is relatively high, so the relation is not as pronounced as for varying coarse material (*Figure 21c*). The snout height varies between 1 and 3 cm.

The maximum width also displays an optimum (of ~0.3 m) located between 5-15 wt% clay (*Figure 21d*). The trend is therefore similar to velocity and runout length. The maximum width of the deposit is not smaller for long debris flows but larger (*Figure 19A* and *Figure 19B*). Snout width shows larger scatter, but is relatively constant (~0.1 m) and therefore not depended on clay content.

Levee length as a function of clay content is the fourth graph that presents an optimum between 5-15 wt% clay. Levee length is as expected directly related to the runout length. Without levees the flow is not confined and a pancake-like deposit develops. *Figure 19D* shows that for very high clay contents there is no levee formation. In mixtures with high clay contents the properties of clay are dominant and the mixture is very viscous. This prevents particle sorting in the flow and therefore levee formation.

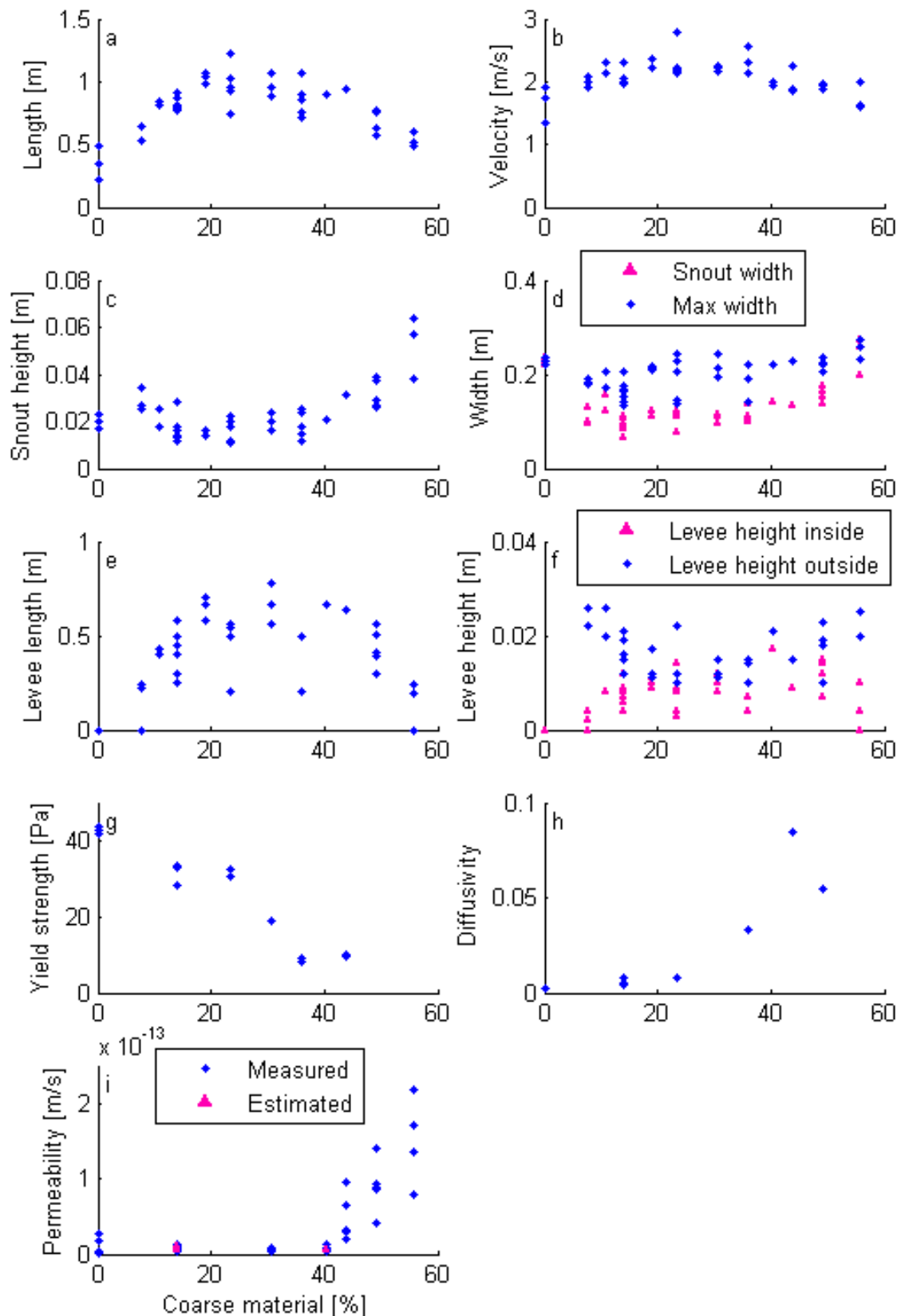


Figure 18: Different variables as a function of mass percentage coarse material (basalt). a) runout length, b) velocity in the channel, c) snout deposit height, d) maximum and snout deposit width, e) levee length, f) levee height in reference to the inside and outside of the deposit, g) yield strength, h) diffusivity, i) permeability.

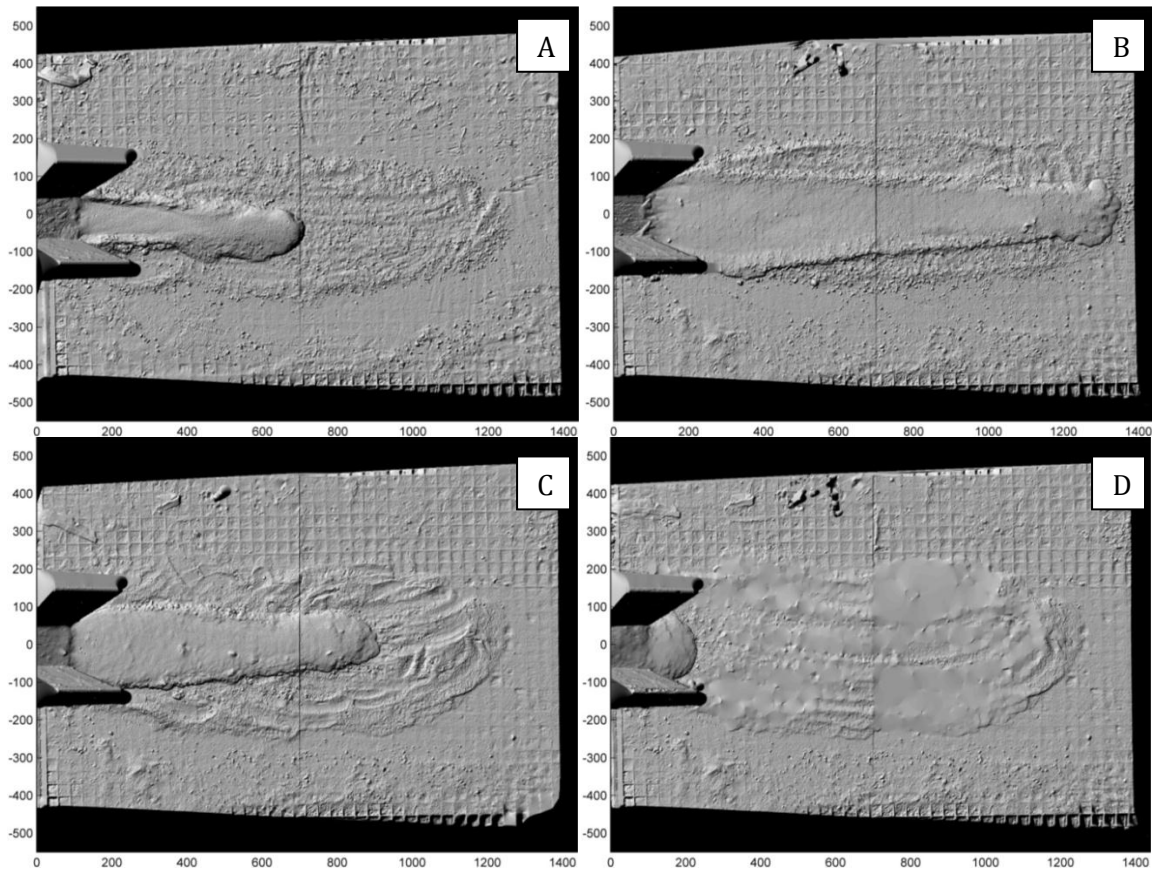


Figure 19: Hill shade DEMs of experimental debris-flow deposits for different percentages of clay content. A) exp119 0%, B) exp166 10.80% C) exp165 18.03%, D) exp163 22.30%.

Levee height in reference to the outflow plain decreases with clay content, but there is large scatter (Figure 21f). With an increase in clay content the levees become less pronounced and decrease in height probably to compensate for their length. If the deposit is longer, material is more spread out and the height decreases, therefore less high levees are needed. Levee height in reference to the middle of the deposit shows an optimum but at a different wt% clay (~5%) compared to runout length. Longer debris flows have more pronounced levees, which is expected because of infilling. More mass is used for the long deposit, so less material is available to fill between the levees. The position of the optimum is not the same, because from ~5wt% clay levees become less pronounced in general and the length of the debris flow is no longer relevant.

The yield strength shows a small decrease from ~50 Pa to ~20 Pa followed by a large increase for increasing clay content up to 290 Pa (Figure 21g). The minimum in yield strength correlates with the other maxima and minima around 10 wt% clay. Diffusivity exhibits an exponential function (Figure 21h). Diffusivity rapidly decreases for increasing clay content and then approaches zero. This was also observed during the debris-flow experiments, because clay rich deposits needed a long time to dry/consolidate and did not wet the sand bed around it. Very viscous flows have high yield strengths up to 300 Pa which prevents them from flowing onto the outflow plain. Diffusivity might contribute to the fact that low clay contents develop short deposits as well. But the lower yield strength for low clay contents means that shear stress is more rapidly below the yield strength.

Permeability is depended on clay content. Larger clay content decreased the permeability. Small clay particles decrease the permeability because they fill the pores between larger grains making it more difficult for the water to flow through the pores. Changing the clay content might have an effect on the porosity of the sediment mixture. This is however not the case (Figure 21k),

which means that not the total volume of the pores decreased with clay content, but only the volume of the individual pores slowing water flow through the sample.

In contrast with these results, Iverson (1997) found an exponential relation between permeability and porosity (Figure 21f). He used the fluid fraction of the debris flow as a measure for porosity which includes suspended clay, while only the water fraction without clay is used. Adding clay to the porosity fraction is not in agreement with the definition of porosity, which is the amount of space between particles. To calculate porosity the difference in weight of dried and saturated samples was divided by the density of water. Even if Iverson's measure of porosity is accepted, the fluid fraction can only be used as a measure of porosity if the mixture is not over or under saturated, which would lead to an over or under estimation of porosity.

EFFECT OF WATER

For the lowest percentage of water content the mixture did not come out of the barrel in which the sediment was mixed and for the highest percentage the deposit became longer than the raster. From observations it was already clear that when more water was added to the mixture, the debris flow became longer, faster and thinner. This is also visible in the DEMs (Figure 20) and measurements (Figure 23).

The runout length plotted against the mass percentage of water shows a slightly concave, but almost linear relation (Figure 23a). This relation is very strong. A 4% change in the weight percent of water in the mixture can make a difference between no debris flow coming out of the channel and a debris-flow deposit of a meter long. The runout length is expected to theoretically increase to infinity if infiltration is not taken into account, because the mixture will eventually become a liquid flow (Newtonian) instead of a debris flow (Bingham) when more water is added. If the flow becomes an Newtonian flow infiltration is the only factor limiting outflow length.

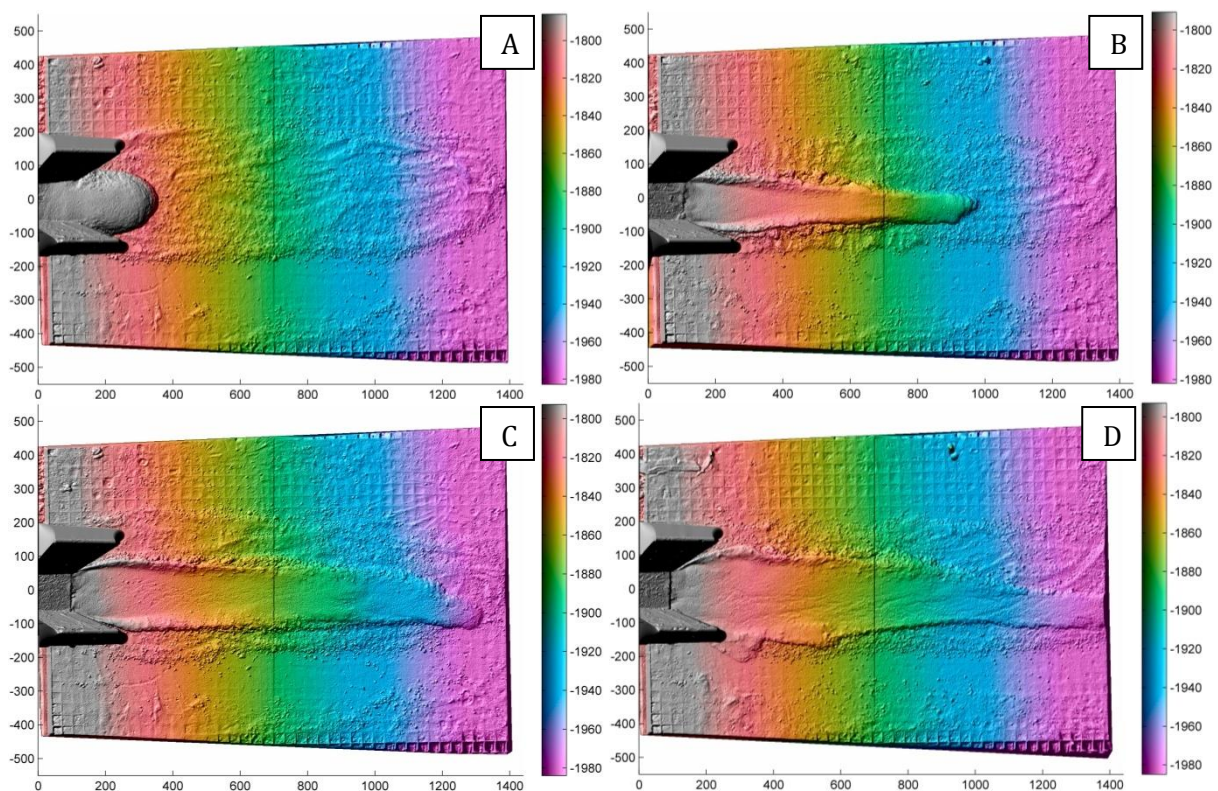


Figure 20: DEMs of experimental debris-flow deposits for different percentages of water content. A) exp146 20.00%, B) exp132 23.08% reference mixture, C) exp148 26.47%, D) exp161 31.03%.

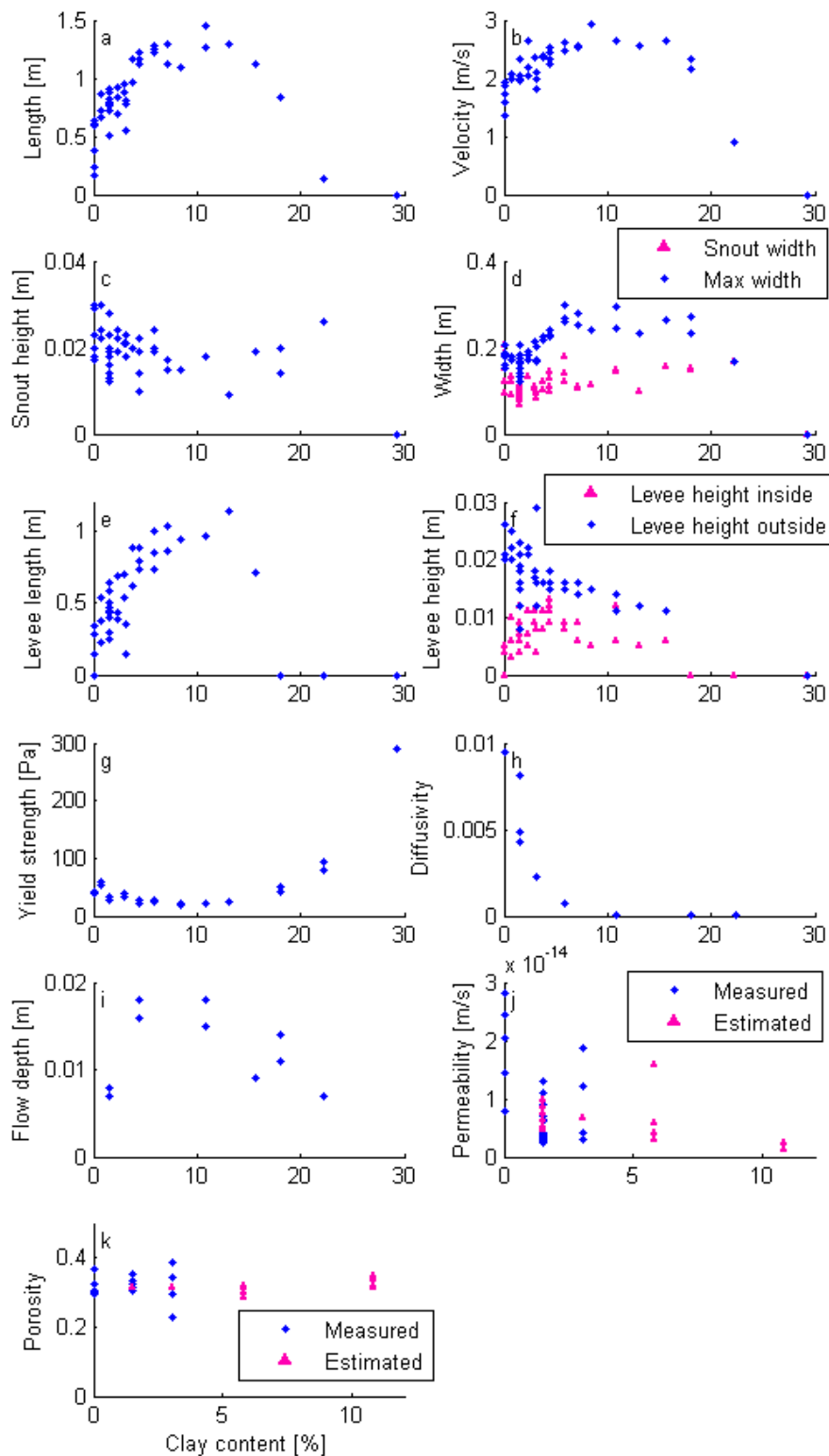


Figure 21: Different variables as a function of mass percentage clay (kaolinite). a) runout length, b) velocity in the channel, c) snout deposit height, d) maximum and snout deposit width, e) levee length, f) levee height in reference to the inside and outside of the deposit, g) yield strength, h) diffusivity, i) flow depth at the apex, j) permeability, k) porosity.

The velocity shows a similar but less linear relation as runout length (*Figure 23b*). More water increases the velocity of the mixture up to $\sim 3\text{m/s}$. The maximum velocity approaches the velocity of water flow under these conditions.

Snout height shows the inverse trend of runout length (*Figure 23c*). It decreases almost linear for an increasing amount of water from 5.5 to 1 cm. The relation is less clear than the relation for runout length because there is a lot of scatter between 20 and 25 wt% water. The first data point has a thickness of zero because no deposit formed on the outflow plain. The mixture did not come out of the barrel. Snout height is mainly determined by mass conservation. When the debris flow is short, the thickness of the deposit is larger. This is also visible in the DEMs (*Figure 20*).

For low water content the width is relatively constant, so the maximum width is similar to the snout width (*Figure 23d*). However, for high water content the maximum width differs significantly from the snout width. The maximum width increases slightly with increasing water content from 0.2 to 0.4 m, while snout width is very scattered.

Levee length increases linearly with increasing water content similar to the runout length (*Figure 23e*), again confirming that levees are necessary to form elongated deposits. The longer the deposit the longer the levees are.

The thickness of the levees compared to the outflow plain decreases with more water, while it increases compared to the middle of the deposit (*Figure 23f*). The thicknesses become similar with more water, which means that the infilling between the levees becomes less for longer flows, because more mass is transported downslope. This might also be the reason why levees become lower ($\sim 1.2\text{ cm}$). Furthermore, the levees do not need to be as high, because the width also increases, which decreases flow thickness because the flow is more spreaded.

To summarize, when the flow is more watery, the viscosity and yield strength go down, and the flow becomes increasingly more like a Newtonian fluid. This eases the flow in all dimension, resulting in faster velocity, lower thicknesses, larger widths, more flow downslope and less infilling.

EFFECT OF DEBRIS-FLOW SIZE

The last debris-flow composition variable that was tested is total amount of water and material. The smallest amount of 1950 g was not enough reach the outflow plain. The largest of 11050 g was just enough to not flow over the raster and was also about the largest mixture that was possible to mix in the barrel (*Figure 22B*).

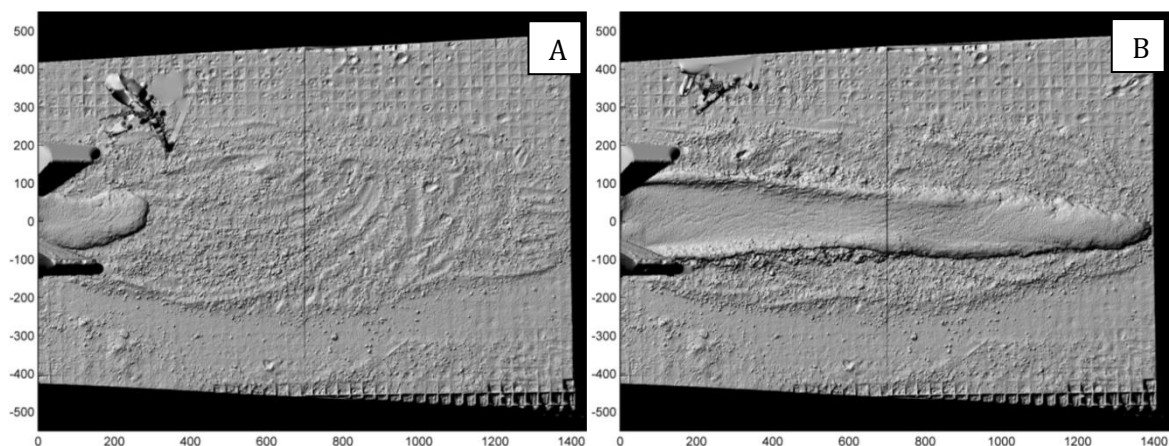


Figure 22: Hillshades of experimental debris-flow deposits for different amounts. A) exp207 2600g, B) exp211 11050g.

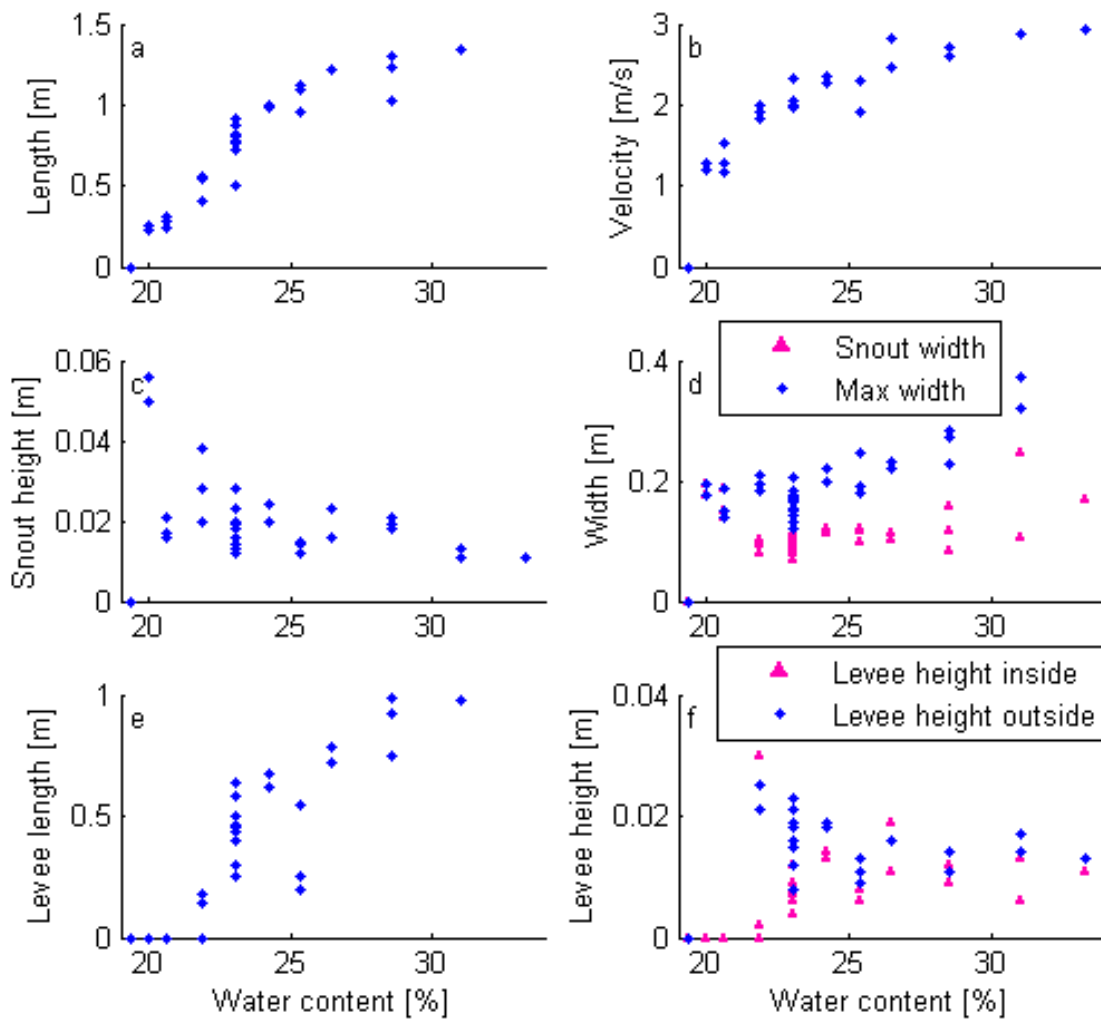


Figure 23: Different variables as a function of mass percentage water. a) runout length, b) velocity in the channel, c) snout deposit height, d) maximum and snout deposit width, e) Levee length, f) Levee height in reference to the inside and outside of the deposit.

Length (Figure 24a), velocity (Figure 24b), maximum width (Figure 24d), levee length (Figure 24e) and flow depth (Figure 24g) show an increase for larger input of material. These relations are expected, simply because more material makes larger flows and deposits. Larger flows experience relatively less friction and have therefore larger velocities and flow depths as well. Experiments with 9750 g material deviate notably from the trend line in Figure 24e and Figure 24f. It is unclear why these experiments deviate. These experiments were done in the first non-electronic flume by other students under slightly different circumstances, which might explain the deviation from the other results. Another explanation might be that there was something different about the sediment mixture, since multiple experiments show deviating results.

Larger amounts have no effect on the snout. Snout thickness (Figure 24c) shows no trend and snout width is constant for different amounts (Figure 24d). For deposit width another trend is observed. For low amounts the maximum width is similar to the snout width, but for larger amounts the difference becomes larger.

Levee height relative to the outflow plain does not show a trend on first sight (Figure 24f). But if we eliminate the results from 9750 g that were just discussed we can conclude that the levee height is relatively constant, although the scatter is still large. The levee height relative to the middle of the deposit increases slightly. This is probably caused by a lack of deposition and infill at the beginning of the deposit with long deposits that entered the plain under high velocities. The high velocities might have prevented any deposition at the beginning of the outflow plain.

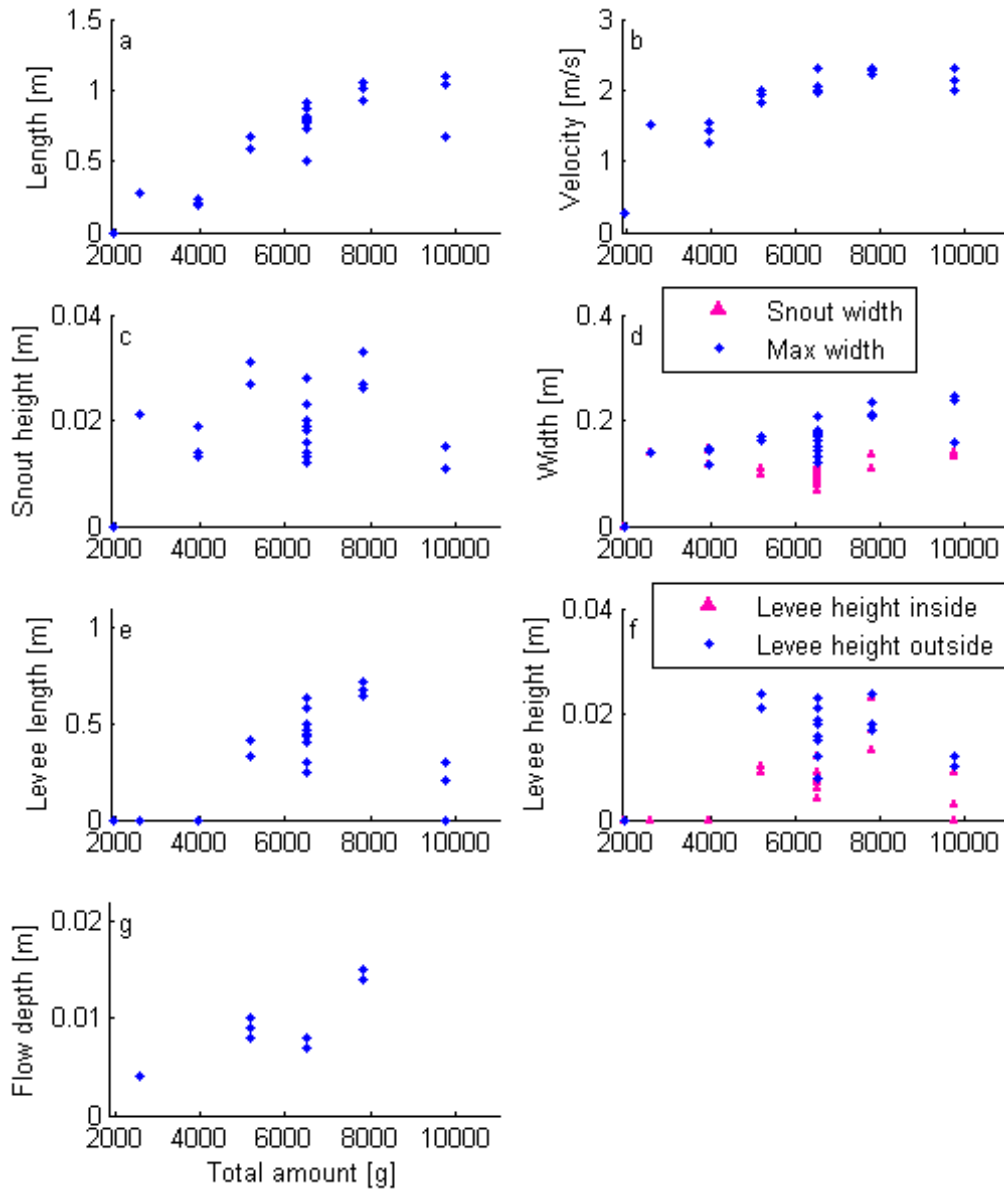


Figure 24: Different variables as a function of total amount. a) runout length, b) velocity in the channel, c) snout deposit height, d) maximum and snout deposit width, e) Levee length, f) Levee height in reference to the inside and outside of the deposit, g) flow depth at the apex.

EFFECT OF TERRAIN PARAMETERS ON DEBRIS FLOW MORPHOLGY

EFFECT OF OUTFLOW PLAIN SLOPE

The effects of varying outflow plain slope are illustrated in *Figure 25*. Since outflow plain has no effect on what happens in the channel, flow depth and velocity are not included.

Runout length is slightly effected by changes in the outflow plain slope (*Figure 25a*). Higher slopes slightly increase the runout length, because higher gradients increase the gravitational force in the direction of motion.

The measurements for snout height (*Figure 25b*) and levee length (*Figure 25d*) for different plain slopes are very scattered and do not seem influenced by the slope. The snout height measurements are scattered around an average of about 0.02 m.

Snout width and maximum width also do not seem to be influenced by outflow plain slope (*Figure 25c*). But in contrast to snout height measurements, the width measurements are very constant. The maximum width is about 0.2 m and the snout width about 0.1 m.

Levee height relative to the outflow plain decreases slightly with increasing slope, probably because mass from the levees is used to develop longer deposits. Height relative to the middle of the deposit increases slightly, this might be because there is less vertical infill if the infill area is larger. In this case, the relative increase in levee height is not caused by higher velocities creating more downward transport over the second hatch, because channel velocities are constant.

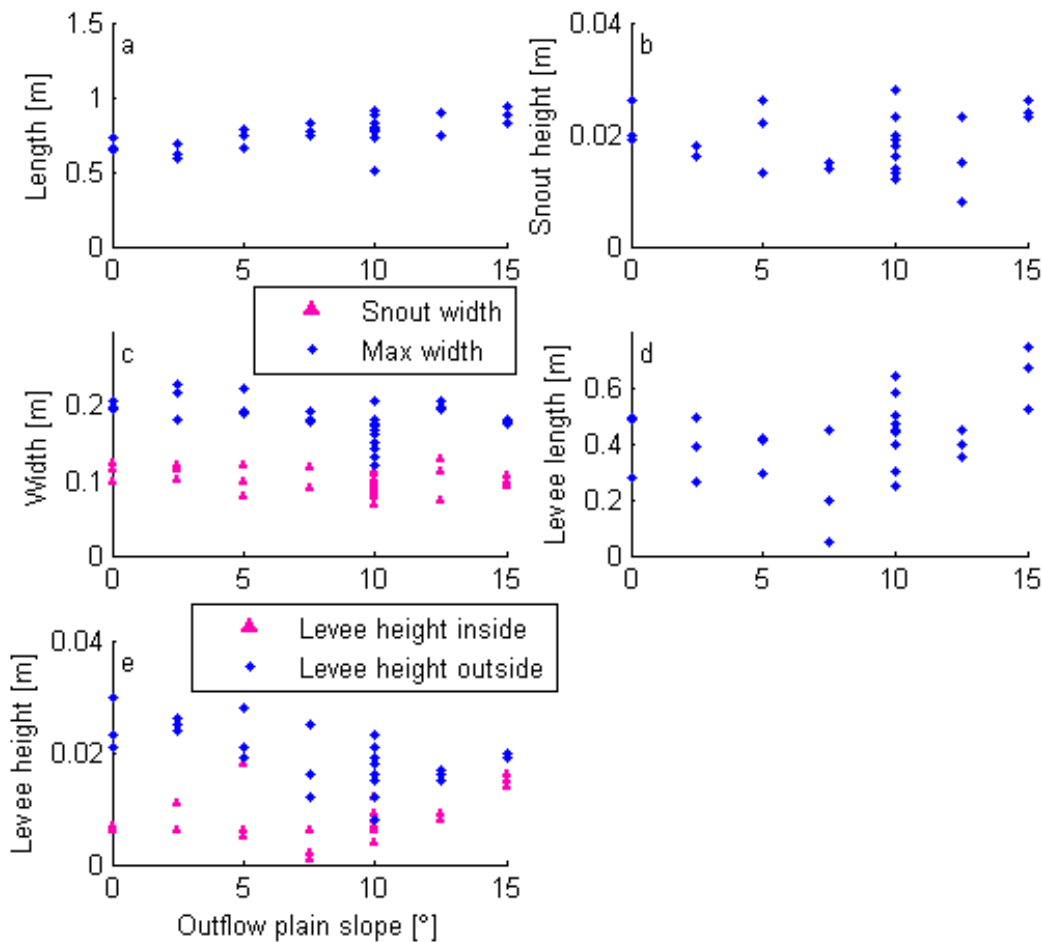


Figure 25: Different variables as a function of outflow plain slope. a) runout length, b) snout deposit height, c) maximum and snout deposit width, d) Levee length, e) Levee height in reference to the inside and outside of the deposit.

EFFECT OF CHANNEL SLOPE

Figure 26 shows the results for variations in channel slope. For the lowest channel slope the mixture did not come out of the channel.

Higher channel slopes lead to higher runout lengths (*Figure 26a*). The relation is linear but not very strong. Higher slopes also lead to slightly higher velocities (*Figure 26b*). These velocities contribute to longer runout lengths. Larger gradients increase the downward velocity and therefore downward transport by larger gravitational attraction in the direction of movement.

Snout height is randomly scattered around an average of a little over 0.02 m (*Figure 26c*). This suggests that channel slope does not influence the snout height. This is also the case for snout

width which seems relatively constant and randomly scattered as well (Figure 26d). The maximum width increases with velocity and runout length (Figure 26d).

The precision of the trend in levee length is poor, but can be described as an increasing trend with larger channel slopes (Figure 26E). As seen before this is directly related to the increase in debris-flow length.

Levee height in relation to the outflow plain is relatively constant (Figure 26f) and probably not influenced by channel slope. But levee height relative to the middle of the deposit increases with higher slopes. Again this might be caused by higher velocities when reaching the outflow plain which prevents deposition at the beginning.

Flow depth slightly increases (Figure 26G). This suggest that higher velocities create larger flow depths.

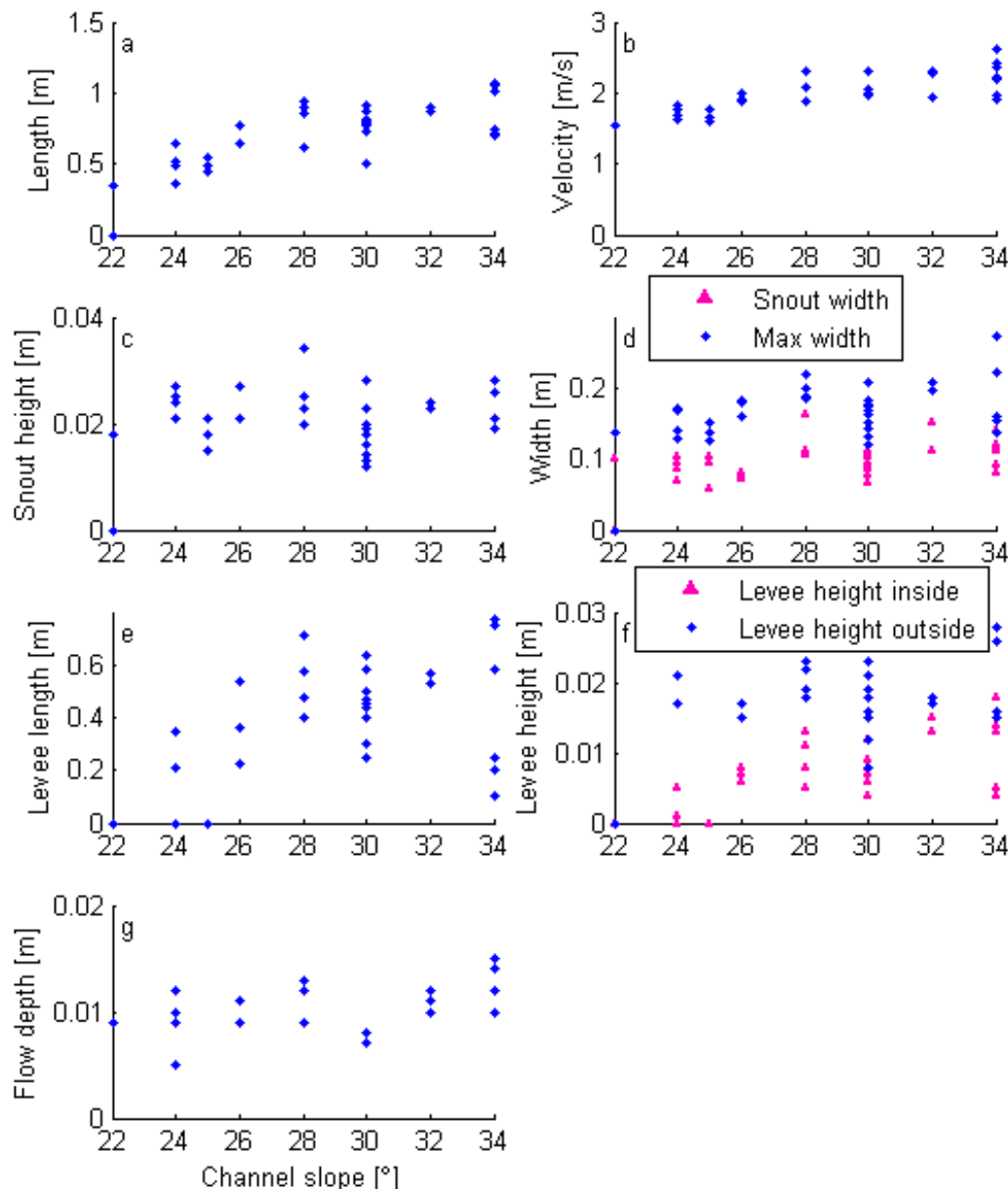


Figure 26: Different variables as a function of channel slope. a) runout length, b) velocity in the channel, c) snout deposit height, d) maximum and snout deposit width, e) levee length, f) levee height in reference to the inside and outside of the deposit, g) flow depth at the apex.

EFFECT OF CHANNEL WIDTH

Figure 27 shows the results for the different channel widths that were tested.

The length shows a decrease with decreasing channel width (Figure 27a). This is most likely related to friction which effects the velocity (Figure 27b). Even though the mixtures and slopes are the same the velocity decreases for smaller channels.

As expected the debris-flow width is also influenced by the channel width but not very much (Figure 27d). The maximum width slightly decreases and snout width slightly increases with decreasing channel width. The trend in maximum width can be explained by a smaller apex, which better confines the flow entering the plain. Maximum width is generally observed close to the apex. The snout width gets smaller when the apex and maximum width are wider and the deposit longer. This is probably because of the mass distribution through the deposit.

Snout height does not seem to be influenced by channel width (Figure 27c).

Levee length increases with runout length, as for all previous variables (Figure 27e). The levee height measured on the outside does not show a trend, but the height on the inside increases for larger channel widths. Wider channels generate deposits with a large surface area, therefore the infill will be spread over a larger area and becomes therefore less high with expanding width, increasing the levee height.

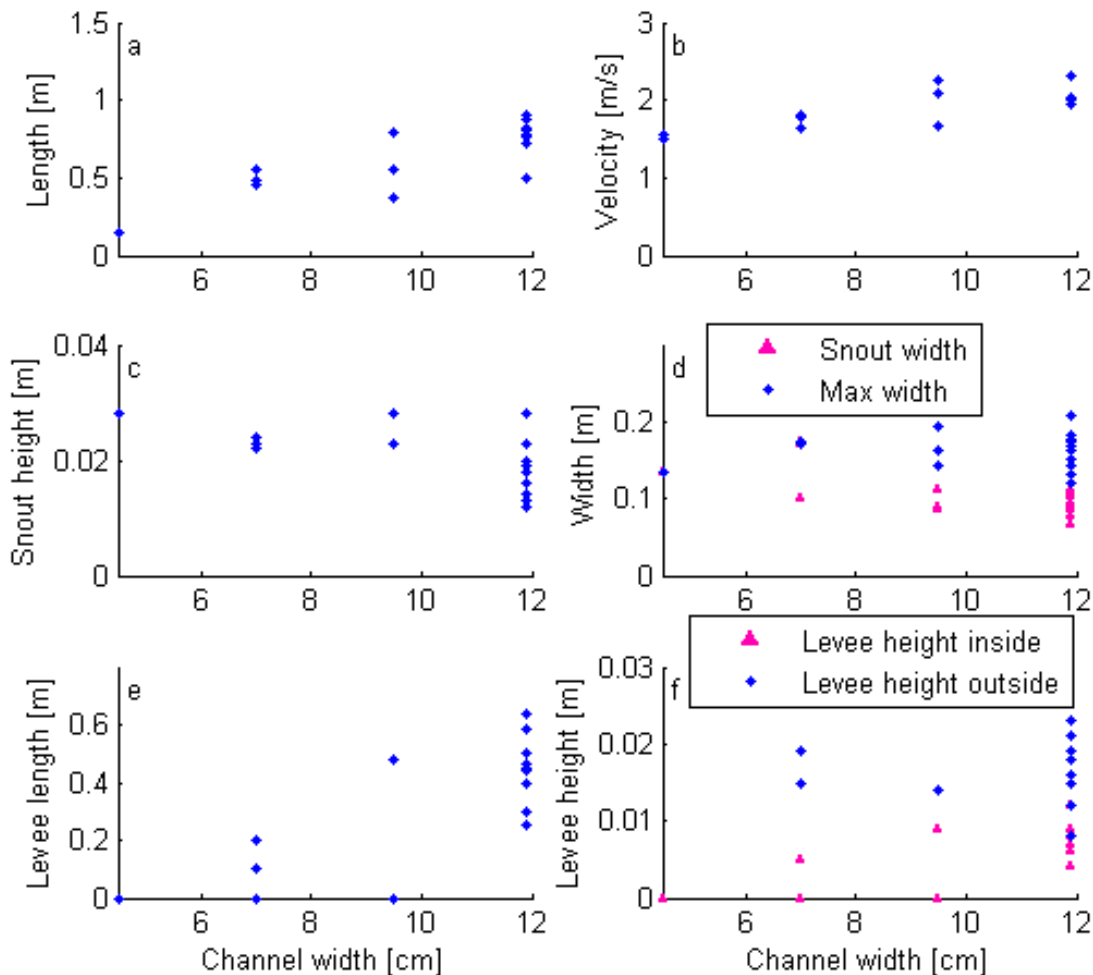


Figure 27: Different variables as a function of channel width. A) runout length, B) velocity in the channel, C) snout deposit height, D) maximum and snout deposit width, E) levee length, F) levee height in reference to the inside and outside of the deposit.

EFFECT OF CHANNEL LENGTH

Another variable that was tested is channel length. Five experiments with the reference mixture were done in this longer channel. Because a slope of 28° was used for these experiments, they could not be compared to the reference experiments. The results were plotted in the figure of channel slope versus runout length and velocity (Figure 28).

The results show that the experiments were very similar to the experiments performed in the shorter channel with a slope of 28° . On average they seem slightly shorter but still fit in the general trend (Figure 28a). This deviation might have been caused by the length of the channel, but might also be due to internal variation. If the channel would have any effect it is expected that more grain segregation takes place because the flow is longer in motion. This did not appear to be so from observations. Furthermore there would be a chance that velocities are larger at the end of the channel, because there is more time to gain speed. This was also not the case (Figure 28b). Therefore it is not likely that the longer channel had any significant effect on the deposit.

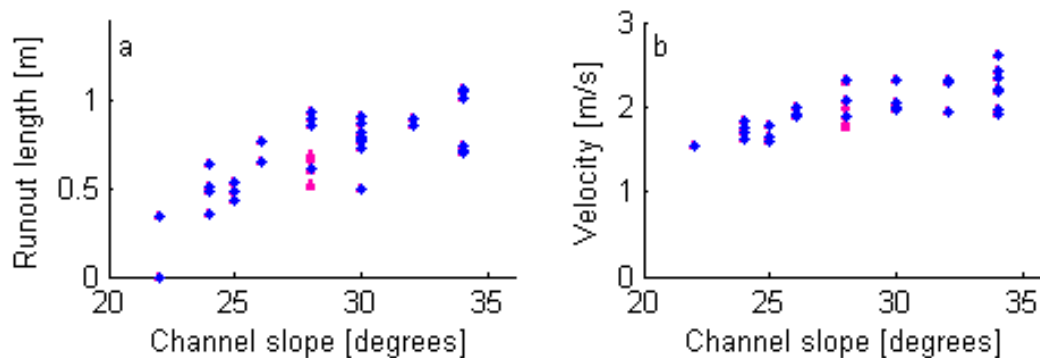


Figure 28: A) Runout length and B) velocity as a function of channel slope. Long channel experiment shown in red.

EFFECT ON FLOW CHARACTERISTICS: VELOCITY AND FLOW DEPTH

Observed surface velocity distributions were similar to surface velocities studied by Johnson et al. (2012) by the use of particle tracking in the USGS flume. In the review it was mentioned that surface velocities are faster in the middle causing deposition of levees at the sides. Additionally the middle of the debris flow shoulders the coarse material from the snout towards the side supplying levees with coarse material. These processes were observed together with important processes like grain segregation and prove that from this point of view these experiments represent natural debris flow very well (Figure 29).

Velocity was affected by all variables that were tested. This is in agreement with Takahashi (1981) who mentioned that debris-flow velocities show a wide variation because not only debris characteristics like grain size and concentration matter, but also the passage characteristics like width and slope. Campbell (1975) discussed that flow velocity was determined by fluidity of the flow, channel slope



Figure 29: Time lapse, top view photographs.

and channel length. Fluidity and slope were found to be very important in this research, but channel length was found to be unimportant. Different channel lengths yielded similar results for velocity. It is likely that shorter channels than the two tested channels might lead to different results, because equilibrium velocity is not reached.

In general, larger velocities were generated when gradient increased, flow depth increased or friction decreased either by decreasing viscosity, skin friction or internal friction. All variation in the different variables can roughly be explained by these three terms. The gradient could be increased by increasing the channel slope. A larger amount of material increased the flow depth, but also experienced relatively less skin friction. Increased channel width also creates less skin friction. Increased water content mostly decreased the viscosity of the flow. Increased coarse material content also decreased the viscosity, but too much coarse material created snout friction and internal friction by grain collisions in the flow. The clay content experiments showed these effects as well, but in opposite order: increased clay content first decreased internal collisional friction and when more clay was added it increased viscosity.

The results showed that flow depth is most clearly influenced by amount of material and clay content and less by channel slope. It was already discussed that a larger amount of material increases the flow depth, but the effect of clay on flow depth is less clear. Because flow depth and flow velocity could not be studied separately, it is not clear if clay content directly influences the flow depth or indirectly by velocity.

Water and coarse material content probably also have an effect on flow depth, but this data was not collected. According to Davies (1990) adding coarse grains increases flow depth until a certain point when it becomes constant (Figure 30). This study used a moving belt on which the experiments took place and could therefore study velocity and flow depth separately. Flow depth did not only influence velocity, but larger velocities also increased flow depth (Figure 30).

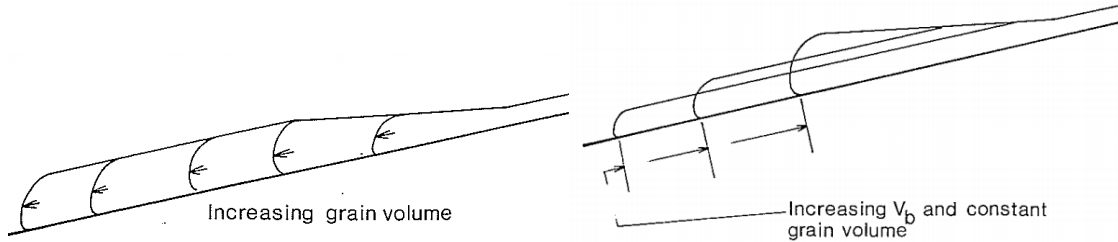


Figure 30: Simplified flow geometry A) with increasing grain volume and constant bed speed, B) with increasing bed speed for constant sediment mixture (Davies, 1990).

shows also a clear linear relation between velocity and flow depth. Larger velocities are related to higher flow depths. In more detail this figure indicates different trends for channel slope and amount of material. The linear trend for channel slope is significantly steeper than for amount of material. These differences can be explained by the relations that were discussed. Channel slope only has an indirect effect on flow depth, but increases velocity significantly. Amount of material has a direct effect on flow depth, because larger volumes have per definition larger depths and indirectly larger flow depths are generated because velocity increases due to relatively less skin friction. Flow depth and velocity are not the only factors influencing each other, different flow depths can exist for the same velocity.

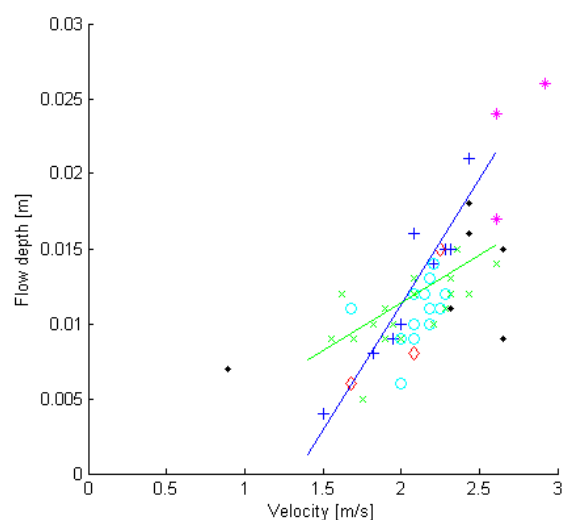


Figure 31: Flow depth plotted against velocity for all data sorted by tested variable. Trends lines are plotted for channel slope and amount of material series

EFFECT ON SNOT HEIGHT

The results showed that debris-flow snout height was not influenced by amount, slopes or channel width, only by clay, water and coarse material content. This means that debris-flow composition is the only factor influencing the snout height and not topography or volume. Johnson (1970) already noted that snout height and flow depth are dependent on debris strength, especially small changes in water content have large effects. This is also observed in the results presented here. Water content and coarse material effect the snout height the most.

Debris-flow composition exerts its effect on snout height by its effect on flow characteristics. It is not likely that velocity is important, since slope, volume and channel width do not influence snout height even though they do influence velocity. It is expected that flow depth has a larger influence on snout height than velocity, but this hypothesis cannot be tested since flow depth data is not available for the coarse material experiments and for a large part of the water and clay content experiments.

The yield strength looks to affect snout height in *Figure 18* but in *Figure 21* this is not observable.

Simply the accumulation of coarse material at the front is the most important factor influencing snout height. This explains why the trend with clay content is less clear than with coarse material. The trend in clay content can be explained by the influence of clay on kinetic sieving. A larger clay content decreases sediment sorting by increasing the viscosity, which decrease the formation of a large coarse snout. For very large clay contents the snout thickness increases again, because the flow length is significantly shorter en one unsorted pancake is formed, because it is not spread out, it is relatively thick. This is also the reason for high values for low coarse material contents.

EFFECT ON DEPOSIT WIDTH

The results showed that deposit width is dependent on all variables except outflow plain slope. When discussing snout width and maximum width separately it becomes clear that snout width is determined relatively similar to snout height. Parameters that are important are water and coarse material content. It is not likely that velocity influences snout width because a lot of boundary conditions influence velocity but turned out not to influence snout width.

In *Figure 32* snout height and width are plotted. A lot of data point have similar widths and heights because they are visible in a large cluster. For some data points of the series of water and coarse material content, a trend is visible. Debris-flow deposits with larger snout widths also have larger snout heights.

The maximum width shows a relation with water, clay, amount, channel slope and channel width. This is significantly different from the variables related to snout width. Even though coarse material is the most important factor influencing snout width, it is not relevant to the maximum width. The location where maximum width occurs is generally the impact place where the flow from the channel hits the plain. Because of the angle difference between the plain and the channel the impact force is large and creates a wide splash before flowing down the outflow plain. This impact force is larger for higher velocities (*Figure 33*) except for the coarse material content runs. This has to do with levee formation by coarse grains. The levees confine the flow and prevent lateral spreading. Levees are also formed in flows with less coarse material, but these are suspected to be less strong and they form less rapidly.

In real debris flows the transition from channel to outflow plain will be more gradual. A maximum width as produced in the experiments is therefore not likely to occur. The compare relative width to natural debris flows, the snout width is a better measure.

Since snout width is influenced by different parameters than maximum width, they are basically unrelated, only slightly by water content. Larger water content both increases snout width and maximum width.

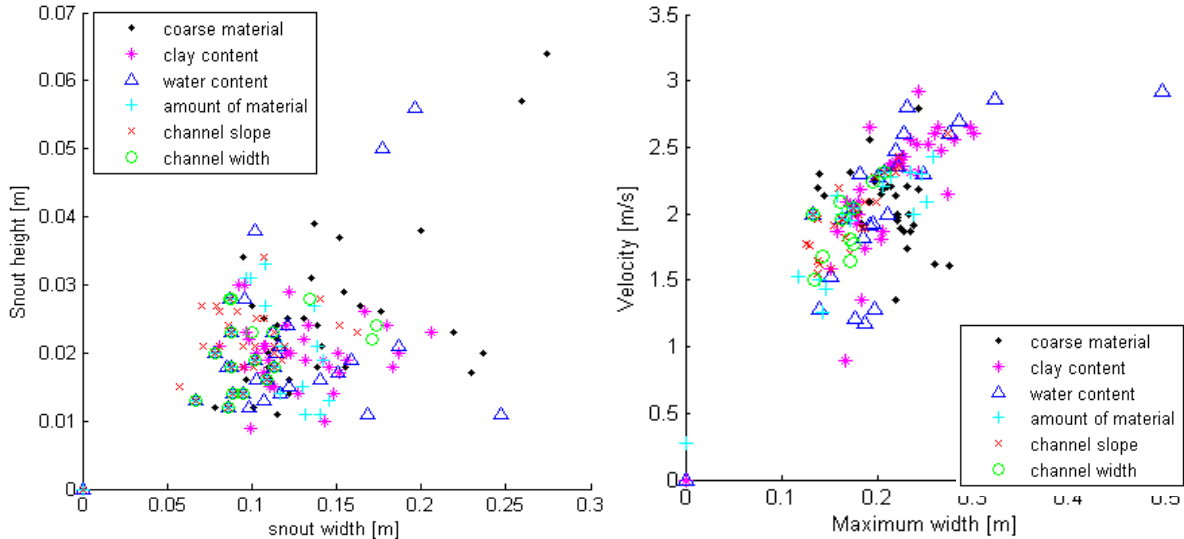


Figure 32: Snout height plotted against snout width.
 Figure 33: Velocity as a function of maximum width.

EFFECT ON LEVEE HEIGHT

Levee height relative to the outflow plain is not determined by amount of material and shows large scatter for channel slope and channel width. For larger water, coarse material and clay contents and for larger outflow plain slope levees become less pronounced. Levees do not need to be high for high water and clay contents because this also increases width, which decreases the thickness of the flow on the outflow plain. Higher runoff velocities might also play a role in the development of smaller levee heights. Higher velocities transport more material downslope leaving less time and material to develop levees. The only problem with this theory is that higher velocities by increased channel slope do not influence levee height (Figure 34).

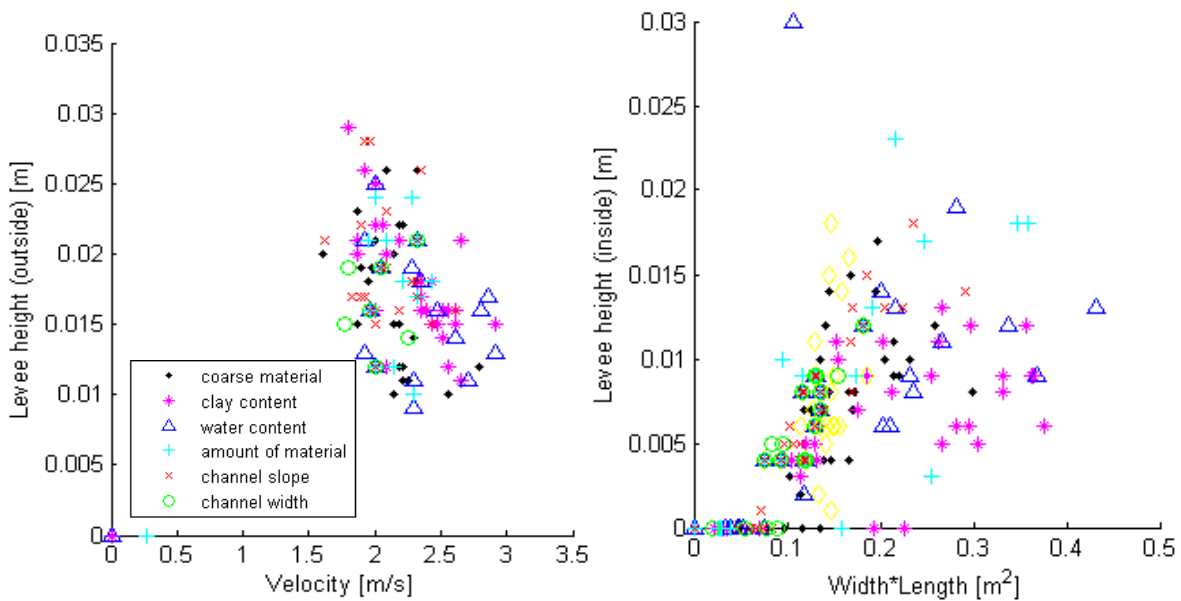


Figure 34: Levee height measured on the outside of the deposit as a function of velocity.

Figure 35: Levee height measured relative to inside of the deposit as a function of infill area. Infill area is calculated by deposit width times length.

The height of the levees compared to the height of the deposit is mostly a measure of the amount of infill after deposition. Because the amount of material that passes the second hatch is slightly influenced by the velocity, this influences the levee height. Also wider and longer deposits have more room for infilling. The same volume of material results in a smaller deposit thickness if the area is larger, hence also larger relative levee height (Figure 35).

EFFECT ON LEVEE LENGTH

Levees are thought to be very important in determining the length of debris flows. The development of levees confines the flow focusing the flow forward and preventing the material being deposited as a pancake. Levee length displays the same trend as runout length in the results. The length of the levees is always ~ 0.3 m shorter than the total deposit length. In all experiments showing levee length against outflow length (Figure 36) it is a linear relation and almost parallel to the $x=y$ line (runout length = levee length). An exception from the line a large amount of data points plot on the horizontal axis, representing the absence of levees. The absence of levees can be caused by high viscosity deposits with a lot of clay or a limited amount of water. Another type of circular deposits is formed by more granular-like flows with a high coarse material content. These deposits are on the threshold of being a debris flow. Incidentally deposits were filled up so much that levees were invisible.

The results for levee length show that without levee formation deposits cannot become longer than about 0.5 m. Lateral constriction by levee formation is therefore an essential process in the development of elongated deposits. This is in agreement with statements and observations from other authors (Iverson, 2003; Zanuttigh and Lamberti, 2007).

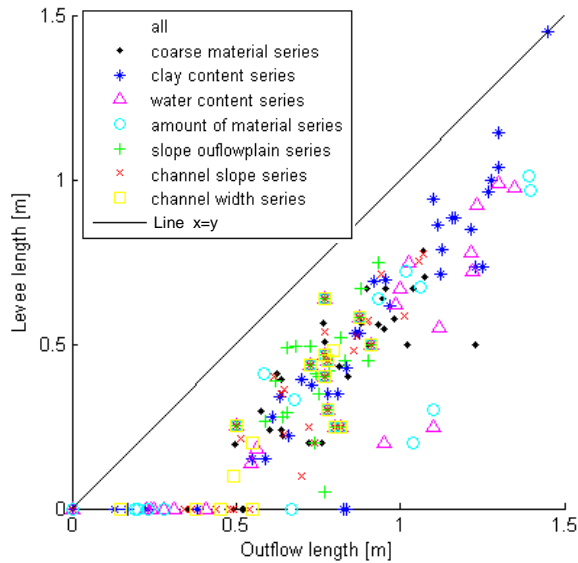


Figure 36: levee length of all experiments as a function of outflow length.

EFFECT ON RUNOUT LENGTH

The single debris-flow experiments showed that the runout length of a debris flow depends on all of the tested variables; coarse material, clay content, water content, feeder channel slope, runout plain slope, channel width and amount of material.

From the results it became clear that levee formation is a very important process in developing long debris flows. Additionally flow velocity always shows the same trend as runout length. Higher velocities indicate that there is more energy available to transport the material downslope. It was observed that many of the other dimensions like width and height decreased when the runout length increased. When more material is transported downslope less material and time is available to develop thick and wide deposits. Because the same amount of material was used each run, some dimensions decreased for longer deposits because of the mass balance. Runout length is probably the most important debris-flow dimension for risk assessment or prediction methods. Therefore, many authors have discussed prediction equations to determine runout length. Many of these equations were classified and analyzed by Rickenmann et al. (2005) and D'Agostino et al. (2010). Many use a volume balance approach in the form of $A = kV^d$ (Dagostino et al., 2010). For which A is the flooding area, V is the total volume and k and d are determined empirically. This semi-empirical relation is used by different authors with different constants (Iverson et al., 1998; Crosta et al., 2003). This volume based approach takes very few conditions directly into account. Roughly said larger debris flows have longer runout lengths (Takahashi, 1991). Not only debris-flow composition is included empirically, but also topography constraints and slopes. These volume-based equations can be used in the same study area where weathering products and topography are relatively constant over time. For a more universal method different equations are needed.

A theoretical non-empirical equation was developed by Hungr et al. (1984) and Takahashi (1991) based on momentum balance (equation 8). This equation was concluded to be the best runout length predictor by Rickenmann (2005).

$$R = \frac{\{u \cos(\theta_u - \theta_d)[1 + gh \cos \theta_u / 2u^2]\}^2}{g(S_f \cos \theta_d - \sin \theta_d)} \quad eq. 8$$

$R = runout\ length [m]$

$\theta_d = plain\ slope [^\circ]$

$\theta_u = channel\ slope [^\circ]$

$u = velocity\ entering\ plain [m/s]$

$h = \text{flow depth entering plain [m]}$
 $S_f = \text{friction slope [}^\circ\text{]}$

The equation assumes constant discharge and no change in width. The friction slope is assumed to be constant and accounts only for sliding friction.

This equation includes most of the boundary conditions measured that have influence on runout length, only channel width is not included. Mixture variables express their influence by velocity, friction and flow depth.

When R was calculated for the reference experiments, it was estimated between ~ 0.0008 and 30 m. This large range is caused by estimations on S_f . Many authors use this as a calibration parameter. Rickenmann (2005) correctly assumes that S_f reflects material characteristics.

This is also the largest problem with this equation. S_f includes more than only sliding friction when S_f is calibrated against results. It then accounts for everything that is not accounted for in the equations like width changes, pore pressure changes and other forms of friction.

A good equation containing all parameters that affect runout length was not found. Better runout length estimations are mostly done by the use of numerical models.



Figure 37: Photograph fan 1, 22 debris flows with 2x coarse material content (23.47wt%).

FAN EXPERIMENTS

The results of the fan experiments are presented in this section. Three fans are discussed in detail, because they were made by the present author, but more experimental fans were made with this experimental setup. Data and knowledge from these fans were also available and will be used in the discussion for further analysis.

The first fan that was made was built up by 22 debris flows with equal sediment-water mixtures (23.47 wt% coarse material, *Appendix II*) (*Figure 37*). In

Figure 38 the different flows are indicated with different colors. The second fan was built up by 6 debris flows that all had the same amount, reference boundary conditions and reference water content, but not the same sediment composition. The compositions of the flows are listed in *Appendix II*. The third fan was built up of 19 debris flows, with a similar composition and setup as the reference experiments.

The top-view photographs and movies show a flow by flow buildup of the fans (*Figure 39, Figure 40* and *Figure 41*). It is clearly visible that a deposit on average has a smaller runout length than the preceding deposit on fan 1 and 3. Because of the decrease in runout length the fan did not grow larger than the length of the first debris flow. In contrast, the deposits of fan 2 did not get significantly shorter, which was a surprising result, but it was also surprising that all flows deposited right on top of each other. Their preferential path is on top of the previous smooth deposit instead of on the larger gradient leading to the rough terrain of the outflow plain. Preferential deposition on top of each other was not caused by levee formation because levee formation occurred also on fan 1 and 3. When it became clear that the runout lengths of fan 2 would not decrease for at least another few experiments, other mixtures that would result in shorter flows were tried. Surprisingly, this did not go as expected, because these flows also gained longer runout lengths compared to the single debris-flow experiments. This had probably to do with smoothing of the bed by the clay rich deposits. Only a high viscosity mixture of 15x the amount of clay produced shorter deposits. Due to the low usability (not representative of an average debris-flow fan) of these extreme clay content mixtures it was decided not to continue this fan.

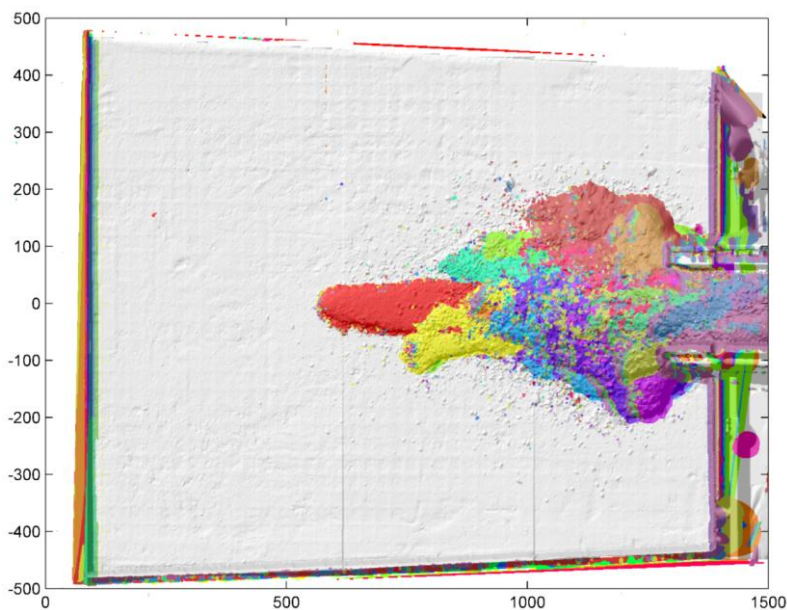


Figure 38: Different debris flows indicated with a different color on a hill shade map. Every color is the difference between two successive DEMs.



Figure 39: Top-view photographs of different steps in the formation of fan 1 after debris flows 2, 9, 16 and 22. Movie showing all top-view photographs (http://youtu.be/_bWJwCAXD0).



Figure 40: Top-view photographs of different steps in the formation of fan 1 after debris flows 2, 3, 4 and 6. Movie showing all top-view photographs (<http://youtu.be/C5SjM3lnZ0g>).



Figure 41: Top-view photographs of different steps in the formation of fan 1 after debris flows 2, 12 and 19. Movie showing all top-view photographs (http://youtu.be/B_oqo4FnRHw).

In regard to fan 1 and 3 it was also noticeable that flows did not always flow in the direction of the largest gradient. Large slope angles, almost vertical, developed just after the fan apex. The steep slopes did not collapse when they dried, because the deposits were strongly consolidated. The width of the deposits is larger for stacked debris flows compared to single debris flows. There is no clear trend, but it is clear that all stacked deposits are wider than average single debris flows. The sides of the flow often flow off the steep edges of the previous deposit making them wider.

Sorting patterns are visible on the surface of fan 1 and 3. Compared to fan 1 surface sorting patterns were less clear on fan 3. Similar to the single debris flows, coarse fronts and levees were less pronounced with the reference mixture than with the coarser mixture. Coarse snouts, coarse levees and watery tails are visible on fan 1 while only some weakly pronounced levees and fine infilling were visible on fan 1.

Although sorting was less clear on fan 3, the lobes were clearer. Individual lobes could no longer be recognized at the surface, because of the steep edges. This was less pronounced on fan 1 because levees and snouts were affected by drying. When the deposits dried, some loose gravel would roll down the fan, which could be seen on the bed around the fan (Figure 37) and as small spots on the colored hill shade (Figure 38).

Even though some sorting was visible at the surface of the fans, this was not visible in the fan stratigraphy (Figure 43 and

Figure 44). Cross-sections were made every 10 cm of fan 1 and 3 to study the vertical sorting patterns. The cross sections of both fans did not show any sorting patterns. The only difference was that there was clearly less coarse material on the inside of fan 3 compared to fan 1.

The long profile of the first fan shows the variation in slope of the fans (*Figure 42*). The final slopes of fan 1 and fan 3 show a similar trend. The bottom of the fans shows a slope parallel to the outflow plain ($\sim 10^\circ$), because it was determined by only one debris flow. Then the slope increased to $\sim 30^\circ$, parallel to the channel slope. Steepest part of fan 1 is between 1200 and 1500 mm. In this location the slope ($\sim 35^\circ$) was steeper than the channel slope and decreases again after 1500 mm. The steepest part of fan 3 is higher ($\sim 45^\circ$) at approximately the same location (between 1200 and 1400 mm). The average slope of fan 1 was $\sim 24^\circ$ and $\sim 28^\circ$ if the slope of the first debris flow is not taken into account. The average slope of fan 3 was $\sim 26^\circ$ and $\sim 28^\circ$ if the slope of the first debris flow was not taken into account. This is approximately the same as in fan 1. This indicates that coarse material content has no significant effect on fan slope.

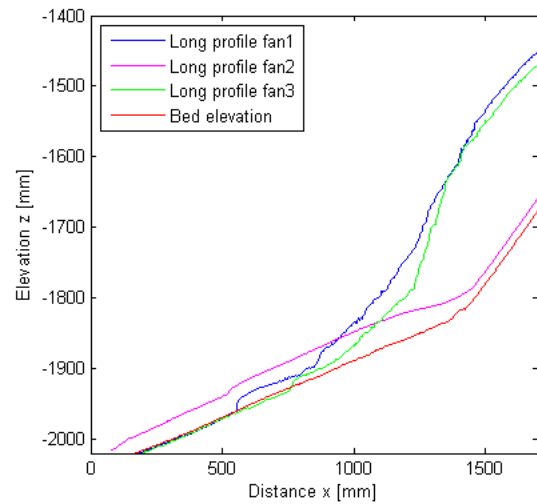


Figure 42: Long profile elevation of fans 1, 2 and 3. Red line indicates the bed elevation.

From the cross sections is visible that the fan 1 (*Figure 45*) has grown as wide as 400 mm. Line 4 shows the largest width. This is within the area with the largest slope. This cross-section is the first cross-section outside the channel. The width therefore changed largely between line 3 and 4, which could be the reason that the slope is higher at this location. The flow was confined before the end of the channel and after the end of the channel it could spread rapidly resulting in a smaller deposit depth. The cross-sections on fan 3 show a width of ~ 350 mm, which is slightly narrower than fan 1 (*Figure 46*). The height difference between line 3 and 4 is also larger than for fan 1. This is related to the maximum slope at this location which is also larger for fan 3.



Figure 43: Cross-sections of fan 1 at 8, 24 and 44 cm from the apex.

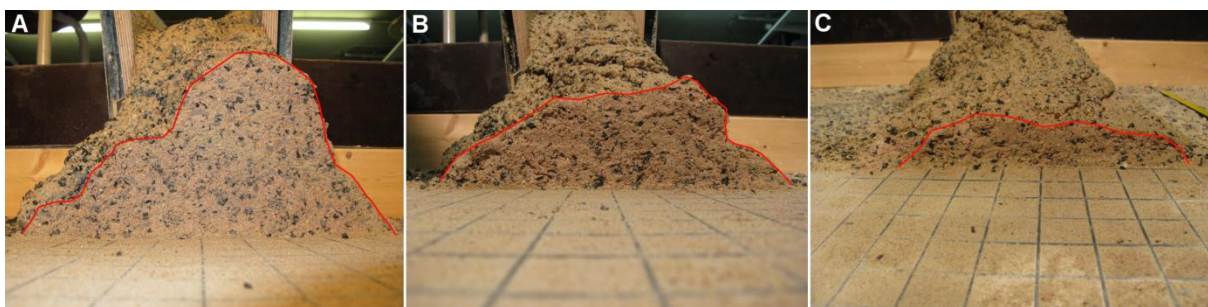


Figure 44: Cross sections of fan 3 at 10, 20 and 40 cm from the apex.

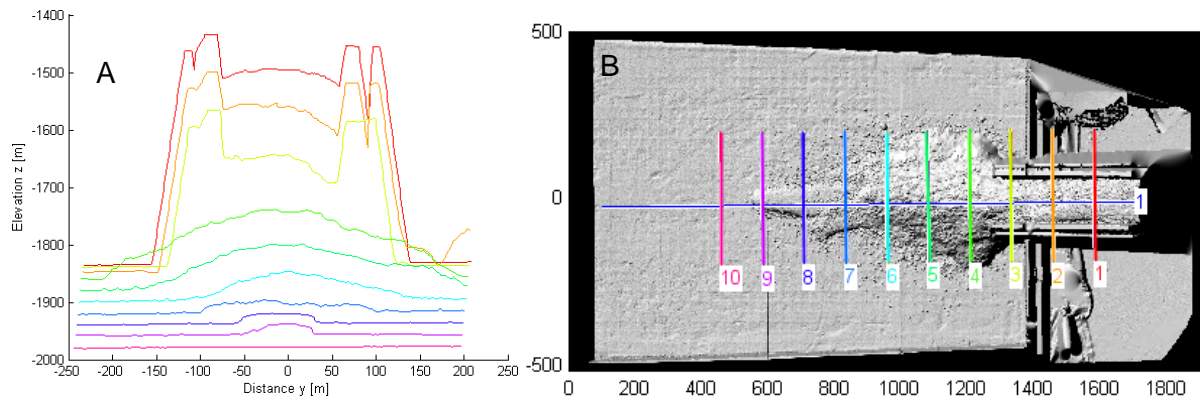


Figure 45: Cross-sections fan 1. A) Elevation, B) location of cross-sections and long profile.

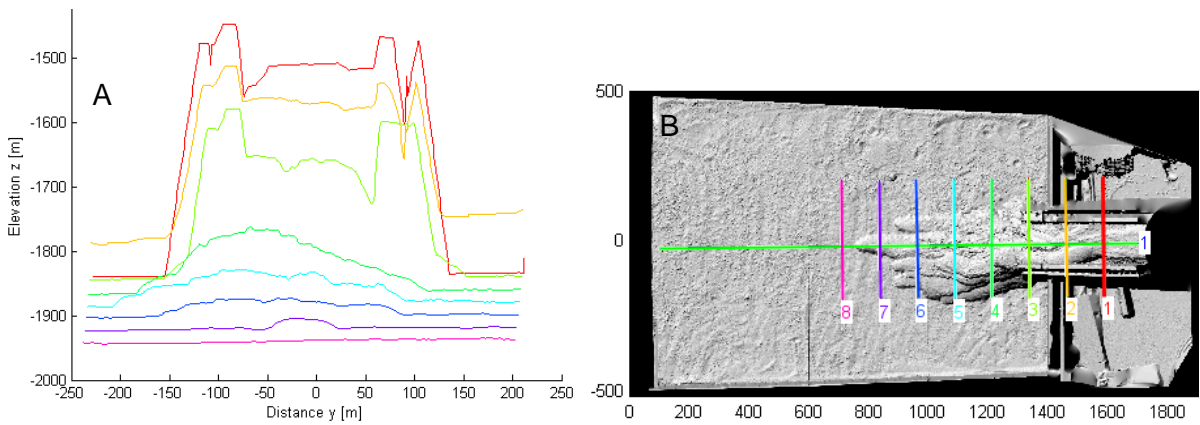


Figure 46: Cross-sections fan 3. A) elevation, B) location of cross-sections and long profile.

DISCUSSION

In this chapter the implications of the results are discussed, followed by a discussion about dimensionless parameters and scaling issues. Finally, the experiments are compared with other experimental studies and Martian debris flows.

IMPLICATIONS FOR DEBRIS FLOW RISK ASSESSMENT

The results of the previous chapter have shown which boundary and initial conditions are effecting debris-flow dimensions and processes and to what degree. This information can be used for debris flow risk assessment.

Runout length is an essential parameter of debris-flow deposits in relations to hazard assessment. The length of natural debris flows can be very unpredictable. Experiments showed that runout length is influenced by both topography and composition, runout length is therefore the most difficult parameter to predict.

The experimental results have shown that a debris flow composition of 20-30 wt% coarse material and 5-15 wt% clay develop the longest debris flows. Mountain regions with weathered material close to these compositions should therefore be extra alert for long runout lengths and also focus on protecting areas that are not directly situated near the source area. These abundances might be slightly different for natural debris flows, but attention should in general be paid to source areas with large varieties in grain sizes in combination with relative large abundances of clay and a significant fraction of coarse grained material including gravel, pebbles, cobbles and boulders.

The experiments have also showed that larger water content increases the runout length. The water content is very difficult to predict, because the water content depends on the water source, but also when the debris flow is triggered. Although the debris flow will be less destructive when the debris flow gains more Newtonian flow characteristics with increasing water content, the flow will also be less confined and will probably affect a larger area downslope. Debris flow behavior occurs from about ~22 wt% water, the upper limit was not found.

Higher channel and plain slopes and larger channel widths all contribute to an increase in runout length, and also flow velocity. Especially steep mountain areas are therefore vulnerable for very destructive debris flows.

COMPARISON OTHER SMALL SCALE EXPERIMENTS

Many small scale debris-flow experiments have been performed by other authors before this research. Fairfield (2011) summarized these experimental debris flow studies in her literature review. Although many experiments have been performed, only few study debris-flow deposits. Most flume experiments are focused on studying rheologic parameters, flow behavior or snout formation. The experiments are performed in rotating flumes (Kaitna and Rickenmann, 2005; Kaitna et al., 2007), on conveyor belt flumes (Hirano and Iwamoto, 1978; 1981; Davies, 1990; Hübl and Steinwendtner, 2000), re-circulating flumes (Armanini et al., 2005; Larcher, 2007) or open flume experiments (Van Steijn et al., 1989; Gregoretto, 2000; Parsons et al., 2001; Ghilardi, 2003; D'Agostino et al., 2010; Fairfield, 2011; Bettella et al., 2012). There are only few open flume experiments similar to this study and the deposit is generally not studied.

Four papers that include an experimental study that include some form of a deposit study are discussed in relation to the experiments of this thesis.

Fairfield (2011) does some analysis on flow width, depth and length. These experiments show some similar conclusions to the experiments of this thesis. High flow velocities relate to long lengths and higher slopes increase flow velocity. Because the experiments did not flow onto a plain but stopped in the channel flume, the dimensions cannot be compared (*Figure 47a+b*). The

width of the flow was constrained by the channel instead of levees. Fairfield also concluded that debris-flow composition has a large influence on flow mobility. She concluded that more gravel or clay generally decreases velocity, length and depth. This was also noted in the experiments of this thesis, but only for large percentages of clay and coarse material. For small clay and coarse percentages length, velocity and depth increases. All these parameters show an optimum for varying clay or coarse material content.

Bettella et al. (2012) also did some open flume experiments to study debris-flow deposits (Figure 47c). It was found that runout length increases with water concentration and decreases with smaller grain diameters. The experiments of this thesis agree with the first conclusion, but only partially with the second. An increase in clay content or a decrease in coarse material content can be viewed as a decrease in average grain size. This research discovered that a clear optimum was present in runout length for both content variables and not solely a decrease. Bettella et al. (2012) also discussed that friction number might be an indication for more elongated deposits, but the results of this thesis show that even though this seems to work for variation over clay content (Figure 50f/Figure 21a), it does not agree with Figure 50e/Figure 18a for coarse material variations. This is a difference that is probably generated by the limited amount of experiments that were performed by Bettella et al. (2012). Sufficient experiments need to be performed over a wide range to view the complete runout length trend.

Liu (1996) also found that steeper slopes increase velocity and runout length. From comparing the deposits visually it becomes clear that deposits from Liu (1996) show much less characteristic debris flow morphologies (Figure 48a). This is also the case for deposits from Van Steijn et al. (1989) (Figure 48b). There is no levee formation, no coarse snout formation and most of the deposits are not very elongated. The runout length is not very long. This might not have implications for the velocity to relative runout length, but is of importance when other dimension like width/height ratios is studied.

From this analysis is discovered that no extensive experimental studies are done in relation to debris flow deposits. Experiments that are performed often lack the morphologic similarity of the deposits to natural deposits, even though typical channel processes, like grain segregation, are often present. Additionally, the number of experiments in the researches are limited and therefore fail to predict the complete trend. This indicates that this research is very important in making the next step in this research field.

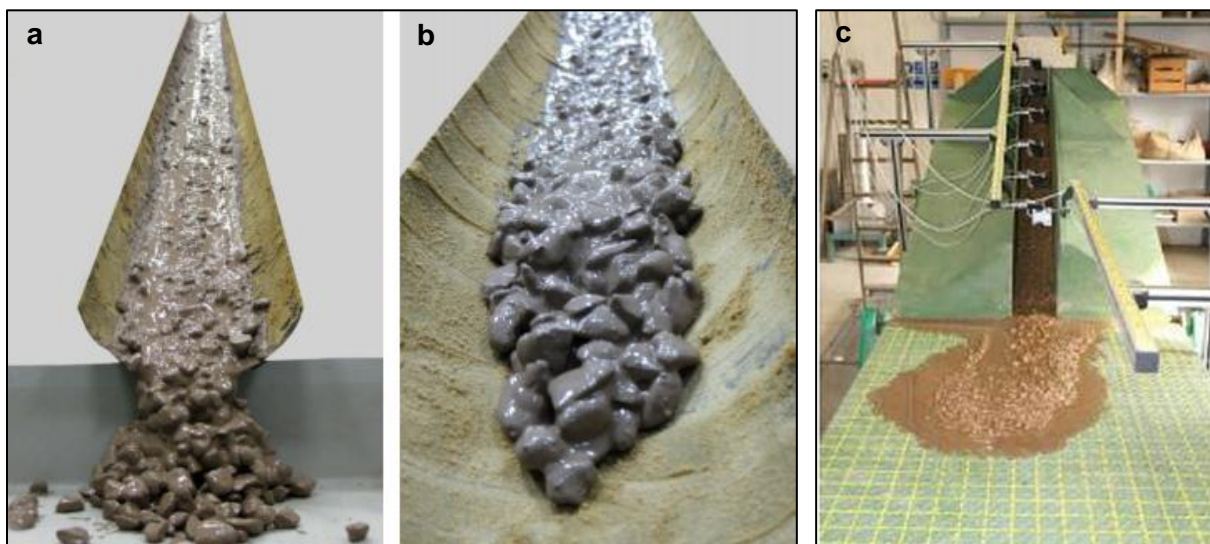


Figure 47: Small-scale debris-flow experiments by different authors, a+b) Fairfield (2011), c) Bettella et al. (2012).

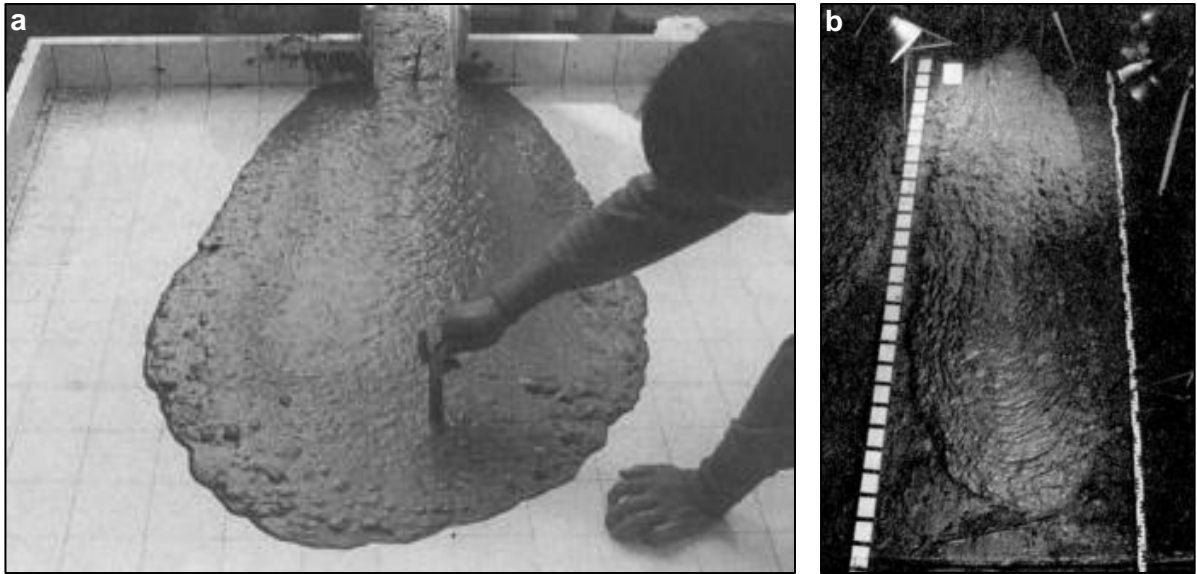


Figure 48: Small-scale debris-flow experiments by different authors, a) Liu (1996), b) van Steijn et al. (1989).



Figure 49: Photographs of natural debris flows. A) Downfan view from apex of Dolomite fan, Owens Valley, of paired levees 150–250 cm tall deposited during a 1984 debris-flow event (Blair and McPherson, 2009). B) Overview of 1984 debris-flow deposits (light) on the Dolomite fan consisting of proximal levees (upper arrow) and distal lobes (lower arrow) (Blair et al., 2009). C) Lobe-shaped deposits produced by the 1993 pyroclastic flows of Lascar volcano (Chile), levees enriched in large pumices (flow moving ahead) (Felix and Thomas, 2004). D) Natural levee along debris flow channel a few years after the event, Cresta Reit, Bormio (Sondrio), Italy (Zanuttigh and Lamberti, 2007).

COMPARISON NATURAL DEBRIS FLOWS

Visual comparison of natural debris flows with the scale experiments show many similarities. The most important processes that occur in natural debris flows are represented in the small scale experiments: grain segregation, excess pore pressure, coarse snout formation, levee formation and a comparable stopping mechanism. These processes lead to morphologies that are comparable to natural debris flows.

Examples of levees of natural debris flows are shown in *Figure 49a, b, c* and *d*. The levees of the experiments look like these levees. They confine the flow and consist of coarser material than the rest of the deposited material. The natural debris show steep edges and end in a lobe (*Figure 49b* and *c*) similar to the small-scale experiments. Different debris flows on the same show similar characteristics. They approximately have the same length, width, similar looking levees and lobes (*Figure 49*). This is logical since the source are of debris flows on fans is the same. Therefore composition of debris flows is very similar and additionally they flow through the same environment with channel width, slope and fan slope. These parameters only change slightly. The largest difference is in water content.

A study of field data showed some indications that the relations found in this thesis will also be relevant for natural debris flows. Data from different field sites mentioned in Zanuttigh and Lamberti (2007) show that runout length is larger for higher velocities and larger volumes. And field data of several debris flows in the Dolomites, eastern Italian Alps, shows that height is larger for larger volumes (D'Agostino et al., 2010). Unfortunately not much variables are available from field data, which makes further analysis of the experimental relations difficult with the data available.

NON-DIMENSIONAL PARAMETERS

Because measurements are obtained from small-scale experiments, comparison of the absolute measured results with natural debris flows is not directly possible. To do this dimensionless numbers are necessary. Six dimensionless numbers are discussed distinguishing five stress generation processes in a steady shear flow of uniform mixture, identical grains and water: (1) inertial grain collisions, (2) grain contact friction, (3) viscous shear, (4) inertial (turbulent) fluid velocity fluctuations, and (5) solid-fluid interactions (Iverson and Denlinger, 1987). To further assess how representative the small scale experiments are for natural debris flows the results are compared to data from natural debris flows and large scale experiments. Different authors have determined values for dimensionless parameters and Iverson (1997) calculated the dimensionless parameters for three natural debris flows and experiments in the USGS flume (*Table 4*).

To calculate these dimensionless parameters some material properties needed to be calculated. Fluid fractions, solid fractions and fine fractions were calculated from the debris-flow composition. These fractions were used to calculate interstitial fluid density (*equation 9*), debris-flow density (*equation 10*) and viscosity (*equation 11*). Sediment density was obtained from weight measurements of the permeameter samples (*Appendix III*). Results from sieving and permeameter measurement were used as values for characteristic diameter δ and permeability k . Additionally, velocity u and flow depth h were used from debris-flow experiment measurements to approximate the shear rate $\gamma (=u/h)$ (Iverson et al., 2010; Zhou and Ng, 2010). The friction angle was estimated at 30° for all compositions.

$$\begin{aligned}\rho_f &= \rho_s v_{\text{fines}} + \rho_w (1 - v_{\text{fines}}) && \text{eq. 9} \\ \rho_f &= \text{density fluid constituents [kg/m}^3\text{]} \\ \rho_s &= \text{sediment density [kg/m}^3\text{]} \\ \rho_w &= \text{water density [kg/m}^3\text{]} \\ v_{\text{fines}} &= \text{fine volume fraction of fluid [-]}\end{aligned}$$

$$\rho = \rho_s v_s + \rho_f v_f \quad \text{eq. 10}$$

$\rho =$ debris flow density [kg/m^3]
 $\rho_s =$ sediment density [kg/m^3]
 $\rho_f =$ density fluid constituents [kg/m^3]
 $v_s =$ solid volume fraction [-]
 $v_f =$ fluid volume fraction [-]

$$\mu = (1 + 2.5v_{\text{fines}} + 10.05v_{\text{fines}}^2 + 0.00273 \exp(16.6v_{\text{fines}}))\mu_w \quad \text{eq. 11}$$

$\mu =$ effective viscosity [$\text{Pa} \cdot \text{s}$]
 $\mu_w =$ viscosity pure water [$\text{Pa} \cdot \text{s}$]
 $v_{\text{fines}} =$ fine volume fraction of fluid [-]

Some values were not available for all mixtures for which dimensionless numbers were calculated. These values were estimated by the trend observed for these variables. In *Appendix V* these values are indicated with orange.

In *Table 3* real, experimental and typical values for different properties are indicated (Iverson, 1997). The values of the calculated and measured properties are indicated in the second column and are within or close to the range of typical values. This indicates that these values can safely be used for further calculations. The largest deviations are found for permeability and viscosity.

Table 3: Ranges and values of different properties. Values are shown for this thesis, the USGS flume and three real debris flows (Oddstad 1982, South Toutle river 1980, Osceola mudflow 5700 B.P.). Additionally typical values are given. (Iverson, 1997)

Parameter	Thesis	USGS	Natural flows	Typical values
δ [m]	0.0005-0.002	0.001	0.001	10^{-5} -10
γ [1/s]	105-295	100	1-10	
ρ_s [kg/m^3]	2300-3000	2700	2700	2500-3000
ρ_f [kg/m^3]	1000-1462	1100	1100-1200	1000-1200
μ [$\text{Pa} \cdot \text{s}$]	0.001-0.004	0.001	0.1-0.01	0.001-0.1
k [m^2]	10^{-15} - 10^{-13}	10^{-11}	10^{-12} - 10^{-11}	10^{-13} - 10^{-9}
v_s	0.4-0.6	0.6	0.6	0.4-0.8
v_f	0.3-0.6	0.4	0.4	0.2-0.6
Φ (°)	30	40	30	25-45

Bagnold (1954) developed a dimensionless number to express the importance of grain collision versus viscosity. The Bagnold number N_{bag} is the ratio between the inertial grain stress and viscous shear (*equation 12*) (as cited in Iverson, 1997).

The Bagnold number increases for larger coarse material content and decreases for larger clay content (*Figure 50a* and *Figure 50b*). Larger Bagnold numbers indicate a higher importance of collisional shear over viscous shear. Observations had already showed high viscosities of clay rich mixtures which is in agreement with these results.

Comparison with large scale debris flow show that the Bagnold number is in the same range as in the USGS flume experiments, but differ from the values of natural debris flows, which are much lower (*Table 4*). Bagnold (1954) determined the transition from macro-viscous flows to grain inertial flows in which collisional shear is dominant at 200 (as cited in Iverson, 1997). The Bagnold number exceeds 200 for all experiments with less than ~ 10 wt% clay (*Figure 50, Appendix V*). This means that the effect of viscosity is relatively smaller and collision forces larger in the experiments, because the shear rate is 10 to 100 times higher due to thin fast flows on steep slopes (Iverson, 1997).

Implications of this are that the debris-flow experiments are effected more by the coarse grained fraction compared to natural debris flows. This can be explained by the relative large grain sizes compared to the size of the flow. So when debris-flow compositions of small-scale experiments

are compared to compositions of large debris-flows, the coarse fraction is probably underestimated in the small experiments because it has a larger effect on the morphology.

$$N_{Bag} = \frac{\rho_s \gamma \delta^2 v_s}{\mu (1-v_s)} \quad \text{eq. 12}$$

N_{Bag} = Bagnold number [–]
 ρ_s = sediment density [kg/m³]
 γ = shear strain rate [s⁻¹]
 δ = characteristic diameter [m]
 μ = effective viscosity [Pa]
 v_s = granular volume fraction [–]

Another dimensionless number that is often used is the Savage (1984) number N_{sav} . This is the ratio of inertial grain stress to shear stress by contact friction (*equation 13*). This equation accounts for the effect of buoyancy due to pore-fluid weight.

The Savage number decreases for large coarse material content and also decreases for a larger clay content (*Figure 50c* and *Figure 50d*). This means that for both trends contact friction becomes relatively more important compared to inertial grain stress. Grain collisions are less likely in easy flowing mixtures with a lot of clay which explains *Figure 50d*, but we have seen from the Bagnold number that collision forces relatively increase for mixtures with a larger coarse material content. To explain the decrease of the Savage number, the contact friction has to increase more. Earlier in this thesis large friction of a coarse grained front was discussed, which could play an important role in decreasing the Savage number. Increase in frictional stresses by coarse snouts was also observed by Bettella et al. (2012).

Savage and Hutter (1989) concluded that the transition from dominantly friction to dominantly collision is at 0.1 for dry granular flows, which is lower than the friction number of all experimental results, which means that grain inertial stress is dominant in all experiments. Similar to the Bagnold number is much higher that for large scale flows (*Table 4*), this difference is caused by 10-100 times higher shear rate and the implications of that are that the coarse grain fraction has a larger effect than in large scale debris-flows.

$$N_{Sav} = \frac{\rho_s \gamma^2 \delta^2}{(\rho_s - \rho_f) g h} \quad \text{eq. 13}$$

N_{Sav} = Savage number [–]
 ρ_s = sediment density [kg/m³]
 ρ_f = density of fluid constituents [kg/m³]
 γ = shear strain rate [s⁻¹]
 δ = characteristic diameter [m]
 g = gravitational acceleration [m/s²]
 h = flow depth [m]

The friction number N_{fric} is the Bagnold number divided by the Savage number ($N_{fric} = N_{Bag} / N_{Sav}$) (Iverson and LaHusen, 1993). This is the ratio of shear stress by grain contact to viscous shear stress. Bagnold, Savage and friction numbers were calculated (*Appendix V*) and plotted (*Figure 50*).

The friction number increases with coarse material content, but decreases with clay content from 5 wt% clay on (*Figure 50e* and *Figure 50f*). The optimum that is visible in the friction number by varying clay content is located at the same weight percentage clay as the optima in *Figure 21*. A higher friction number might therefore be an indication for longer, clay rich debris flows. It is expected that viscous shear gradually increases for higher clay contents. So, to gain an optimum in the friction number the contact friction has to increase more until 5 wt% clay. This suggests that clay increases friction between the material and the channel.

Because Bagnold and Savage numbers are large compared to large scale debris flows, low values are expected for the friction number compared to large scale debris flows, since $N_{Bag} \sim f(\gamma)$, $N_{Sav} \sim f(\gamma^2)$ and $N_{fric} = N_{Bag}/N_{Sav}$ (Table 4). This shows that friction is relatively less important in small scale experiments. The transition from viscosity dominated to contact friction dominated was determined at $N_{fric} > 1400$ (Iverson and LaHusen, 1993) obtained from the original equation that was not edited by Iverson (1997). These results can therefore not be compared.

Other dimensionless numbers are the mass number N_{mass} which is the ratio of solid inertia to fluid inertia (equation 14) (Iverson, 1997), the Darcy number N_{Dar} which describes the tendency of pore fluid pressure to buffer grain interaction (equation 15) (Iverson, 1997) and the grain Reynolds number N_{Rey} which is the ratio between the solid inertial stress and fluid viscosity shearing. The Reynolds number is calculated as the Bagnold number divided by the mass number ($N_{Rey} = N_{Bag}/N_{mass}$). These numbers are also plotted in Figure 50.

The mass number increases with coarse material and decreases with clay (Figure 50g and Figure 50h). But the change is much larger for clay content than for coarse material content. Solid inertia is more important with a high mass number compared to fluid inertia. The mass number from the experiments is close to the mass numbers of flows in the USGS flume and natural debris flows (Table 4).

The Darcy number shows an optimum around 30 wt% coarse material and shows an increase for clay (Figure 50i and Figure 50j). For high Darcy numbers a fluid matrix prevents grain interaction which is easy with clay available and difficult with a large amount of coarse grains. The Darcy number falls in the range of the natural debris flows and is a better representation of natural debris flows compared to the USGS flume flows (Table 4). Iverson and LaHusen (1989) showed experiments with Darcy numbers between 1000 and 6000 and reported strong solid-fluid interaction. The experiments of this thesis also showed strong solid-fluid interactions for much larger Darcy numbers, so these numbers do not define boundaries.

The Reynolds number increases with coarse material and decreases with clay (Figure 50k and Figure 50l). Larger Reynolds numbers indicate larger inertial effects and deviate from ideal viscous flow. This shows that for clay, viscosity is relatively more important and inertia is more important for coarse material. The Reynolds number is in the same order as for the USGS flume, but much higher than for the natural debris flows (Table 4). This is again caused by larger values of the Bagnold number by large shear rates. Vanoni (1975) discussed that typically inertia starts to be important for fluid flow if $N_{Rey} > 0.1$. This is the case for all experiments, but not for two of the three natural debris flows. This might be because lahars and mudflows have a finer grained composition than standard debris flows generating less grain inertia. This has no further implications for the experimental analysis.

$$N_{mass} = \frac{\rho_s \cdot v_s}{\rho_f \cdot 1 - v_s} \quad eq. 14$$

$$N_{mass} = \text{Mass number} [-]$$

$$\rho_s = \text{sediment density [kg/m}^3]$$

$$\rho_f = \text{density fluid constituents [kg/m}^3]$$

$$v_s = \text{granular volume fraction} [-]$$

$$N_{Dar} = \frac{\mu}{v_s \rho_s \gamma k} \quad eq. 15$$

$$N_{Dar} = \text{Darcy number} [-]$$

$$\mu = \text{effective viscosity [Pa]}$$

$$v_s = \text{granular volume fraction} [-]$$

$$\rho_s = \text{sediment density [kg/m}^3]$$

$$\gamma = \text{shear strain rate [s}^{-1}]$$

$$k = \text{hydraulic permeability [m}^2/\text{s]}$$

Dimensionless numbers can vary for different parts of the flow (Iverson, 1997; Iverson et al., 2010). This is due to grain size variations in the flow and flow depth. For example, coarse

material accumulates in the flow front which also has a larger flow depth. This has an effect on shear rate γ and characteristic grain size δ . Additionally grain size and water distribution may affect permeability and effective viscosity.

To summarize, the small scale experiments are for each dimensionless parameter as accurate as large scale experiments in the USGS flume. In general for experiments, collisional shear is relatively more important and frictional shear less important than for natural flows because of larger shear rate. Although collisional shear is more important, the contribution of friction and viscosity is not insignificant. To improve these dimensionless numbers in the future, it should be investigated if velocity divided by flow depth is really a good measure for shear rate, since Iverson (1997) only mentions it as an estimation. If the current method estimates shear rate properly, it should be researched if thicker debris flows with lower velocities can also be developed in the lab, which should in theory result in lower shear rates. The implications from relatively larger grain inertial stress is that the effects of the coarse grained fraction (causing the most collisional forces) is overestimated.

Table 4: Dimensionless parameters calculated for USGS flume, three real debris flows (Iverson, 1997) and experiments of this thesis.

Parameter	Experiments	USGS	Oddstad debris flow Jan 4, 1982	South Toutle River May 18, 1980	Osceola Mudflow ~5700 B.P.
N_{Bag}	34-1571	400	4	0.2	0.4
N_{Sav}	0.3-3.5	0.2	0.0002	0.000006	0.0000001
N_{fric}	82-1741	2000	20,000	30,000	400,000
N_{mass}	0.9-3.3	4	4	4	4
N_{Dar}	31,909-4,406,812	600	60,000	2,000,000	60,000,000
N_{Rey}	29-498	100	1	0.04	0.01

STOPPING MECHANISM

Even though different dimensions of the deposit are discussed in relation to boundary and initial conditions, it is not yet clear what causes the flow to stop. To stop a debris flow it is necessary that the total shear stress becomes smaller than the yield strength. Shear stress is dependent on normal stress on shear surface, pore-fluid pressure, cohesion and angle of internal friction (*equation 1*). The results have shown that pore-fluid pressure, yield stress, skin friction and internal friction (viscosity or grain-collision) vary for different mixtures which makes assessment of the stopping mechanism difficult.

According to Major (1997) deposit dimensions are a reflection of deposit strength which is influenced by permeability, pore-fluid pressure and frictional strength at the margins. This suggest that the internal friction of the flow is of less importance for the stopping mechanism.

To assess the stopping mechanism it should be determined if diffusivity is small enough to sustain excess pore-fluid pressure longer than time before deposition. In natural debris flows and USGS debris flows diffusivities fall in the range of 10^{-3} - 10^{-7} m²/s (Iverson, 1997; Major and Iverson, 1999; Major, 2000). It is noted that diffusivities can be higher in debris-flow snouts, but when diffusivities are higher on average debris flows are more likely resemble rock avalanches (Iverson and Denlinger, 2001). According to non-dimensional numbers, experiments with large coarse material content (>3x reference; 30.54 wt%) should be considered rock avalanches (*Figure 50*). Even though this proves that pore pressure loss might be an important stopping mechanism for large coarse material content experiments, here they are not considered rock avalanches because typical debris-flow morphologies are observed.

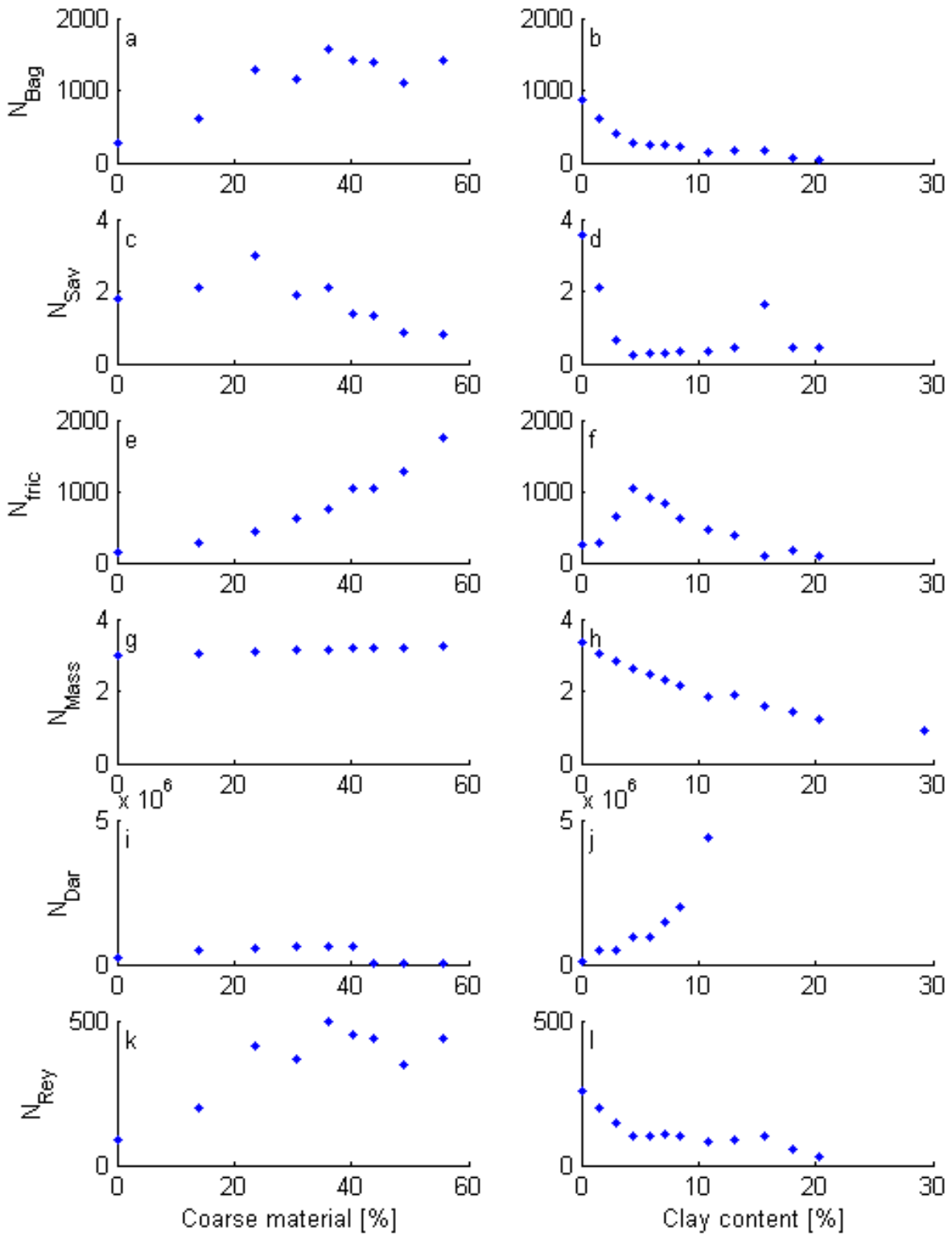


Figure 50: Non-dimensional numbers a,b) Bagnold number, c,d) Savage number, e,f) Friction number, g,h) Mass number, i,j) Darcy number, k,l) Reynolds number as a function of a,c,e,g,i,k) coarse material content and b,d,f,h,j,l) clay content.

Friction at the flow margins is mainly caused by development of a coarse flow front. Coarse flow front cause a lot of friction because the coarse material rather slides and rolls than flows down the slope. This because the coarse front loses pore pressure relatively rapidly. This relates back to the previous paragraph. It is thought that loss of pore pressure together with friction of coarse flow front decrease the length of the deposit for debris-flow compositions with a large coarse material content.

For high clay contents the stopping mechanism is different. Diffusivity and permeability indicate that there is no significant pore-fluid pressure loss during transport (*Figure 21h* and *Figure 21j*). For higher clay content viscous forces become more important and also the yield strength (*Figure 21g*). More important than frictional forces of the margins, because coarse front development is limited. When yield stress increases for clay content shear stresses are earlier below the flow threshold. This means that the length of the flow for clay rich mixtures with a relatively low coarse material content are determined by the yield strength.

SCALING PARAMETERS

Some issues with (small scale) experiments have already been discussed. Apparently experiments have the tendency to develop relatively higher grain inertial (collisional) stresses compared to other stresses. Iverson et al. (2010) developed seven dimensionless scaling parameters that show how well debris-flow dynamics are described in experiments. Of these seven parameters three are discussed here that are really scale depended (Iverson et al., 2010). Y defines the scale dependence of the yield strength (*equation 16*). Flow depth is the only parameter that changes with scale. Therefore the effect of yield strength can be expected to decrease with size (Iverson et al., 2010). Calculated values for this parameter are not significantly different (*Table 5*), but are difficult to compare. The scaling parameters show a wide range for the experiments including values similar to large and small scales calculated by Iverson et al. (2010), but Iverson et al. (2010) used a standard mixture to calculate for different scales, this mixture is not comparable with mixtures used for the experiments of this thesis. If it is assumed that the effect of yield stress also decreases with size for the mixtures used in this thesis, small scale flows are less easily put in motion and stop more easily by yield stress. This is why a second hatch opens in the experimental channel after 1.5 seconds. Because the flow stops earlier, the deposit would be flooded with the finer material of the tail if the hatch did not exist. Because we want to study the deposit, the flow is diverted at the moment when the deposit stops growing in length and width.

$$Y = \frac{\tau_y}{\rho_0 g H} \quad \text{eq. 16}$$

τ_y = yield stress [Pa]

ρ_0 = density [Pa]

g = gravitational acceleration [m/s^2]

H = flow depth [m]

Parameters N_{R2} and N_P show the scale-dependence of pore-fluid viscosity (Iverson et al., 2010). N_{R2} is a Reynolds number with characteristic velocity \sqrt{gL} (*equation 17*). It shows the effect of viscosity on the total shear resistance. L is the surge length but was estimated by the flows length for the experiments of this thesis and was assumed equal for all experiments. H and L are the parameters that are scale depended and decrease both with size. Because viscosity was typically a factor 100 smaller the smaller H and L are partially compensated. The range falls between estimated values for small scale experiments and the USGS flume by Iverson et al. (2010) (*Table 5*).

$$N_{R2} = \frac{\rho_0 H \sqrt{gL}}{\mu} \quad \text{eq. 17}$$

$\rho_0 = \text{density [Pa]}$

$g = \text{gravitational acceleration [m/s}^2\text{]}$

$H = \text{flow depth [m]}$

$L = \text{surge length [m]}$

$\mu = \text{effective viscosity [Pa} \cdot \text{s]}$

N_p indicates the effect of pore pressure persistence. It is calculated by the ratio of time the debris flow is in motion divided by the pore pressure diffusion (*equation 18*). N_p has much larger values for small-scale experiments (*Table 5*). This indicates that pore pressure diffusion is very rapid even though diffusion is smaller than the reference diffusion of Iverson et al. (2010). If $N_p > 1$ pore pressure disappears during motion. This would be a problem in the simulation of debris flows, since formation of excess pore pressure is an essential process in debris flow motion. Visual observations do not support this result. Deposits maintained high pore pressure for at least a few seconds up to hours after deposition, this was observed by shaking the deposit which liquefied the deposit a second time and wet areas around the deposit developed also not immediately. Exceptions are the mixtures with a very large weight percentages of coarse material. These mixtures are on small scale considered to be in the transitional regime from debris flow to rock slide. But due to the scaling effect of pore pressure persistence these flows are probably more like debris flows on the natural scale.

$$N_p = \frac{D\sqrt{L/g}}{H^2} \quad \text{eq. 18}$$

$L = \text{surge length [m]}$

$g = \text{gravitational acceleration [m/s}^2\text{]}$

$H = \text{flow depth [m]}$

$D = \text{hydraulic diffusivity [m}^2\text{/s]}$

Table 5: Values for dimensionless scaling parameters for different debris-flow sizes of similar composition ($\delta=0.01m$, $\rho_s=2700\text{kg/m}^3$, $\rho_f=1200\text{kg/m}^3$, $\tau_y=100 \text{ Pa}$, $\mu=0.1 \text{ Pa}\cdot\text{s}$, $D=10^{-5} \text{ m}^2\text{/s}$) (Iverson et al., 2010). Second column range of the parameters for this thesis is included, same composition was not possible.

Parameter	Thesis	Bench-top	USGS	Full-scale	
H		0-0.02	0.03	0.3	3
Y		0.009-0.5	0.2	0.02	0.002
N_{R2}		$2 \cdot 10^4$ - $2 \cdot 10^5$	$3 \cdot 10^3$	$1 \cdot 10^5$	$3 \cdot 10^6$
N_p		$2 \cdot 10^{-3}$ - $2 \cdot 10^2$	$6 \cdot 10^{-3}$	$2 \cdot 10^{-4}$	$6 \cdot 10^{-6}$

The scaling parameters suggest that the scaling effects of small scale experiments are less than expected. This is mainly because the sediment mixtures are not comparable. Viscosity is approximately a factor 100 smaller. Iverson et al. (2010) noted that increasing clay content largely effects viscosity and yield strength in small-scale experiments, while at large scales the effect of clay content on pore-fluid pressure and friction reduction are larger. In the experimental results all four effects are observed. For little additions of clay we have seen that pore fluid pressure increased (*Figure 21*) and friction decreased (*Figure 50*). Yield stress only increased significantly for very large clay additions (*Figure 21*). Viscosity is per definition an exponential increase with fine fraction (*equation 10*), and therefore in these experiments clay content. This suggests that we can assume the concerns of Iverson et al. (2010) are found to be of limited influence on the experimental results. This is probably because lower viscosities were accepted in the experiments to compensate for the negative effects of viscosity on small scales. Low viscosity values were obtained by a low silt content of the mixture leading to a low fine fraction.

It is not unusual for small scale experiments to change a parameter or boundary condition to compensate for scaling effects. For example small-scale meandering river experiments use natural sediment sizes to generate hydraulic rough conditions and use higher slopes to generate sediment transport which is necessary due to relatively large grains and low water depths (van Dijk et al., 2012).

MARTIAN DEBRIS-FLOW FANS

Visual observations of Martian fans show many morphological characteristics of debris-flow fans on Earth and experimental fans. The debris-flow fans on HiRISE image PSP_006837_1345_RED (*Figure 53*) found by Johnson et al. (2013) are discussed in more detail.

The Martian HiRISE image shows a lot of boulders on the debris-flow fans (*Figure 53B*). It suggests transportation of very coarse grained material, which could not have happened by purely fluvial flow. Many boulder sizes are seen at the surface, varying from 3 m down to pixel size. This suggests a wide variety of grain sizes are transported, typical and essential for debris flows.

Levees are also spotted in this HiRISE image (*Figure 53C*). Even though many levees appear to be covered by lobes. Levees are a pronounced morphology at the fan surface typical for debris flows. Levees are more pronounced in the outer bends of the flow path.

Lobes are the most characteristic morphologies that are found on debris-flow fans on Mars (*Figure 53C*). Lobes are very characteristic for debris flows because they have a typical form that is not generated by other transport processes, because it is typically for a yield stress fluid. The steep edges of the lobes show distinct individual deposits.

A dataset (supplied by Tjalling de Haas) from measurements of lobes on Mars was used to compare experimental debris-flow dimensions to Mars. Debris flows on Mars are on average 8 meter wide, 21 m long and 1 m high (*Table 6*). This is on average 92 times wider, 27 times longer, 51 times higher and 74003 times bigger in volume than the experiments. Results have showed that lobe height is only depended on debris-flow composition. In theory some information about the composition can be obtained from Martian lobe heights and visual observations.

Table 6: Martian lobe dimensions (Tjalling de Haas) and average dimensions reference experiments.

	<i>Width</i>	<i>Length</i>	<i>Height</i>	<i>Volume</i>
Min	3.10	7.90	0.22	15.14
Median	7.65	18.60	0.82	110.84
Average	8.44	21.50	0.91	222.01
Max	30.10	80.00	2.10	2203.74
Av ref exp	0.091	0.773	0.018	0.003

Many stacked debris flows are found that retreat in runout length. This was also observed in the fan experiments 1 and 3. This suggest that runout lengths are not increased by debris flows deposited earlier like in fan experiment 2. This indicates that the clay content is not extremely high, approximately lower than ~6 wt%.

Boulder concentrations are not larger in levees and snouts. This suggests that not a very large coarse material content is present. But this cannot be concluded for certain, because only individual boulders can be observed from the satellite images and no finer sorting patterns. By observation of the appearance of the lobes coarse material content is estimated at ~10-30 wt% coarse material.

The width/height ratio can give information about the internal friction of the flow. Very viscous flows have steep edges, just as flows with a large internal grain friction. More easily flowing flows have generally less steep edges and become wider and less high. This leads to higher width/height ratios that can be cause by for example small amounts of clay, large amounts of

water and little amounts of coarse material. A histogram with width/height ratios of the Martian debris flow lobes is shown in *Figure 51*.

The width/height ratio is plotted for water, clay and coarse material (*Figure 52*). Although there is large scatter in all of the figures, the trend is still visible. Snout/lobe width is used for width and snout/lobe height is used for height. If it is assumed that the debris-flows on the studied Martian fan are approximately of the same composition, typical width/height ratios from the histogram (*Figure 51*) can be compared to width/height ratios of the experiments. This is a reasonable assumption since debris flows in the same region are generated in the same source area and therefore a similar sediment composition.

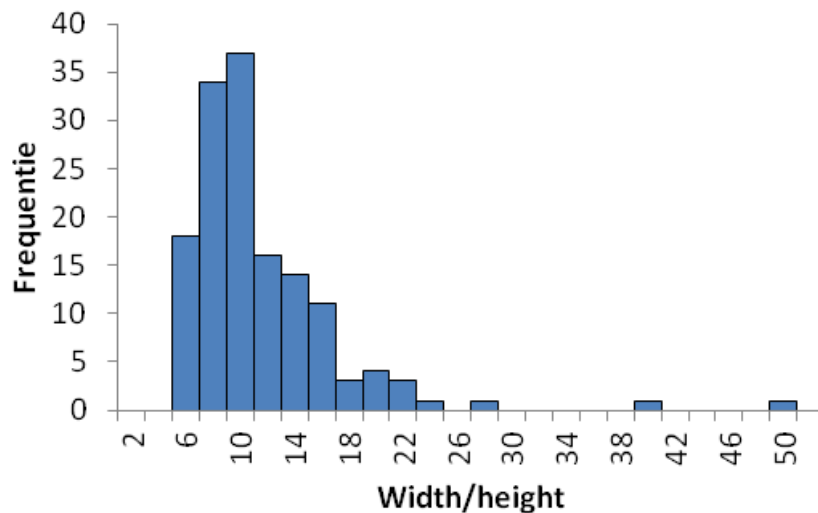


Figure 51: Histogram with width/height ratios of Martian debris flow lobes (dataset Tjalling de Haas).

The histogram indicates that typical width/height ratios are around 8. This is relatively high in all the graphs of *Figure 52*. It is expected that experimental width/height ratios are slightly underestimated, since it was observed that stacked debris flows on fans have larger widths than single debris flows. Although the ratios are underestimated, a rough indication of Martian debris-flow composition can be given.

The width/height ratios for varying coarse material content shows an optimum (*Figure 52a*). Small ratios for low and high percentages and high ratios for 20-40 wt%. The Martian ratios intersect the graph in the optimum. This indicates coarse material percentages of 20-40 wt%. This coincides with estimations of visual observations made before.

The width/height ratios for clay also show an optimum in the graph (*Figure 52b*). Intersection points are near 10 wt% clay and 15 wt%. Between 10-15 wt% the ratio is higher and otherwise lower. If these values are compared with the estimations of the visual observation a weight percentage of 10 is more likely than 15. Although the effect of clay was thoroughly researched, the effect of only 1 mineral (kaolinite) was tested. According to Yu et al. (2013) other clay minerals like montmorillonite and illite create higher yield strengths.

The width/height ratios for water content show approximately an exponential increase (*Figure 52c*). This exponential function would intersect with the characteristic Martian width/height ratio around 30 wt% or 50 vol% water. As discussed earlier, these percentages are probably lower due to underestimation of the width.

So to summarize, Martian fan show many morphological similarities to the debris-flow experiments and are therefore very likely formed by debris flows. Visual observations indicate that the Martian debris flows contain approximately less than 6wt% clay and 10-30wt% very coarse material. Width/height ratios indicate 20-40 wt% coarse material, ~10 wt% clay and ~30% water, but the percentages are likely to be a bit lower since experimental ratios are underestimated.

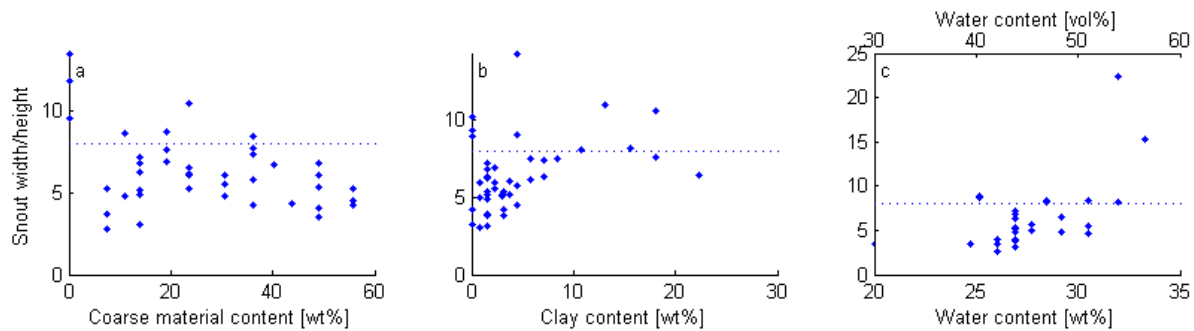


Figure 52: Experimental width/height ratios for a) coarse material content, b) clay content and c) water content.

IMPROVEMENTS AND FUTURE RESEARCH

Although scaling issues and failed experiments were already extensively discussed, more difficulties and limitations appeared during this thesis.

The largest limitation of the experiments is that the experiments were not performed under Martian conditions. The low temperature and pressure could have significant effects on debris-flow motion and deposition. Especially when water sublimates processes might play a role that are not occurring on Earth. The effect of smaller gravity is not expected to make a large difference, but should be studied as well. The comparison with Mars can be improved if these effects are studied.

Another limitation of the experiments is that an erodible bed is absent. No sediment can be entrained during motion in the channel. This was practical in the analysis because the volume and composition is in this way controlled, but important processes might be overlooked because entrainment always occurs in natural flows.

Furthermore, improvements can be made in the experiments by better control of the moisture content on different places in the experimental set up. Drying the subbed (sand in the raster) before each experiment as well as the top layer might improve the repeatability of the results. Moreover, the moisture in the barrel and the channel is important to keep the same for all experiments.

Measurements for flow depth and velocity were not very accurate. It was obtained from movies by hand. This could be improved.

Looking back at the discussion of the scaling parameters, improvements can be made in shear rate. It should be tested if h/u is a good estimation for shear rate. If so, experiments with ticker and slower debris flows should be tried to develop to make them more similar to natural debris flows according to the non-dimensional numbers.

Shear stress measurements should be made in the future, if possible, because then the moment of deposition (stopping mechanism) can be studied better.

In the scope of future space mission, it would be useful to obtain close up images of debris-flow fan surfaces. With close up images, grain sorting pattern give more information about the debris flow and the material involved.

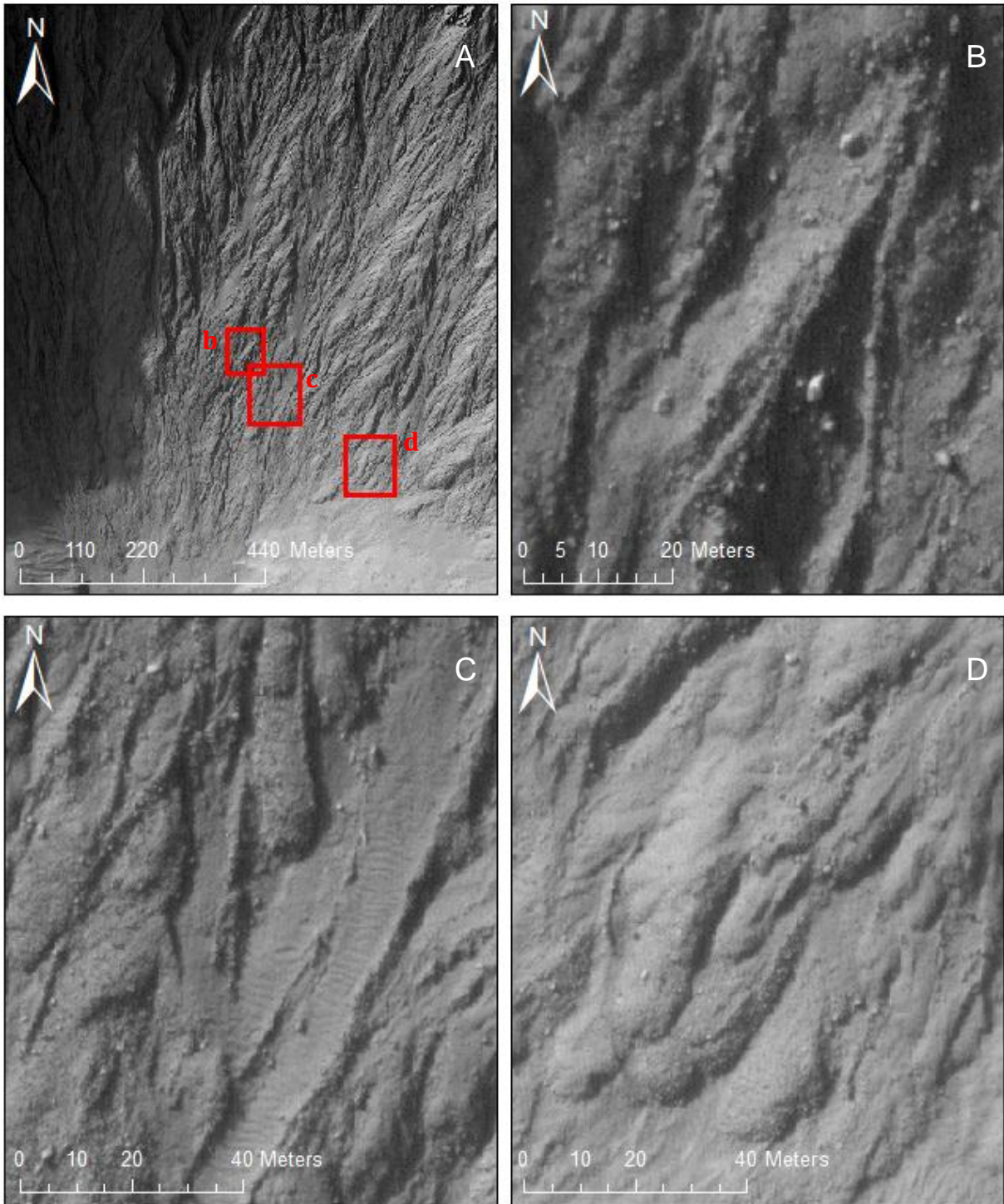


Figure 53: HiRISE (PSP_006837_1345_RED) image with debris-flow fans Mars. A) Overview with frames indicating location of other images. Zoomed in on, B) boulders, C) levees, D) lobes.

CONCLUSION

The small-scale experimental debris-flow morphologies are similar to natural debris flows. The morphologies that are well represented in experiments are coarse levees, lobes, steep edges, coarse snouts, watery tail and no stratification after deposition. Processes typical for debris flows such as grain segregation, shouldering and liquefaction were also present.

Debris-flow morphologies are influenced by terrain related boundary conditions (channel slope, outflow plain slope, channel width) and debris-flow composition (clay, coarse material, water, amount). Snout width and height are only determined by water and sediment concentrations, while runout length is controlled by composition and topography.

Long debris flows are a big hazard in mountainous areas. The longest debris flows occurred for 20-30 wt% coarse material and 5-15% clay. Debris flows behavior was observed from ~22 wt% water. Additionally to the composition, high slopes and wide channels increase runout length.

Debris flow length is limited by the possibility to build levees, yield stress, friction of the flow front or pore pressure loss. Yield stress is dominant stopping mechanism for clay rich debris-flow compositions. For high coarse material content the frictional forces of the snout are significant, but rapid pore-fluid pressure loss as well.

Scaling issues were limited. Most of the dimensionless numbers and scaling parameters of the experiments were similar to results from the USGS flume. Relatively high grain inertial (collisional) stresses were calculated in the analysis implicating a relative higher effect of coarse grained material. Effects of viscosity were expected to be large, but due to a low fine fraction no scaling issues were discovered in relation to viscosity. Pore pressure dissipation was expected to be a problem, but not observed.

In relating the effects of boundary and initial conditions to debris flow morphology on Mars, it was found that the Martian debris flows contain approximately less than 6 wt% clay, 10-30 wt% very coarse material and a bit less than 27 wt% water. Determined by visual comparison and width-depth ratios of debris flow snouts. Although this is only a very rough estimation, percentages might be a bit lower, since deposition width of debris flows is larger on fans compared to single debris-flow experiments.

ACKNOWLEDGEMENTS

I would like to thank Tjalling de Haas for close supervision of my master thesis, providing a subject for this thesis, guiding me through months of experiments and helping me to understand the experimental results. Secondly, I want to thank Maarten Kleinhans for further supervision and ideas for this thesis. Furthermore I like to thank Marcel van Maarseveen, Bas van Dam, Henk Markies and especially Chris Roosendaal of the technical staff for developing the experimental set-ups and for all the technical support with problems I encountered during the experiments. I also would like to thank Bas van der Meulen and Jasper Leuven for reviewing my thesis. Finally I would like to thank Ivar Lokhorst and Jasper Leuven for developing a good method to generate debris flows and for their data set with which I could continue my research.

REFERENCES

- Armanini, A., Capart, H., Fraccarollo, L., Larcher, M. (2005). Rheological stratification in experimental free-surface flows of granular-liquid mixtures. *Journal of Fluid Mechanics*, 532:269-319.
- Bagnold, R. A. (1954). Experiments on a Gravity-Free Dispersion of Large Solid Spheres in a Newtonian Fluid under Shear. *Proceedings of the Royal Society of London: series A, Mathematical and Physical Sciences*, 225:1160:49-63.
- Battella, F., Bisantino, T, D'Agostino, V., Gentile, F. (2012). Debris-flow runout distance: laboratory experiments on the role of Bagnold, Savage and friction numbers. *WIT transactions on Engineering Sciences*. 73:27-36.
- Blair, T. C., McPherson, J. G. (2009). Processes and forms of Alluvial fans. In: Parsons, A. J., Abrahams, A. D. (eds.) *Geomorphology of desert environments*, 2nd ed. Springer, the Netherlands, 413-467.
- Branney, M. J., Kokelaar, P. (2002). *Pyroclastic Density Currents and the Sedimentation of Ignimbrites*. Geological Society Memoir, 27.
- Campbell, R. H. (1975). Soil slips, debris flows, and rainstorms in the Santa Monica Mountains and vicinity, southern California. U.S. Geological Survey Professional Paper, 851.
- Christensen, P. R. (2003). Formation of recent Martian gullies through melting of extensive water-rich snow deposits. *Nature*, 422:45-48.
- Conway, S. J., Balme, M. R., Murray, J. B., Towner, M. C., Kim, J. R. (2008). Icelandic debris flows and their relationship to Martian gullies. In: *Workshop on Martian Gullies, Theories and Tests*. Lunar and Planetary Institute, Houston, Texas, USA.
- Costa J. E. (1984). Physical geomorphology of debris flows. In: Costa, J. E., Fleisher, P. J. (eds.) *Developments and applications of geomorphology*. Springer, Berlin, 268–317.
- Costard, F., Forget, G., Mangold, N., Peulvast, J. P. (2002). Formation of Recent Martian Debris Flows by Melting of Near-Surface Ground Ice at High Obliquity. *Science*, 295: 110-113.
- D'Agostino, V., Cesca, M., Marchi, L. (2010). Field and laboratory investigations of runout distances of debris flows in the Dolomites (Eastern Italian Alps). *Geomorphology* 115:294–304.
- Davies, T. R. H. (1990). Debris-flow surges – experimental simulation. *Journal of hydrology*, 29:1:18-64.
- De Haas, T., Hauber, T., Kleinhans, M. G. (2013). Local late Amazonian boulder breakdown and denudation rate on Mars. *Geophysical Research Letters*, 40:1-5.
- Fairfield, G. (2011). Assessing the dynamic influences of slope angle and sediment composition on debris flow behaviour: An experimental approach. Durham theses, Durham University, 3265.
- Gaidos, E. J. (2001). Cryovolcanism and the Recent Flow of Liquid Water on Mars. *Icarus*, 153:218–223.
- Ghilardi, P. (2003). Experimental Observations of Granular Debris Flows. *Geophysical Research Abstracts*, 5:13705.
- Gilmore, M. S., Phillips, E. L. (2002). Role of aquicludes in formation of Martian gullies. *Geology*, 30:1107-1110
- Gray, J. M. N. T., Thornton, A. R. (2005). A theory for particle size segregation in shallow granular free-surface flows. *Proceedings Royal Society of America*, 461:1447-1473.
- Gregoretto, C. (2000). The initiation of debris flow at high slopes: experimental results. *Journal of Hydraulic Research*, 38:2:83-88.
- Heldmann, J. L., Mellon, M. T., (2004). Observations of martian gullies and constraints on potential formation mechanisms. *Icarus*, 168:285-304.

- Hirano, M., Iwamoto, M. (1981). Measurement of debris flow and sediment-laden flow using a conveyor-belt flume in a laboratory. *Erosion and Sediment Transport Measurement, Proceedings of the Florence Symposium, IAHS*, 133:225-230.
- Hirano, M., Iwamoto, M., Saruwatari, H. (1978). Some experimental studies of flow in flume with belt-conveyor bed. *Proceedings of the 22th Japanese Conference on Hydraulics*, 283-289.
- Hüble, J., Steinwendter, H. (2000). Estimation of Rheological Properties of Viscous Debris Flow Using a Belt Conveyor. *Physics and Chemistry of the Earth (B)*, 25:9:751-755.
- Hungr, O., Evans, S. G., Bovis, M. J., Hutchinson, J. N. (2001). A review of the classification of Landslides of the Flow Type. *Environmental & Engineering Geoscience*, 7:3:221-238.
- Hungr, O., Morgan, G. C., Kellerhals, R. (1984). Quantitative analysis of debris torrent hazards for design of remedial measures. *Canadian Geotechnical Journal*, 21:4:663-677.
- Ikeya, H. (1989). Debris flows and its countermeasures in Japan. *Bulletin of the international association of engineering geology*, 40:1:15-33.
- Iverson, R. M. (1997). The Physics of Debris Flows. *Reviews of Geophysics*, 35:3:245–296.
- Iverson, R. M. (2003). The debris-flow rheology myth. In: Chen, C. (eds.) *Debris-Flow Hazards Mitigation: Mechanics, Prediction, and Assessment*. Millpress, Rotterdam, 303-314.
- Iverson, R. M., Denlinger, R. P. (2001). Flow of variably fluidized granular masses across three-dimensional terrain: 1. Coulomb mixture theory. *Journal of Geophysical Research*, 106:B1:537-552.
- Iverson, R. M., LaHusen, R. G. (1989). Dynamic Pore-Pressure Fluctuations in Rapidly Shearing Granular Material. *Science*, 246:796-799.
- Iverson, R. M., LaHusen, R. G. (1993). Friction in Debris Flows: Inferences from Large-scale Flume Experiments. *Hydraulic Engineering*, 2:1604-1609.
- Iverson, R. M., Logan, M., LaHusen, R. G., Berti, M. (2010). The perfect debris flow? Aggregated results from 28 large-scale experiments. *Journal of Geophysical Research*, 115:F03005.
- Iverson, R. M., Vallance, J. W. (2001). New views of granular mass flows. *Geology*, 29:115-118.
- Johnson, A. M. (1970). Formation of debris flow deposits. *Physical Processes in Geology: San Francisco*, Freeman, Cooper, Co, 433-448.
- Johnson, C. G., Kokelaar, B. P., Iverson, R. M., Logan, M., LaHusen, R. G., Gray, J. M. N. T. (2012). Grain-size segregation and levee formation in geophysical mass flows. *Journal of geophysical research*, 117:F01032.
- Johnsson, A., Reiss, D., Hauber, E., Hiesinger, H., Zanetti, M. (2014). Evidence for very recent melt-water and debris flow activity in gullies in a young mid-latitude crater on Mars. *Icarus*, 235:37-54.
- Kaitna, R., Rickenmann, D. (2005). Debris flow experiments in a vertically rotating drum. In *Geophysical Research Abstracts*, 7:07959.
- Kaitna, R., Rickenmann, D., Schatzmann, M. (2007). Experimental study on rheologic behaviour of debris flow material. *Acta Geotechnica*, 2:71-85.
- Kean, J. W., McCoy, S. W., Tucker, G. E., Staley, D. M., Coe, J. A. (2013). Runoff-generated debris flows: Observations and modeling of surge initiation, magnitude, and frequency, *Journal of Geophysical Research: Earth Surface*, 118:2190-2207.
- Lanza, N. L., Meyer, G. A., Okubo, C. H., Newsom, H. E., Wiens, R. C. (2010). Evidence for debris flow gully formation initiated by shallow subsurface water on Mars. *Icarus*, 205:103-112.
- Larcher, M., Fraccarollo, L., Armanini, A., Capart, H. (2007). Set of measurement data from flume experiments on steady uniform debris flows. *Journal of Hydraulic Research*, 45:59-71.
- Lee, P., Cockell, C. S., Marinova, M. M., McKay, C. P., Rice Jr., J. W. (2001). Snow and ice melt flow features on Devon Island, Nunavut, Arctic Canada as possible analogs for recent slope flow features on Mars. In: *32nd Lunar and Planetary Science Conference*. Lunar and Planetary Institute, Houston, Texas, USA.
- Liu, X. (1996). Size of a debris flow deposition: model experiment approach. *Environmental Geology*, 28:2:70-77.

- Lokhorst, I. (2013). Debris fans on planet Mars, a morphological analysis. BSc Thesis Earth Sciences, Utrecht University.
- Major, J. J. (1997). Depositional Processes in Large-Scale Debris-Flow Experiments. *The Journal of Geology*, 105:3: 345-366.
- Major, J. J. (2000). Gravity-driven consolidation of granular slurries – Implication for debris-flow deposition and deposition characteristics. *Journal of Sedimentary Research*, 70:1:64-83.
- Major, J. J., Iverson, R. M. (1999). Debris-flow deposition: Effects of pore-fluid pressure and friction concentrated at flow margins. *Geological Society of America*, 111:10:1424-1434.
- Malin, M. C., Edgett, K. S. (2000). Evidence for Recent Groundwater Seepage and Surface Runoff on Mars. *Science*, 288:2330-2335.
- Malin, M. C., Edgett, K. S., Posiolova, L. V., McColley, S. M., Noe Dobrea, E. Z. (2006). Present-Day Impact Cratering Rate and Contemporary Gully Activity on Mars. *Science*, 314:1573-1577.
- Mathewson, C. C., Keaton, J. R., Sant, O. M. (1990). Role of Bedrock Ground Water in the Initiation of Debris Flows and Sustained Post-Flow Stream Discharge. *Bulletin of the Association of Engineering Geologists*, 27:1:73-83.
- Mellon, M. T., Phillips, R. J. (2001). Recent gullies on Mars and the source of liquid water. *Journal of Geophysical Research*, 106:E10: 23165-23179.
- Parsons, J. D., Whipple, K. X., Simoni, A. (2001). Experimental Study of the Grain-Flow, Fluid-Mud Transition in Debris Flows. *The Journal of Geology*, 2001:109:427–447.
- Parsons, R. A. (2008). Martian Gully Slope Measurements made using HiRISE stereo pairs. *Lunar and Planetary Science* 39:2328.
- Pierson, T. C. (1980). Erosion and deposition by debris flows at Mt Thomas, North Canterbury, New Zealand. *Earth Surface Processes*, 5:3:227-247.
- Pierson, T. C. (2005). Hyperconcentrated flow – transitional process between water flow and debris flow. In: Jakob, M., Hungr, O. (eds.) *Debris flow hazards and related phenomena*. Springer, Berlin Heidelberg, 159-202.
- Pierson, T. C., Costa, J. E. (1987). A rheologic classification of subaerial sediment-water flows. *Debris flows/avalanches: process, recognition, and mitigation*, 7, 1.
- Reiss, D., Gasselt, S., Neukum, G., Jaumann, R. (2004). Absolute dune ages and implications for the time of formation of gullies in Nirgal Vallis, Mars. *Journal of Geophysical Research*, 109:E06007.
- Rickenmann, D. (2005). Runout prediction methods. In: Jakob, M., Hungr, O. (eds) *Debris-flow hazards and related phenomena*. Springer, Berlin Heidelberg, 305-325.
- Savage, S. B. (1984). The mechanics of rapid granular flows. *Advances in applied mechanics*, 24, 289-366.
- Savage, S. B., Hutter, K. (1989). The motion of a finite mass of granular material down a rough incline. *Journal of fluid mechanics*, 199:177-215.
- Schon, S. C., Head, J. W., Fasset, C. I. (2009). Unique chronostratigraphic marker in depositional fan stratigraphy on Mars: Evidence for ca. 1.25 Ma gully activity and surficial meltwater origin. *Geology*, 37:2:207-210.
- Sharp, R. P., Nobles, L. H., (1953). Mudflood of 1941 at Wrightwood, Southern California. *Geological society of America*, 64:5:547-560.
- Sparks, R. S. J. (1976). Grain size variations in ignimbrites and implications for the transport of pyroclastic flows. *Sedimentology*, 23:147-188.
- Takahashi, T. (1981). Debris Flow. *Annual Review Fluid Mechanics*, 13:57-77.
- Takahashi, T. (1991). Debris flow. *International Association for Hydraulic Research*. A. A. Balkema, Rotterdam.
- van Dijk, W. M., van de Lageweg, W. I., Kleinhans, M. G. (2012). Experimental meandering river with chute cutoffs. *Journal of Geophysical Research*, 117:F03023.

- Van Steijn, H., Coutard, J. P. (1989). Laboratory experiments with small debris flows: physical properties related to sedimentary characteristics. *Earth surface processes and landforms*, 14:587-596.
- Vanoni, V. A. (1975). *Sedimentation Engineering*. American Society of Civil Engineering, New York, 54:745.
- Yu, B., Ma, Y., Qi, X. (2013). Experimental study on the influence of clay minerals on the yield stress of debris flows. *Journal of Hydraulic Engineering*, 139:364-373.
- Zanuttigh, B., Lamberti, A. (2007). Instability and surge development in debris flows. *Reviews of Geophysics*, 45:RG3006.
- Zhou, G. G. D., Ng, C. W. W. (2010). Dimensional analysis of natural debris flows. *Canadian Geotechnical Journal*, 7:719-729.

APPENDIX

- Appendix I: Data table of all dingle debris-flow experiments
- Appendix II: Table with composition of flows in fan experiments
- Appendix III: Table with results and calculations related to permeameter experiments.
- Appendix IV: Table with results and calculations related to yield-strength experiments.
- Appendix V: Table with calculation on non-dimensional numbers and scaling parameters.
- Appendix VI: Table with Martian lobe dimensions

The data and appendices of this thesis are not included but can be requested by contacting me or Tjalling de Haas.